

การแตกย่อยพอลิเอทิลีนชนิดความหนาแน่นสูงและพอลิโพรพิลีน
เร่งปฏิกิริยาด้วยคอมพอสิตแซคเอสเอ็ม-5/อะลูมินัมเอชเอ็มเอส



นายรังสรรค์ เกตสุทัต

สถาบันวิทยบริการ
จุฬาลงกรณ์มหาวิทยาลัย

วิทยานิพนธ์นี้เป็นส่วนหนึ่งของการศึกษาตามหลักสูตรปริญญาวิทยาศาสตรมหาบัณฑิต

สาขาวิชาปิโตรเคมี และวิทยาศาสตร์พอลิเมอร์

คณะวิทยาศาสตร์ จุฬาลงกรณ์มหาวิทยาลัย

ปีการศึกษา 2550

ลิขสิทธิ์ของจุฬาลงกรณ์มหาวิทยาลัย

**CRACKING OF HIGH DENSITY POLYETHYLENE AND
POLYPROPYLENE CATALYZED BY ZSM-5/Al-HMS COMPOSITE**



Mr. Rangson Katsutath

**สถาบันวิทยบริการ
จุฬาลงกรณ์มหาวิทยาลัย**

**A Thesis Submitted in Partial Fulfillment of the Requirements
for the Degree of Master of Science Program in Petrochemistry
and Polymer Science**

Faculty of Science

Chulalongkorn University

Academic Year 2007

Copyright of Chulalongkorn University


Thesis Title CRACKING OF HIGH DENSITY POLYETHYLENE
AND POLYPROPYLENE CATALYZED BY
ZSM-5/Al-HMS COMPOSITE

By Mr.Rangson Katsutath

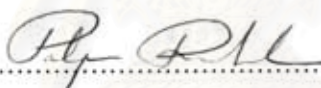
Field of Study Petrochemistry and Polymer Science


Thesis Advisor Assistant Professor Soamwadee Chaianansutcharit, Ph.D.

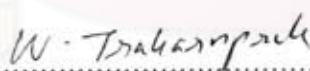
Accepted by the Faculty of Science, Chulalongkorn University in Partial Fulfillment
of the Requirements for the Master's Degree



.....Dean of the Faculty of Science
(Professor Supot Hannongbua, Ph.D.)

THESIS COMMITTEE


.....Chairman
(Professor Pattarapan Prasassarakich, Ph.D.)


.....Thesis Advisor
(Assistant Professor Soamwadee Chaianansutcharit, Ph.D.)


.....Member
(Associate Professor Wimonrat Trakarnpruk, Ph.D.)


.....Member
(Aticha Chaisuwan, Ph.D.)

รังสรรค์ เกตสุทัต : การแตกย่อยพอลิเอทิลีนชนิดความหนาแน่นสูงและพอลิโพรพิลีนเร่งปฏิกิริยาด้วยคอมพอสิต แซคเอสเอ็ม-5/อะลูมินัมเอชเอ็มเอส. (CRACKING OF HIGH DENSITY POLYETHYLENE AND POLYPROPYLENE CATALYZED BY ZSM-5/Al-HMS COMPOSITE)

อ.ที่ปรึกษา: ผศ. ดร. โสภวดี ไชยอนันต์สุจริต, 127 หน้า.

วัสดุคอมพอสิตของสารที่มีรูพรุนขนาดเล็กและสารที่มีรูพรุนขนาดกลาง ได้ถูกนำมาใช้เป็นตัวเร่งปฏิกิริยาการแตกย่อยของพลาสติกพอลิเอทิลีนความหนาแน่นสูงและพอลิโพรพิลีน โดยวัสดุคอมพอสิตจะประกอบด้วยสารที่มีรูพรุนขนาดเล็กแซคเอสเอ็ม-5 ที่สัดส่วน โมลาร์ของซิลิกาต่ออะลูมินาในเจลเท่ากับ 40 และสารที่มีรูพรุนขนาดกลางอะลูมินา-เอชเอ็มเอสที่สัดส่วน โมลาร์ของสัดส่วนซิลิกาต่ออะลูมินาในเจลเท่ากับ 20 60 และ 200 ซึ่งถูกนำมาผสมโดยวิธีทางกายภาพ โดยตรวจสอบลักษณะด้วยเทคนิคการเลี้ยวเบนของรังสีเอ็กซ์ ไอซีพี-เออีเอส อะลูมิเนียมนิวเคลียร์แมกเนติกเรโซแนนซ์ชนิดสปินนวมเฉพาะ การดูดซับไนโตรเจน การคายแอมโมเนียโดยใช้อุณหภูมิที่ตั้งโปรแกรม และ กล้องจุลทรรศน์แบบส่องกราด ได้ศึกษาการแตกย่อยแบบใช้ตัวเร่งปฏิกิริยาของพอลิเอทิลีนความหนาแน่นสูงและพอลิโพรพิลีนบนตัวเร่งปฏิกิริยาแซคเอสเอ็ม-5/อะลูมินัมเอชเอ็มเอสชนิดต่างๆภายใต้ภาวะที่แตกต่าง เมื่อใช้ แซคเอสเอ็ม-5/อะลูมินา-เอชเอ็มเอสเป็นตัวเร่งปฏิกิริยา ค่าการเปลี่ยนของพลาสติกทั้งสองชนิดสูงขึ้นอย่างมากเมื่อเทียบกับการแตกย่อยแบบไม่ใช้ตัวเร่งปฏิกิริยา ค่าการเปลี่ยนและปริมาณของผลิตภัณฑ์ส่วนที่เป็นแก๊ส ของเหลวและปริมาณ ไคกซ์ขึ้นกับอุณหภูมิของปฏิกิริยา อัตราส่วนของตัวเร่งปฏิกิริยาต่อพลาสติก อัตราส่วนน้ำหนักของแซคเอสเอ็ม-5ต่ออะลูมินัมเอชเอ็มเอส และอัตราส่วนของซิลิกอนต่ออะลูมิเนียมในอะลูมินัมเอชเอ็มเอส ความเลือกจำเพาะต่อชนิดผลิตภัณฑ์มีการเปลี่ยนแปลงเพียงเล็กน้อย ส่วนที่เป็นแก๊สที่ได้จากการแตกย่อยพอลิเอทิลีนความหนาแน่นสูง และพอลิโพรพิลีนประกอบด้วยโพรพิลีน ไอโซบิวทิลีน และสารคาร์บอนห้าอะตอมขึ้นไปเป็นส่วนใหญ่ ผลิตภัณฑ์ส่วนที่เป็นของเหลวที่ได้จากการแตกย่อยพลาสติกทั้งสองชนิดส่วนใหญ่อยู่ในช่วง C_3 ถึง C_8 ภาวะที่เหมาะสมของการแตกย่อยด้วยตัวเร่งปฏิกิริยาคอมพอสิตแซคเอสเอ็ม-5/อะลูมินา-เอชเอ็มเอส คือที่อุณหภูมิ 400 องศาเซลเซียส, อัตราส่วนของแซคเอสเอ็ม-5ต่ออะลูมินัมเอชเอ็มเอส 1:1 และอัตราส่วนของซิลิกอนต่ออะลูมิเนียมในอะลูมินัมเอชเอ็มเอสเป็น 60 ซึ่งอัตราส่วนของตัวเร่งปฏิกิริยาต่อพลาสติกของพอลิเอทิลีนความหนาแน่นสูงและพอลิโพรพิลีนใช้เป็นร้อยละ 10 และ 5 โดยน้ำหนักตามลำดับ ตัวเร่งปฏิกิริยาแซคเอสเอ็ม-5/อะลูมินัมเอชเอ็มเอส-60 (1:1) ที่ใช้งานแล้วสามารถทำให้กลับคืนสภาพเดิมได้ด้วยการเผา และความว่องไวของตัวเร่งปฏิกิริยาที่นำกลับมาใช้ใหม่ไม่แตกต่างจากตัวเร่งปฏิกิริยาที่ยังไม่ใช้งาน

สาขาวิชา.....ปิโตรเคมีและวิทยาศาสตร์พอลิเมอร์.....ลายมือชื่อนิสิต.....รังสรรค์ เกตสุทัต
ปีการศึกษา.....2550.....ลายมือชื่ออาจารย์ที่ปรึกษา.....โสภวดี ไชย

4772432023: MAJOR PETROCHEMISTRY AND POLYMER SCIENCE
 KEY WORD: MICROPOROUS MATERIAL/ MESOPOROUS MATERIAL/
 COMPOSITE / ZSM-5/Al-HMS / CATALYTIC CRACKING / HDPE / PP

RANGSON KATSUTATH: CRACKING OF HIGH DENSITY
 POLYETHYLENE AND POLYPROPYLENE CATALYZED BY
 ZSM-5/Al-HMS COMPOSITE. THESIS ADVISOR: ASSISTANT
 PROFESSOR SOAMWADEE CHAIANANSUTCHARIT, Ph.D., 127 pp.

Composites of microporous and mesoporous materials have been studied as catalyst in the cracking of high density polyethylene (HDPE) and polypropylene (PP). Microporous ZSM-5 with the Si/Al molar ratio in gel of 40 and mesoporous Al-HMS with the Si/Al molar ratios in gel of 20, 60 and 200 were physically mixed. All synthesized catalysts were characterized using XRD, ICP-AES, ^{27}Al -MAS-NMR, N_2 adsorption-desorption, NH_3 -TPD and SEM techniques. Catalytic cracking of HDPE and PP over various ZSM-5/Al-HMS catalysts were studied under different conditions. When ZSM-5/Al-HMS was used as catalyst, the conversions of both plastics greatly increased comparing with those in the absence of catalyst. The conversions and yields of gas fraction, liquid fraction and solid coke depended on reaction temperature, catalytic to plastic ratios, weight of ZSM-5 per Al-HMS ratios, and Si/Al ratios in Al-HMS. The product selectivity was not significantly changed. The gas fraction obtained by HDPE and PP cracking composed mainly propylene, iso-butylene and C_5^+ . The liquid fraction obtained by cracking of both types of plastic mainly composed of hydrocarbons in the range of C_7 to C_8 . The optimal condition for catalytic cracking of composite ZSM-5/Al-HMS catalyst in this work was at the temperature of 400°C , ratio of ZSM-5 per Al-HMS as 1:1, and the Si/Al ratio of Al-HMS as 60. The catalyst to plastic ratios for HDPE and PP were 10 and 5 wt%, respectively. The reuse of ZSM-5/Al-HMS-60 (1:1) catalyst was performed by calcination. The activity of the reused catalyst for one cycle was not much different from the fresh catalyst.

Field of Study: Petrochemistry and Polymer Science Student's Signature: *Ran K.*

Academic year: 2007 Advisor's Signature: *Soamwadee Chait*

ACKNOWLEDGEMENTS

The success of this thesis can be attributed to the extensive support and assistance from Assistant Professor Soamwadee Chaianansutcharit and Dr. Aticha Chaisuwan, my thesis advisor and thesis committee. I deeply thank them for their valuable advice and guidance in this research and their kindness throughout this study.

I would like to gratitude to Professor Pattarapan Prasassarakich and Associate Professor Wimonrat Trakarnpruk as the chairman and member of this thesis committee, respectively, for all of their kindness and useful advice in the research.

I would like to gratefully thank PTT Chemical Public Company Limited for supporting the standard mixtures for GC analysis. Moreover, I would like to thank Department of Chemistry and Program of Petrochemistry and Polymer Science, Faculty of Science, Chulalongkorn University for the valuable knowledge and experience. I would like to thank the Graduate School, Chulalongkorn University for supporting a research fund. I would like to thank the Rachadapisek Endowment of Chulalongkorn University, for supporting me as a research assistant. In addition, Thailand Japan Technology Transfer Project supported a loan by Japan Banks for International Cooperation (TJTTP-JBIC) for instrument support. Furthermore, I would like to thank the members of Materials Chemistry and Catalysis Research Unit for consideration and generosity.

For all of my friends, I greatly appreciate their help and encouragement throughout the course of my research and study.

CONTENTS

	Page
ABSTRACT IN THAI	iv
ABSTRACT IN ENGLISH	v
ACKNOWLEDGEMENTS	vi
CONTENETS	vii
LIST OF TABLES	xi
LIST OF FIGURES	xiii
LIST OF SCHEMES	xviii
LIST OF ABBREVIATIONS	xix
CHAPTER I INTRODUCTION	1
1.1 Plastic	2
1.2 Polyolefin	4
1.3 Literature review	5
1.4 Objectives	9
CHAPTER II THEORY	11
2.1 Catalysis	11
2.2 Zeolites	13
2.2.1 Zeolite structures	14
2.2.2 Acid sites of zeolites	15
2.2.3 Shape selectivity	17
2.2.4 Factors influencing zeolite formation	19
2.2.4.1 Reaction mixture components	20
2.2.4.2 Temperature	21
2.2.4.3 Time	21
2.2.5 ZSM-5	21
2.3 Mesoporous materials	22
2.3.1 Mechanism of mesostructure formation	24
2.3.2 Hexagonal mesoporous silica (HMS)	27
2.3.2.1 Hydrogen bonding interaction	28

2.4 Composite material	28
2.5 Characterization methods	28
2.5.1 X-ray diffraction (XRD)	28
2.5.1.1 The Bragg equation	29
2.5.2 N ₂ -sorption	30
2.5.2.1 Isotherms and hysteresis loops	30
2.5.2.2 The BET equation	32
2.5.3 Scanning electron microscopy (SEM)	32
2.5.4 Solid state ²⁷ Al-NMR	33
2.5.5 Temperature-programmed desorption (TPD)	33
2.5.6 Inductively coupled plasma atomic emission spectroscopy (ICP-AES)	34
2.6 Cracking reaction	36
2.6.1 Thermal cracking	36
2.6.2 Catalytic cracking	38
2.6.3 Proposed cracking mechanisms of polymer	41
2.6.4 Reactions of Paraffins	45
CHAPTER III EXPERIMENTS	47
3.1 Instruments and apparatus	47
3.2 Chemicals and gases	49
3.3 Synthesis of catalysts	50
3.3.1 Synthesis of Al-HMS with a Si/Al mole ratio in gel of 20	50
3.3.1.1 Preparation of Al-HMS with various Si/Al mole ratios	50
3.3.2 Synthesis of pure silica HMS	51
3.3.3 Synthesis of ZSM-5 with a Si/Al mole ratio in gel of 40	52
3.4 Removal of organic template from catalysts	53
3.5 Ion exchange of catalysts	54
3.6 Sample preparation for ICP analysis	55
3.7 Preparing the composite of ZSM-5/Al-HMS	55
3.8 Catalytic cracking of HDPE and PP using ZSM-5/Al-HMS	55
3.8.1 Effect of temperature on activity of ZSM-5/Al-HMS	55
3.8.2 Effect of catalytic to plastic ratio	57

3.8.3 Effect of ZSM-5:Al-HMS ratio in composite catalyst.....	57
3.8.4 Effect of aluminium content in catalyst.....	58
3.8.5 Thermal cracking and catalytic cracking over pure catalyst.....	58
3.9 Recycle of catalyst.....	58
CHAPTER IV RESULTS AND DISCUSSIONS.....	59
4.1 Characterization of catalysts.....	59
4.1.1 The physico-chemical properties of ZSM-5(Si/Al = 40)...	59
4.1.1.1 XRD Results.....	59
4.1.1.2 Elemental Analysis.....	60
4.1.1.3 Nitrogen Adsorption-Desorption.....	61
4.1.1.4 ²⁷ Al-MAS-NMR spectra.....	62
4.1.1.5 NH ₃ -TPD profile.....	63
4.1.1.6 SEM images.....	64
4.1.2 The physico-chemical properties of Al-HMS.....	65
4.1.2.1 XRD Results.....	65
4.1.2.2 Elemental Analysis.....	66
4.1.2.3 Nitrogen Adsorption-Desorption.....	67
4.1.2.4 NH ₃ -TPD profile.....	69
4.1.2.5 ²⁷ Al-MAS-NMR Spectra.....	69
4.1.2.6 SEM Images.....	71
4.2 The characterization of ZSM-5/Al-HMS composite catalysts.....	71
4.2.1 XRD Results.....	71
4.2.2 Nitrogen Adsorption-Desorption.....	72
4.3 Activity of ZSM-5/Al-HMS composite catalysts in HDPE Cracking.....	74
4.3.1 Effect of Temperature.....	74
4.3.2 Effect of catalytic to plastic ratio.....	77
4.3.3 Effect of ZSM-5:Al-HMS ratio in composite catalyst.....	81
4.3.4 Effect of aluminium content in catalyst.....	84
4.4 Activity of ZSM-5/Al-HMS composite catalysts in PP Cracking.....	87
4.4.1 Effect of Temperature.....	87

4.4.2 Effect of catalytic to plastic ratio	91
4.4.3 Effect of ZSM-5:Al-HMS ratio in composite catalyst.....	95
4.4.4 Effect of aluminium content in catalyst.....	98
4.5 Catalyst Regeneration.....	101
4.5.1 The characterization of regenerated catalyst.....	101
4.5.1.1 XRD Results.....	101
4.5.1.2 Nitrogen Adsorption-Desorption.....	101
4.5.2 Activity of regenerated catalyst.....	102
4.5.2.1 Activity of regenerated catalyst in HDPE Cracking..	102
4.5.2.2 Activity of regenerated catalyst in PP Cracking.....	106
CHAPTER V CONCLUSION	109
REFERENCES	111
APPENDICES	119
VITAE	127

สถาบันวิทยบริการ
จุฬาลงกรณ์มหาวิทยาลัย

LIST OF TABLES

Table	Page
2.1 The development of important industrial catalytic process in last 50 years.....	13
2.2 Factors influencing zeolite crystallization.....	20
2.3 Selected variables of gross composition on the final crystalline product in zeolite synthesis	21
2.4 Various synthesis conditions of hexagonal mesoporous materials and the type of interaction between template and inorganic species.....	24
2.5 Properties of some hexagonal mesoporous materials.....	25
2.6 Recommended wavelengths and estimated instrumental detection limits.....	36
3.1 Amounts of aluminum isopropoxide (AIP) in the preparation of Al-HMS with Si/Al mole ratios in gel of 20, 60 and 200.....	51
4.1 Si/Al mole ratios in gel and in catalyst of calcined ZSM-5 (Si/Al = 40).....	61
4.2 BET specific surface area and pore diameter of calcined ZSM-5 (Si/Al = 40).....	61
4.3 Si/Al mole ratios in gel and in catalyst of exchanged Al-HMS with different Si/Al ratios.....	67
4.4 Textural properties of calcined Al-HMS with different Si/Al ratios.....	67
4.5 Ratio of peak area between tetrahedral aluminum and octahedral aluminum of Al-HMS with various Si/Al ratios.....	70
4.6 BET specific surface area and pore diameter of calcined catalysts.....	73
4.7 Thermal and catalytic cracking of HDPE over ZSM-5/Al-HMS-60 (1:1) composite catalysts at various reaction temperatures.....	75
4.8 Thermal cracking and catalytic cracking of HDPE over ZSM-5/Al-HMS-60 (1:1) composite catalysts with various catalytic to plastic ratios.....	78
4.9 Catalytic cracking of HDPE over ZSM-5/Al-HMS-60 composite catalysts with various ZSM-5:Al-HMS ratios in composite catalyst.....	82
4.10 Catalytic cracking of HDPE over ZSM-5/Al-HMS composite catalysts with various Si/Al ratios in Al-HMS.....	85
4.11 Thermal and catalytic cracking of PP over ZSM-5/Al-HMS-60 (1:1) composite catalysts at various reaction temperatures.....	88

4.12 Thermal cracking and catalytic cracking of PP over ZSM-5/Al-HMS-60 (1:1) composite catalysts with various catalytic to plastic ratios.....	92
4.13 Catalytic cracking of PP over ZSM-5/Al-HMS-60 composite catalysts with various ZSM-5:Al-HMS ratios in composite catalyst.....	95
4.14 Catalytic cracking of PP over ZSM-5/Al-HMS composite catalysts with various aluminium contents in Al-HMS	98
4.15 Catalytic cracking of HDPE using the fresh and the regenerated ZSM-5/Al-HMS-60 (1:1) composite catalysts.....	103
4.16 Catalytic cracking of PP using the fresh and the regenerated ZSM-5/Al-HMS-60 (1:1) composite catalysts.....	106



สถาบันวิทยบริการ
จุฬาลงกรณ์มหาวิทยาลัย

LIST OF FIGURES

Figure	Page
1.1 Typical trend of increasing municipal waste.....	1
1.2 Plastic compositions in municipal solid waste	2
1.3 Industry polymer identification coding system	3
1.4 Global plastics consumption 2006	5
1.5 Comparison of pore sizes of zeolite Y and ZSM-5 with the kinetic diameters of some hydrocarbon molecules	6
2.1 Structural genetics of zeolitic materials based tetrahedra TO_4 (T = Si or Al)....	15
2.2 Brønsted acid sites of zeolite.....	16
2.3 The generation of Brønsted and Lewis acid sites in zeolite.....	17
2.4 Diagram depicting three types of selectivity: reactant, product and transition-state shape selectivity.....	18
2.5 Formation of zeolite crystal nuclei in a hydrous gel.....	19
2.6 Structure of ZSM-5 a) The MFI framework topology b) 10-ring viewed along [010] (Straight channel) and c) 10-ring viewed along [100] Zigzag Channel.....	22
2.7 Schematic representations of various types of interaction of surfactant head group with inorganic species: electrostatic in MCM-41 (a) $I^+ X^- S^+$ and FSM-16 (b) $S^+ I^-$, hydrogen bonding in HMS (c) $S^0 I^0$ and SBA-15 (d) $I^+ X^- H^+ S^0$	25
2.8 Schematic representation of the $S^0 I^0$ templating mechanism of formation of HMS.....	27
2.9 The diffraction of X-ray from the parallel crystal planes with interplanar spacing d	29
2.10 Adsorption-desorption isotherms according to the IUPAC classification.....	31
2.11 Hysteresis loops according to the IUPAC classification.....	31
2.12 Cracking mechanisms illustrated by the reaction of <i>n</i> -heptene; adsorption at a Brønsted acid site leads to formation of an adsorbed carbenium ion that can be cracked. Both the β -scission mechanism and the protonated cyclopropane mechanism are shown.....	39
2.13 Monomolecular cracking mechanisms with ZSM-5.....	41

2.14 Bimolecular cracking mechanism of zeolite Y in addition to the monomolecular mechanism.....	42
3.1 Apparatus for synthesis of ZSM-5.....	52
4.1 XRD patterns of as-synthesized of ZSM-5 B1.....	59
4.2 XRD patterns of calcined of ZSM-5: (A) ZSM-5 B1 and (B) mixed ZSM-5.....	60
4.3 N ₂ adsorption-desorption isotherms of mixed ZSM-5 (Si/Al = 40) catalyst.....	62
4.4 ²⁷ Al-MAS-NMR spectrum of mixed calcined ZSM-5 catalyst (Si/Al = 40).....	63
4.5 NH ₃ -TPD profiles of mixed ZSM-5 catalyst Si/Al ratio in gel of 40.....	64
4.6 SEM images of mixed ZSM-5: (A) 1500x and (B) 8000x.....	64
4.7 XRD patterns of as-synthesized of Al-HMS with various Si/Al ratios in gel: (a) Al-HMS 20 (Si/Al = 20), (b) Al-HMS 60 (Si/Al = 60), and (c) Al-HMS 200 (Si/Al = 200).....	65
4.8 XRD patterns of calcined of Al-HMS with different Si/Al ratios in gel: (a) Al-HMS 20 (Si/Al = 20), (b) Al-HMS 60 (Si/Al = 60), and (c) Al-HMS 200 (Si/Al = 200).....	66
4.9 N ₂ adsorption-desorption isotherms and pore size distribution of Al-HMS with various Si/Al ratios in gel of (A) Al-HMS 20 (Si/Al = 20), (B) Al-HMS 60 (Si/Al = 60) and (C) Al-HMS 200 (Si/Al = 200).....	68
4.10 NH ₃ -TPD profiles of Al-HMS with various Si/Al ratios in gel: (A) Al-HMS 20 (Si/Al = 20), (B) Al-HMS 60 (Si/Al = 60), and (C) Al-HMS 200 (Si/Al = 200).....	69
4.9 ²⁷ Al-MAS-NMR spectra of calcined Sample Al-HMS with different Si/Al ratios in gel.....	70
4.12 SEM images of calcined Al-HMS with different Si/Al ratios in gel: (A) Al-HMS 20 (Si/Al = 20), (B) Al-HMS 60 (Si/Al = 60), and (C) Al-HMS 200 (Si/Al = 200).....	71
4.13 XRD patterns of catalysts: (A) Al-HMS-60, (B) ZSM-5, and (C) ZSM-5/Al-HMS-60 (1:1) composite catalyst.....	72
4.14 N ₂ adsorption-desorption isotherms of ZSM-5/Al-HMS-60 ratio 1:1 composite catalyst compared with the pure of ZSM-5 and Al-HMS-60 catalyst: (A) ZSM-5, (B) ZSM-5/Al-HMS-60 (1:1) composite catalyst and (C) Al-HMS-60.....	73
4.15 Accumulative liquid volume of liquid fractions obtained from thermal and catalytic cracking of HDPE over ZSM-5/Al-HMS-60 (1:1) composite catalysts at various reaction temperatures.....	75

4.16 Gas product distributions from catalytic cracking of HDPE over ZSM-5/Al-HMS-60 (1:1) composite catalysts at various reaction temperatures.....	76
4.17 Gas product distributions from thermal cracking of HDPE at various reaction temperatures.....	76
4.18 Carbon distribution numbers of distillate oils from thermal and catalytic cracking of HDPE over ZSM-5/Al-HMS-60 (1:1) composite catalysts at 400°C and 450°C.....	77
4.19 Accumulative volume of liquid fractions obtained by catalytic cracking of HDPE over ZSM-5/Al-HMS-60 (1:1) composite catalysts with various catalytic to plastic ratios.....	79
4.20 Distribution of gas fraction obtained by thermal cracking and catalytic cracking of HDPE over ZSM-5/Al-HMS-60 (1:1) composite catalysts with various catalytic to plastic ratios.....	79
4.21 Carbon number distribution of distillate oils from catalytic cracking of HDPE over ZSM-5/Al-HMS-60 (1:1) composite catalysts with various catalytic to plastic ratios.....	80
4.22 Accumulative volume of liquid fractions obtained by catalytic cracking of HDPE over ZSM-5/Al-HMS-60 composite catalysts with various ZSM-5:Al-HMS ratios in composite catalyst.....	82
4.23 Distribution of gas fraction obtained by catalytic cracking of HDPE over ZSM-5/Al-HMS-60 composite catalysts with various ZSM-5:Al-HMS ratios in composite catalyst.....	83
4.24 Carbon number distribution of distillate oils from catalytic cracking of HDPE over ZSM-5/Al-HMS-60 composite catalysts with various ZSM-5:Al-HMS ratios in composite catalyst.....	84
4.25 Accumulative volume of liquid fractions obtained by catalytic cracking of HDPE over ZSM-5/Al-HMS composite catalysts with various aluminium contents in Al-HMS.....	85
4.26 Distribution of gas fraction obtained by catalytic cracking of HDPE over ZSM-5/Al-HMS composite catalysts with various aluminium contents in Al-HMS.....	86

4.27 Carbon number distribution of distillate oils from the commercial SUPELCO standard gasoline fraction and catalytic cracking of HDPE over ZSM-5/Al-HMS composite catalysts with various aluminium contents in Al-HMS	87
4.28 Accumulative volume of liquid fractions obtained by thermal and catalytic cracking of PP over ZSM-5/Al-HMS-60 (1:1) composite catalysts at 350°C, 400°C and 450°C.....	89
4.29 Distribution of gas fraction obtained by thermal and catalytic cracking of PP over ZSM-5/Al-HMS-60 (1:1) composite catalysts at 350°C, 400°C and 450°C.....	90
4.30 Carbon number distribution of distillate oils from thermal and catalytic cracking PP over ZSM-5/Al-HMS-60 (1:1) composite catalysts at 350°C, 400°C and 450°C	91
4.31 Accumulative volume of liquid fractions obtained by thermal cracking and catalytic cracking of PP over ZSM-5/Al-HMS-60 composite catalysts with various catalytic to plastic ratios.....	93
4.32 Distribution of gas fraction obtained by thermal cracking and catalytic cracking of PP over ZSM-5/Al-HMS-60 (1:1) composite catalysts with various catalytic to plastic ratios	93
4.33 Carbon number distribution of distillate oils from the thermal cracking and catalytic cracking of PP over ZSM-5/Al-HMS-60 composite catalysts with various catalytic to plastic ratios.....	94
4.34 Accumulative volume of liquid fractions obtained by catalytic cracking of PP over ZSM-5/Al-HMS-60 composite catalysts with various ZSM-5:Al-HMS ratios in composite catalyst.....	96
4.35 Distribution of gas fraction obtained by catalytic cracking of PP over ZSM-5/Al-HMS-60 composite catalysts with various ZSM-5:Al-HMS ratios in composite catalyst.....	97
4.36 Carbon number distribution of distillate oils from catalytic cracking of PP over ZSM-5/Al-HMS-60 composite catalysts with various ZSM-5:Al-HMS ratios in composite catalyst.....	97
4.37 Accumulative volume of liquid fractions obtained by catalytic cracking of PP over ZSM-5/Al-HMS composite catalysts with various aluminium contents in Al-HMS.....	99

4.38 Distribution of gas fraction obtained by catalytic cracking of PP over ZSM-5/Al-HMS composite catalysts with various aluminium contents in Al-HMS	100
4.39 Carbon number distribution of distillate oils from the commercial SUPELCO standard gasoline fraction and catalytic cracking of PP over ZSM-5/Al-HMS composite catalysts with various aluminium contents in Al-HMS	100
4.40 XRD patterns of the fresh and the regenerated ZSM-5/Al-HMS-60 (1:1) composite catalyst.	101
4.41 Adsorption isotherms of fresh and regenerated regenerated ZSM-5/Al-HMS-60 (1:1) composite catalyst from N ₂ adsorption measurement.	102
4.42 Accumulative volume of liquid fraction obtained by catalytic cracking of HDPE using the fresh and the regenerated ZSM-5/Al-HMS-60 (1:1) composite catalysts	104
4.43 Distribution of gas fraction obtained by catalytic cracking of HDPE using the fresh and the regenerated ZSM-5/Al-HMS-60 (1:1) composite catalysts	105
4.44 Carbon number distributions of distillate oils obtained by the commercial SUPELCO standard gasoline fraction and catalytic cracking of HDPE using the fresh and the regenerated ZSM-5/Al-HMS-60 (1:1) composite catalysts	105
4.45 Accumulative volume of liquid fraction obtained by catalytic cracking of PP using the fresh and the regenerated ZSM-5/Al-HMS-60 (1:1) composite catalysts	107
4.46 Distribution of gas fraction obtained by catalytic cracking of PP using the fresh and the regenerated ZSM-5/Al-HMS-60 (1:1) composite catalysts	108
4.47 Carbon number distributions of liquid fraction obtained by the commercial SUPELCO standard gasoline fraction and catalytic cracking of PP using the fresh and the regenerated ZSM-5/Al-HMS-60 (1:1) composite catalysts	108

LIST OF SCHEMES

Scheme	Page
3.1 The GC heating program for gas analysis.....	49
3.2 The GC heating program for liquid analysis.....	49
3.3 Preparation diagram for Al-HMS support.....	51
3.4 Preparation diagram for ZSM-5.....	53
3.5 A heating program for organic template removal.....	54
3.6 Ion exchange diagram for catalysts.....	54
3.7 Catalytic cracking apparatus.....	56
3.8 Catalytic cracking Scheme for HDPE and PP.....	57



สถาบันวิทยบริการ
จุฬาลงกรณ์มหาวิทยาลัย

LIST OF ABBREVIATIONS

TPABr	Tetrapropyl ammonium bromide
TEOS	Tetraethyl orthosilicate
Ludox	Colloidal silica
HDA	Hexadecylamine
AIP	Aluminum isopropoxide
BET	Brunauer- Emmett-Teller
BJH	Barret, Joyner, and Halenda
XRD	X-ray Diffraction
SEM	Scanning Electron Microscopy
TPD	Temperature-Programmed Desorption
GC	Gas Chromatography
ICP-AES	Inductively Coupled plasma-Atomic Emission Spectrometer
MAS-NMR	Magic-angle-spinning-nuclear magnetic resonance
PP	Polypropylene
HDPE	High density polyethylene
PE	Polyethylene
PS	Polystyrene
°C	degree Celsius
g	gram (s)
h	hour (s)
mg	milligram (s)
min	minute (s)
ppm	part per million or mg/l
M	molar
%	percent

CHAPTER I

INTRODUCTION

Waste disposal is a serious problem even if the amount of waste per person stays constant over the years. Changing in life style have aggravated the situation.

Municipal waste is thing collected and treated by municipalities. Only part of it comes from households, the rest is caused by small businesses, commercial, and other municipal activities. As shown in Figure 1.1, a trend of municipal waste is rising and growing faster than the population. And, continues to increase for the next decades.

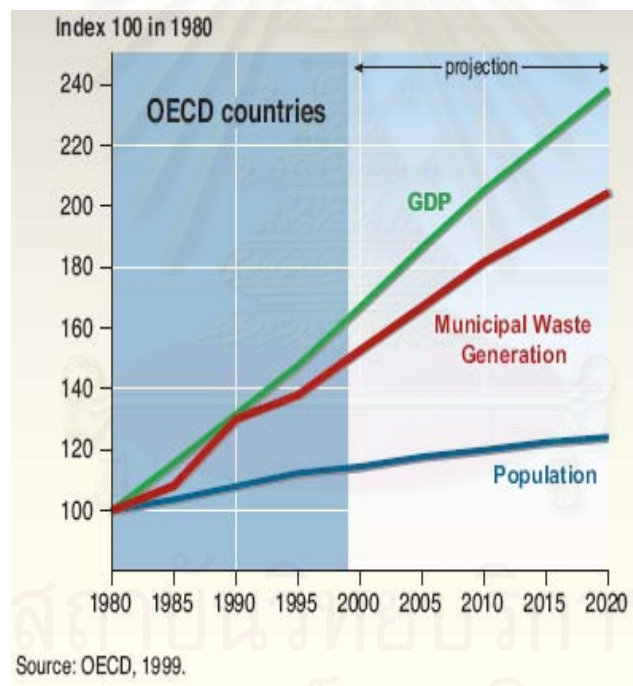


Figure 1.1 Typical trend of increasing municipal waste [1].

The amount and composition of municipal waste depend on many factors, e.g. levels of urbanization, energy choices, waste management strategies, and habits of consumers. Although garbage bins represent only a small part of the total waste generated, it is important that everyone should take an action. We can reduce waste by recycling and avoiding the purchase of over-packaged goods. In many countries,

organic materials and paper are the majority of municipal waste. Large cities tend to generate more wastes. In addition, type of energy source used for cooking, heating and seasonal differences also play a part in the composition of waste. For example in rural communities like in Mongolia there is a large difference between the volume of wood ash produced in summer and winter.

1.1 Plastic

Plastic is used in many aspects of people's lives, such as beverage containers, household items, and furniture. The widespread use of plastics becomes a larger part of the municipal solid waste (MSW) stream in recent decades.

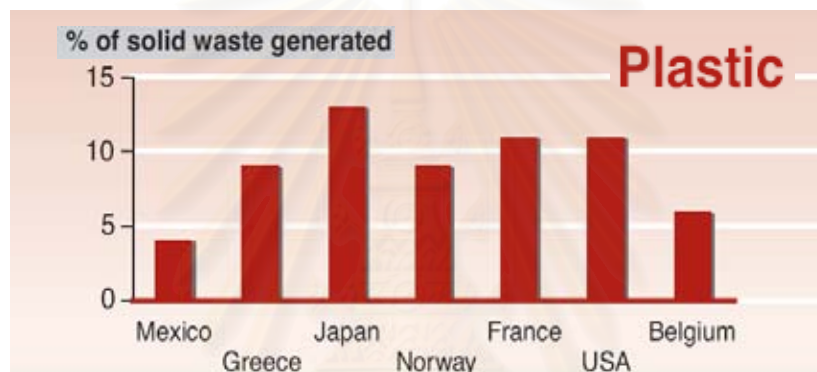


Figure 1.2 Plastic compositions in municipal solid waste [1].

Plastics are polymers, long-chain carbon-based or *organic* molecules. These chains contain fundamental molecular repeating units called *monomers*. The term “plastics” covers synthetic or semi-synthetic organic condensation or polymerization products that can be molded or extruded into objects, films or filaments. The name is derived from the properties in a semi-liquid state that is malleable and plasticity. Plastics vary in temperature tolerance, hardness, and resiliency. The general uniformity of composition and lightness of plastics ensures their use in industrial applications today.

Plastics can be divided into two major categories: thermosets and thermoplastics. A thermoset is a polymer that solidifies or "sets" irreversibly when heated. They are useful for their durability and strength. Thus, they are used primarily in automobiles and construction applications. Other uses are adhesives, inks, and coatings.

A thermoplastic is a polymer in which the molecules are held together by weak bonds, creating plastics that soften when exposed to heat and return to original condition at room temperature. Thermoplastics can easily be shaped and molded into products such as milk jugs, floor coverings, credit cards, and carpet fibers. Thus, it can be easily recycled.

There are many different kinds of plastics, with hundreds of different varieties. All types of plastic are recyclable. To make sorting and recycling easier, the American Society of Plastics Industry developed a standard marking code to help consumers identify and sort the main types of plastic. Their most common codes are presented in Figure 1.3.

Industry polymer identification coding system



Figure 1.3 Industrial polymer identification coding system.

1.2 Polyolefin

Polyolefin is a collective description for plastics, which includes low density polyethylene (LDPE), linear low density polyethylene (LLDPE), high density polyethylene (HDPE) and polypropylene (PP). The commercial success of polyolefin is due to a combination of their flexibility, strength, lightness, stability, impermeability and easy sterilization. This combination makes polyolefins ideally suited for a variety of applications such as food and drink packagings, medical end-uses, domestic appliances, agricultural films, industrial pip, electrical cables and vehicle parts. Besides, polyolefin have some environmental benefits, which are responsive to a range of recovery and recycling solutions, and provide for both energy and material savings due to their process and production efficiency.

Municipal and industrial plastic wastes are treated predominantly in three ways, by landfill, incineration and recycling. Plastics are recycled for both economic and environmental reasons. Recycling of plastics has our obvious benefit of decreasing the amount of used plastics that end up in landfilling and incineration. With increased plastics recycling, fewer natural resources need to be extracted to produce virgin plastic.

Polymer recycling methods can be grouped as follows:

- (1) Mechanical reprocessing of used plastics to form new products. This method has found very limited application it is not generally applicable because of the low quality of the new products and the need for pure waste plastic streams.
- (2) Thermal and/or catalytic degradation of plastic waste to gas and liquid products, which can be utilized as fuels or chemicals. These methods seem to be the most promising to be developed into a cost-effective commercial polymer recycling process to solve the acute environmental problem of plastic waste disposal.[7-9]

Figure 1.4 shows the global consumption of plastics in 2006. Polyethylene (PE) and polypropylene (PP) account for about 62 wt % of total plastics household wastes, and in contrast with other thermoplastics such as polystyrene (PS) or polyethylene terephthalate (PET).

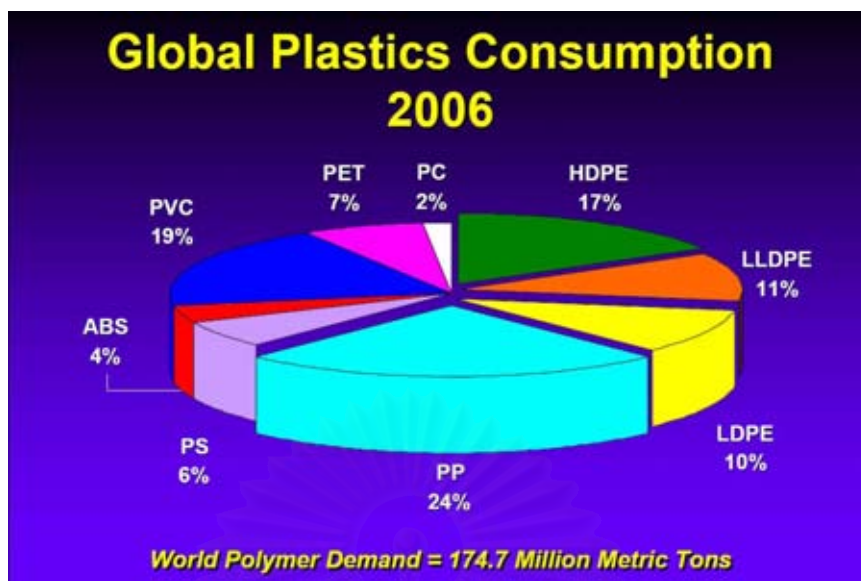


Figure 1.4 Global plastics consumption 2006 [2].

Pure thermal degradation demands relatively high temperatures and its products required further processing for their quality to be upgraded.[10-13]

An interesting alternative is the use of solid-acid catalysts to promote the catalytic degradation of plastic waste. It occurs at lower temperatures and leads to hydrocarbon mixtures with higher commercial value than thermal degradation.[10,14]

1.3 Literature Review

V. J. Fernandes, Jr. *et al.*[17] reported that thermal degradation of HDPE without catalyst gave rise to products distributed over a wide range of carbon atom numbers (C_5 - C_{26}), the main fraction was C_{10} - C_{15} (60.2%). The catalytic reaction led to lighter products (C_5 - C_{26}), predominantly in C_5 - C_9 (73.5%). This behavior was due to the strong acid sites of the ZSM-5 zeolite, which promoted the polymer chains cracking.

D. P. Serrano *et al.*[18] studied the catalytic degradation of polymer over Al-MCM-41, ZSM-5 and silica-alumina catalysts at about 400°C. It was found that amorphous silica-alumina was less active catalyst. The poor activity was probably originated by weak acidity, low surface area and a wide distribution of pore radius present in this material. The authors suggested that these problems overcome by using zeolitic materials as catalysts for the catalytic degradation process, since they had advantages in terms of pore sites distribution and acid strength.

G. Manos *et al.* [19] explored the catalytic cracking of HDPE over ultrastable Y, Y, β zeolites, mordenite, and ZSM-5 at 360°C. The structure of the zeolite framework had a significant influence on the product distribution. Over large-pore USY, Y and β zeolites, alkanes were the main products with less alkanes and aromatics and very small amounts of cycloalkanes and cycloalkanes. For medium-pore mordenite and ZSM-5, alkenes were the major products. The hydrocarbons formed with medium-pore were lighter than those formed with large-pore zeolites. A similar order was found regarding the bond saturation:

(more alkenes) ZSM-5 < mordenite < β < Y < USY (more alkanes)

M. Makkee *et al.*[20] reported the cracking of a straight-run FCC gasoline using ZSM-5 catalyst or FCC base catalyst, Zeolite Y. The components of gasoline that were converted by FCC base catalyst or ZSM-5 were mainly C7⁺ *n*-olefins and *i*-olefins. The ZSM-5 catalyst produced light olefins (LPG-range and some ethene) through cracking of the gasoline-range olefins. The FCC base catalyst not only produced LPG-range olefins by cracking, but also some *i*-paraffins (mainly *i*-butane) and heavier products. All results could be explained by the existence of shape selectivity in the catalysts shown in Fig 1.5. The small pore size of ZSM-5 restricted the entry of large hydrocarbons and promoted a higher interaction with the reaction intermediates. Therefore, the conversion of C7⁺ *n*-olefins and the production of ethene were higher with ZSM-5 than with the base catalyst.

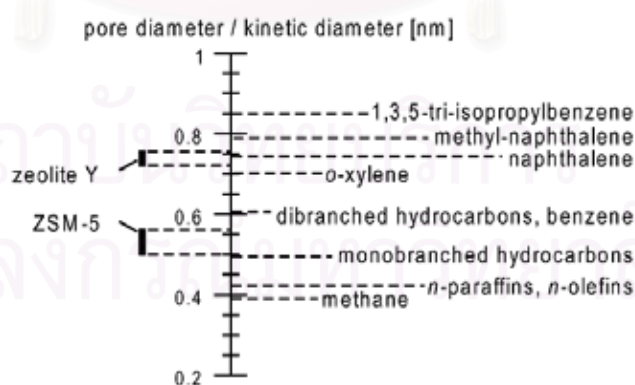


Figure 1.5 Comparison of pore sizes of zeolite Y and ZSM-5 with the kinetic diameters of some hydrocarbon molecules ([20]).

Y. Sakata *et al.* [21] reported catalytic cracking of PE and PP using FSM, silica-alumina, ZSM-5, silicalite, and silica-gel as catalyst by batch operation at

430°C and 380°C. Compared with thermal degradation, FSM catalyst accelerated the initial rate of degradation, increased the liquid product yield and promoted degradation into lower molecular weight products. Silicalite and silica-gel had very negligible effects on polymer degradation. When the batch reaction was repeated four times using FSM catalyst, the extent of the decline in the degradation rate was lower for PE than PP. Compared with the silica-alumina and ZSM-5, which turned completely black in the case of both PE and PP, the deposition of coke on the used FSM catalyst was extremely light. This catalytic effect of FSM for polyolefinic polymer degradation was related to the hexagonal pore structure system of FSM.

D.P. Serrano *et al.* [22] explored the catalytic cracking of PS over HMCM-41, HZSM-5, and amorphous SiO₂-Al₂O₃ at 375°C. The highest catalytic activities were obtained over HMCM-41 (~35%), and thermal cracking (~36%), whereas the conversions of other materials were roughly half of one obtained from the thermal cracking (18.0 and 18.6%, respectively). This fact was explained by the existence of competitive cross-linking reaction promoted by the acid catalysts. The higher the acid strength of the catalyst, the larger the extension of the cross-linking process, HZSM-5 zeolite has high acidity exhibited low cracking activity. These competitive reactions were clearly distinguished by the product distribution. Styrene was the main product in both thermal and catalytic cracking over the HZSM-5 zeolite, whereas silica-alumina and HMCM-41 mainly produced benzene and ethyl benzene.

J. Aguado *et al.*[23] investigated the catalytic cracking of LDPE, HDPE, and PP using Al-MCM-41, ZSM-5, and amorphous silica-alumina as catalysts. The catalytic degradation of both HDPE and LDPE was investigated at 400°C in a batch reactor for 30 min. The cracking activity was observed in the following order; ZSM-5 > Al-MCM-41 > silica-alumina. For HDPE and LDPE, the highest cracking activity was observed over ZSM-5 with conversions close to 100%, which suggested that major factor influencing polyethylene cracking is acidity rather than pore size of catalysts. On the contrary, the catalytic cracking of PP over Al-MCM-41 led to almost 100% conversion whereas the activity obtained over zeolite ZSM-5 was close to that of thermal cracking (11.3%). It was due to steric and/or diffusion hindrances of bulky molecules accessing the pore size of catalyst. With Al-MCM-41 and the amorphous silica alumina the conversion of PP was faster than the case of HDPE and LDPE. It was related to a high proportion of tertiary carbons. The presence of the side-chain

methyl groups increased and effective cross section of the PP molecules, compared to the PE chains, prevented their access to the active sites located within the zeolite pores.

D.P. Serrano *et al.* [24] studied the catalytic cracking of polyolefin mixture consisting of 46.5 wt% LDPE, 25 wt% HDPE and 28.5 wt% PP at 400 °C over a variety of acid solids as catalysts. The activity order was as follows:

n-HZSM-5 > H beta > HMCM-41 >> SiO₂-Al₂O₃ > HZSM-5 > HY > thermal degradation

The cracking activity was related to their properties and the nature of the polyolefin mixture. HMCM-41 gave a high conversion because of its large pore size, promoting the access of polymer molecules to acid sites. In the case of n-HZSM-5 and H beta, the presence of high external surface area enhanced their cracking activities. The differences in product distribution were significantly observed. n-HZSM-5 gave the highest selectivity toward C₁₋₄(50 wt %), H beta produced mainly liquid hydrocarbon C₅₋₁₂(60 wt %), whereas HMCM-41 yielded both C₅₋₁₂(54 wt %) and C₁₃₋₃₀(32 wt %) fractions.

A number of acid, porous solids, such as amorphous silica–alumina, zeolites and ordered mesoporous materials, have been used as catalysts for polyolefin cracking. Mesoporous Al-MCM-41 materials yielded hydrocarbons within gasoline and gasoil fractions, whereas ZSM-5 zeolite produced light products with a great number of gaseous and aromatic hydrocarbons. These results have been interpreted in terms of the cracking mechanism.[25] Polyolefin cracking over Al-MCM-41 proceeds by a random scission mechanism due to its large pore size and mild acidity. In contrast, HZSM-5 zeolite leads to an end-chain cracking pathway, which has been assigned to its strong acidity and small pore size. In order to overcome the limitations of single micro- or mesoporous materials and to combine the advantages of these two types of molecular sieves, a new type of materials containing both types porosity is expected to offer attractive features. Up to now, only a few articles concerning this study have been published.[26-31] For example, Kloetstra *et al.*[26] prepared zeolite faujasite overgrown with a thin layer of mesoporous MCM-41, by successive synthesis of FAU and MCM-41 or by adding FAU crystals to MCM-41 synthesis gel. The composite MCM-41/FAU they made has shown good results in cracking of vacuum gasoil. The same observation was also reported by Guo *et al.* [32] in *n*-heptane cracking using composite MCM-41/Beta.

R.A. Garcí'a *et al.*[33] described the catalytic degradation of HDPE over the composite ZSM-5/Al-MCM-41 compared with the behavior of standard Al-MCM-41 and HZSM-5 samples. The samples so obtained have exhibited remarkable catalytic activity in the HDPE cracking despite the low temperatures (380 °C) and catalyst loadings used (plastic/catalyst mass ratio = 100), leading to polyolefin conversions higher than both Al-MCM-41 and HZSM-5. No conversion was detected in Al-MCM-41, showing that the acidity of this catalyst is not strong enough to promote the HDPE cracking at this temperature. Likewise, a low plastic conversion (5%) was obtained over the pure HZSM-5 catalyst, which can be related to the hindered accessibility of the plastic molecules to the zeolite acid sites. In contrast, both hybrids the composite ZSM-5/Al-MCM-41 materials exhibited significant activity for the HDPE cracking showing a conversion close to 68%. Light hydrocarbons with a narrow product distribution and rich in olefins are the main components obtained over the hybrid and HZSM-5 catalysts, while the production of heavy fractions is negligible.

From these literature reviews, composite material ZSM-5/Al-MCM-41 showed remarkable performance relative to conventional catalyst for catalytic cracking of polyolefin. Despite the catalytic activity, the importance in this reaction involved the narrow product distribution and rich in olefins.

But R. Mokaya *et al.*[34] reported that the mesoporous materials (designated Al-HMS) have physical and textural properties similar to those previously reported for MCM-41 mesoporous materials but exhibit thicker framework walls, significantly higher Brønsted acidity and are consequently more active for the cracking of cumene.

Moreover, Bhatia *et al.*[35] reported that Beta/MCM-41 physical composite showed a higher conversion in the cracking of waste palm oil for the production of liquid hydrocarbons compared to the chemical composite.

Therefore, this work intends to synthesize composite ZSM-5/Al-HMS catalyst by physical mixture method for catalytic cracking of HDPE and PP which is important goal for environmental nowadays.

1.4 Objectives

1. To synthesize and characterize composite material ZSM-5/Al-HMS and develop with various Si/Al molar ratios of Al-HMS.

2. To study the effect of reaction temperature, polymer to catalyst ratio, ratio of ZSM-5 per Al-HMS, and Si/Al ratio of Al-HMS in catalytic cracking of HDPE and PP over ZSM-5/Al-HMS composite.
3. To study on the optimum conditions for cracking of HDPE and PP over fresh compare regenerated catalyst.



สถาบันวิทยบริการ
จุฬาลงกรณ์มหาวิทยาลัย

CHAPTER II

THEORY

2.1 Catalysis

Catalyst technology has played a key role in economic development of countries around the world during the 20th century. The production of chemicals and fuels contributes worldwide over 10 trillion dollars per year.[36] The success of the chemical industries (such as chemicals, polymers, drugs, dyes and fabrics) is based purely on catalyst technology.

Catalyst technology, in principle, was in vogue for centuries on a small scale to produce foodstuff, wines and beverages. It was in the early part of the nineteenth century, that Berzelius first discovered the catalysis phenomenon. Since then, the field of catalysis has been an intriguing and continuing area of development to understand and utilize it for practical purposes. The discovery of new catalysts and their applications has historically led to major innovations in chemical processing. Some of the major catalytic processes developed during the last 50 years are given in Table 2.1.

The beginning of catalyst technology in the modern sense was the large-scale production of sulfuric acid on platinum catalyst in 1875, which was followed by the production of nitric acid and the synthesis of ammonia. The Fischer-Tropsch technology, which was developed later, made the efficient utilization of CO for production of hydrocarbons, liquid fuels and other chemicals. With the discovery of Ziegler-Natta catalyst in 1955, the polymer industry came into its own. Then another significant processes, such as catalytic cracking of petroleum feedstock catalysts, to boost up the gasoline yield, the naphtha reforming and the hydrotreating process.

Table 2.1 The development of important industrial catalytic process in last 50 years.

Year	Process	Catalyst	Area of industry
1950	Mono-metallic reforming	Pt-Al ₂ O ₃	Petroleum
1955	Polymerization	TiCl ₃ / Al(R) ₃	Chemicals
1960	Wacker process	PdCl ₂	Chemicals
1962	Steam reforming	Ni-K- Al ₂ O ₃	Petroleum
1964	Cracking on zeolites	X, Y zeolites	Petroleum
1967	Multi-metallic reforming	Pt-Re, Pt-Ir-Cu	Petroleum
1974	Carbonylation	Rh-I	Chemicals
1976	Auto emissions control	Pt, Pd or Rh/Al ₂ O ₃	Auto-emission control
1980	Selective catalytic reduction	VO _x -TiO ₂ , Zeolites	Environmental control
1988	Selective oxidation	Ti- Silicalite	Chemicals
1988	Chiral catalysts	Cinchonidine-Pt; BINAP	Chemicals
1991	Polymerization	Metallocenes	Chemicals
1980-95	Shape selective reactions	ZSM-5, New zeolites	Chemicals
1980-2000	Organic Chemicals	Various heterogeneous catalysts	Chemicals

Together with homogeneous catalyst; solid acid catalysts were developed and applicable in hydrogenation, disproportionation, carbonylation, oxidation, polymerization and many other processes.

Alumino-silicate, zeolites, was found useful in detergents due to their ion exchange capacity, in catalysis due to their acid-base properties and in adsorption and separation processes due to their molecular sieving properties. The increasing assemblage of different zeolite catalysts along with multiplicity of new reactions were explored in many industrial applications. The new zeolite based catalytic processes are making efficient use of energy and raw materials with minimal impact on the environment. Such catalysts are contributing to solve the environmental problems

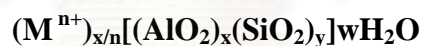
such as removal of hydrocarbons, carbon monoxide and nitrogen oxides from waste and exhaust gases.

2.2 Zeolites

A molecular sieve is a material that has selective adsorption properties and can separate components of a mixture by differentiating in molecular size and shape.[37] Molecular sieves include clays, porous glasses, microporous charcoals, active carbons, etc, but one of the most powerful of molecular sieves are zeolites.

Zeolites are crystalline aluminosilicates with fully cross-linked open framework structures made up of corner-sharing SiO_4 and AlO_4 tetrahedra, named primary structural units. The name "zeolite" comes from the Greek words zeo (to boil) and lithos (stone); and was used for the first time in 1756 by the Swedish mineralogist Cronstedt.[38]

In inorganic chemistry, aluminosilicates are materials composed of Si^{4+} and Al^{3+} . They are formed when some of the Si^{4+} in silicates is replaced by Al^{3+} . For each Si^{4+} ion replaced by an Al^{3+} , the charge is balanced by other positive ions such as Na^+ , K^+ or Ca^{2+} ions. The structural formula of a zeolite is based on the crystallographic unit cell, represented by:



Where M represents the exchangeable cation of valence n and M is generally a Group I or II cation, although other metal, non-metal and organic cations can also balance the negative charge created by the presence of Al in the structure. The Si/Al ratio of the zeolite is indicated by y/x, and w represents the water contained inside the discrete size cages and/or channels of zeolites. In addition to Si^{4+} and Al^{3+} , other elements can also be present in the zeolitic framework. They do not need to be isoelectronic with Si^{4+} or Al^{3+} , but must be able to occupy framework sites.

Zeolites can be divided into natural zeolites like Chabazite, Faujasite or Mordenite, and synthetic zeolites like zeolite A, X and Y or ZSM-5. Natural zeolites have the advantage of their low economic cost while the second group, although they are more expensive, avoid the problem of impurities and changes in chemical composition, and thus enable their properties to be controlled better.

2.2.1 Zeolite Structures

The structure of zeolites is based on an extensive three-dimensional framework in which the tetrahedral sites are linked by oxygen atoms. The result is a uniform microporous structure, which can be formed of channels and/or cavities.

In the zeolite structure, primary individual structural units are assembled into secondary building units called SBU's (Figure 2.1), by means of which the topology of all known molecular sieve framework types can be described.[39] The final framework structure consists of assemblages of secondary units in space, the union of which gives rise to bigger pentasil (a) or sodalitic (b) like-structural units (Figure 2.1). The expansion of these units in the three space directions generates the different zeolitic structures. Therefore, zeolites can be classified according to the framework symmetry as ZSM, FAU, MFI, etc, following the rules described by the International Zeolite Association (IZA).

One of the fundamental characteristics of zeolites is the Si/Al ratio, because several properties such as thermal stability, acidity, and hydrophobic/hydrophilic character are related to it. According to the so-called Loewenstein rule,[40] Al-O-Al linkages in zeolitic frameworks are forbidden. As a result, all aluminate tetrahedra must be linked to four silicate tetrahedra, but a silicate tetrahedron may have five different possible environments: Si(0Al,4Si), Si(1Al,3Si), Si(2Al,2Si), Si(3Al,1Si) and Si(4Al,0Si).

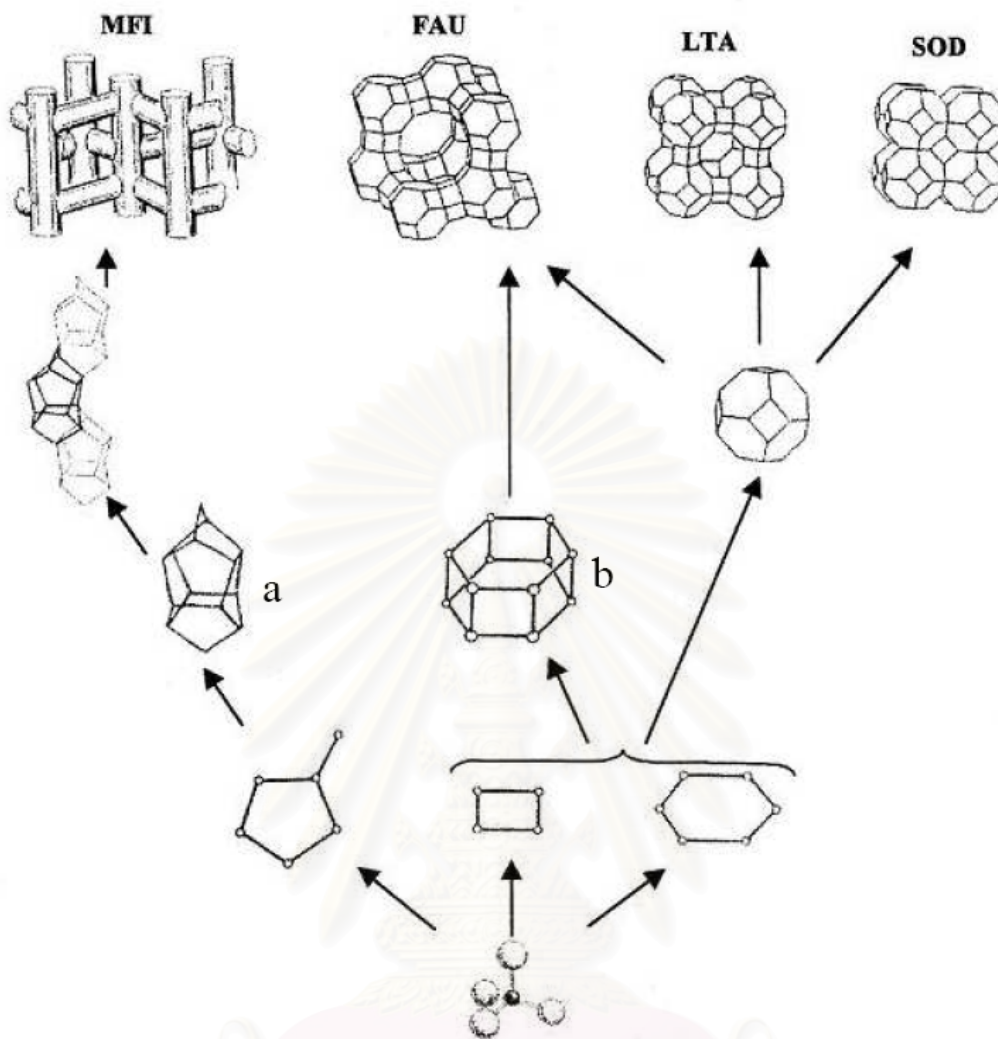


Figure 2.1 Structural genetics of zeolitic materials based tetrahedra TO_4 .
(T = Si or Al).

2.2.2 Acid Sites of Zeolites

If a zeolite structure contains only SiO_4 tetrahedra, it would be electrically neutral and no acidity would be developed on its surface. In fact, Brønsted acid sites are developed when Si^{4+} is isomorphically substituted by a trivalent metal cation, for instance Al^{3+} , and a negative charge is created in the lattice, which is compensated by a proton. The proton is attached to the bridged oxygen atom connected between nearby silicon and aluminum atoms, resulting in the bridged hydroxyl group which is responsible for the Brønsted acid sites of zeolites as shown in Figure 2.2.

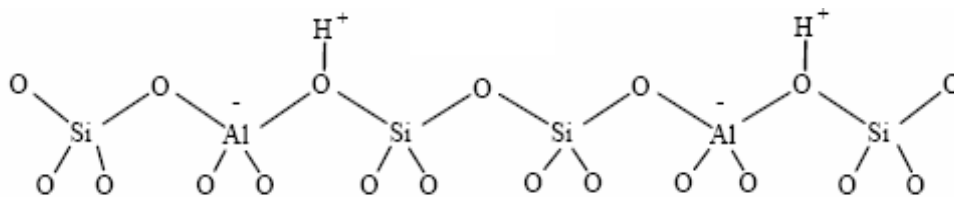


Figure 2.2 Brønsted acid sites of zeolite.

The reactivity of molecular sieve zeolites is determined by active sites provided by an imbalance in charge between silicon and aluminum ions in the framework. Each aluminum atom contained within the framework structure induces a potential active acid site. Classical Brønsted and Lewis- acid models of acidity have been used to classify the acid sites on zeolites. Brønsted acid is a proton-donor and Lewis acid is an electron acceptor. The presence of both types of acid sites in zeolites is shown in Figure 2.3.

Hydrothermal syntheses of silica-rich zeolites generally consist of water as the solvent, a silicon source, an aluminum source, and a structure-directing agent. Better understanding of the effect of the structure-directing agent has long been aimed at. This will entail better control of the resulting structures, and even prediction of the specific structure could be possible. The correlation between the structure-directing agent and the structure of zeolites with high silica content are summarized as follow:

1. Hydrothermal silicate syntheses result in dense crystalline and layered materials when no structure-directing agent is present.
2. Linear structure-directing agents usually result in one-dimensional molecular sieves with 10-ring channels.
3. Branched structure-directing agents tend to form multi-dimensional zeolites with pore diameters of 4-7 Å.
4. One-dimensional, large pore zeolites often result from large polycyclic structure-directing agents.

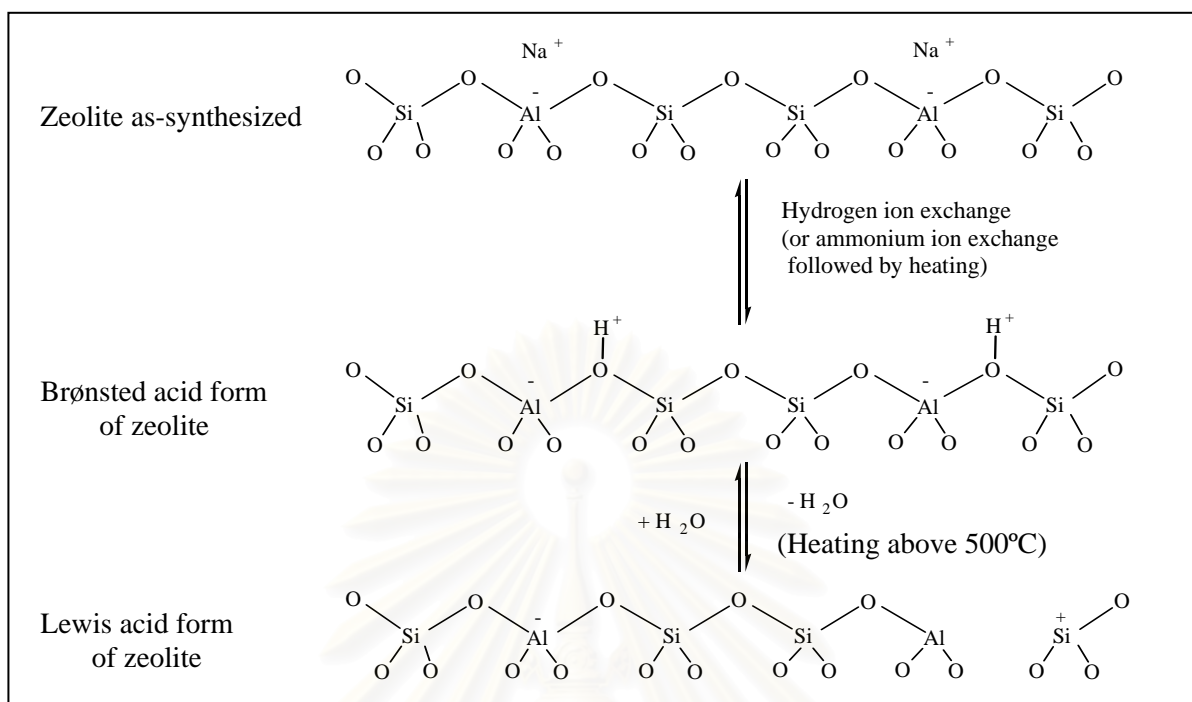


Figure 2.3 The generation of Brønsted and Lewis acid sites in zeolite. [41]

2.2.3 Shape Selectivity

The combination of high internal surface area, acid sites, selective sorption and molecular sieve properties makes zeolites the most useful among versatile heterogeneous catalysts. High internal surface area and acidity give rise to high activity, while selective sorption and molecular sieve properties result in high reaction selectivity. The reaction selectivity can be diffusionaly controlled (reactant or product selectivity) or geometrically controlled (transition state selectivity). The models for types of selectivity is shown in Figure 2.4

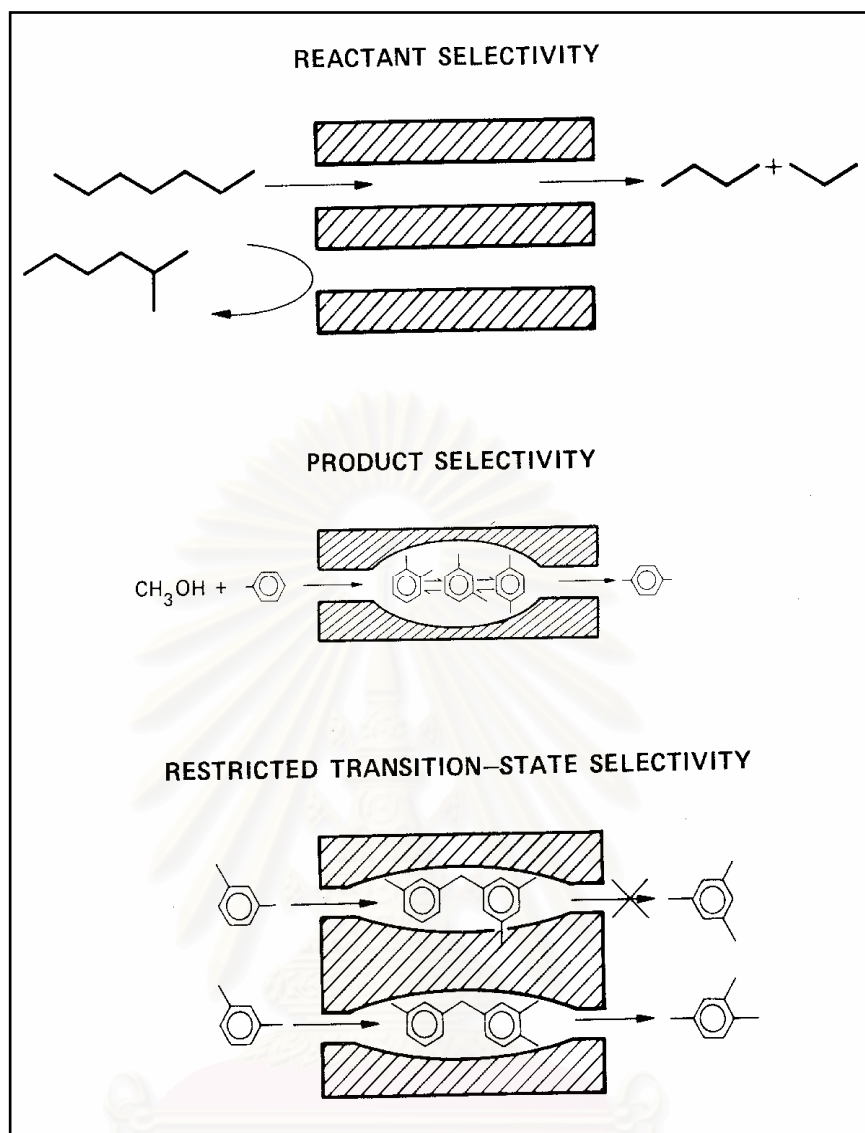


Figure 2.4 Diagram depicting three types of selectivity: reactant, product and transition-state shape selectivity.[42]

Reactant selectivity[41] is observed when only a fraction of the reactant with proper size and shape has access to the active sites, while product selectivity occurs when only some product species with proper dimensions (or shape) can diffuse out of the zeolite channel. Restricted transition-state selectivity will take place when certain reactions will be prevented due to steric and space restrictions.

Molecules with high diffusability will react preferentially and selectively, while molecules which are excluded from the channel will only react on the external surface of zeolite. Products with high diffusivity will be preferentially desorbed

while the bulkier molecules will be converted and equilibrated to smaller molecules, which will diffuse out. The larger (partially dehydrogenated) molecules block the pores and lead to deactivation of catalysts by carbonaceous residues or coke.

2.2.4 Factors Influencing Zeolite Formation

Three variables having major influence on crystallization of zeolite structure are the gross composition of the reaction mixture, temperature, and time.[43] There are also history-dependent factors such as digestion or aging period, stirring, nature (either physical or chemical) of the reaction mixture, and order of mixing.

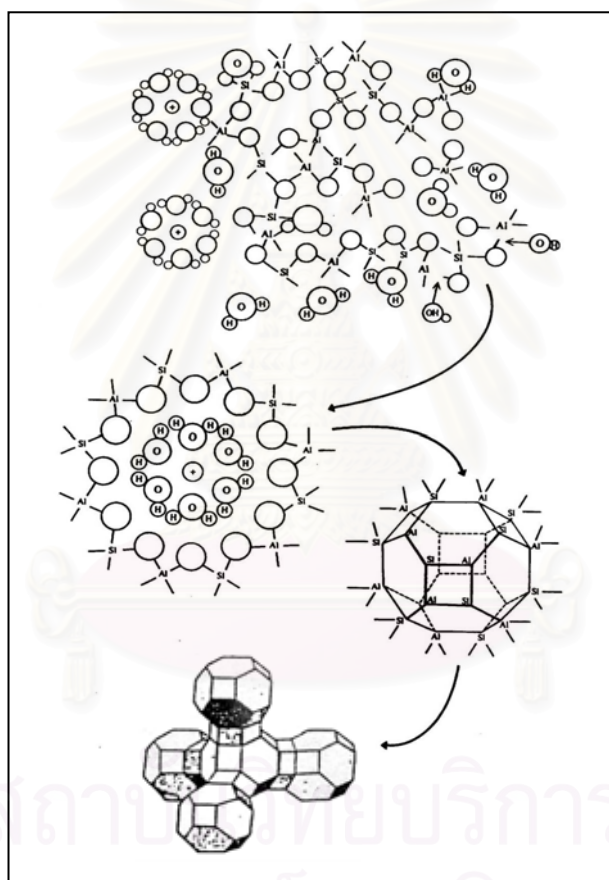


Figure 2.5 Formation of zeolite crystal nuclei in a hydrous gel. [44]

Table 2.2 Factors influencing zeolite crystallization. [43]

<ul style="list-style-type: none"> ▪ Gross composition - $\text{SiO}_2/\text{Al}_2\text{O}_3$ - Cations <ul style="list-style-type: none"> (a) Inorganic (b) Organic 	<ul style="list-style-type: none"> - $[\text{OH}^-]$ - Anions (other than $[\text{OH}^-]$) - $[\text{H}_2\text{O}]$
--	---

- **Time**
 - **Temperature**
 1. Ambient - ca. 25 to 60°C (natural zeolite formation)
 2. Low - ca. 90 to 120°C
 3. Moderate - ca. 120 to 200°C
 4. High - ca 250°C or higher
 - **History-dependent factors**
 1. Aging
 2. Stirring
 3. Nature of mixture
 4. Order of mixing
-

2.2.4.1 Reaction Mixture Components

Each component in the mixture contributes to the characteristics of gel and final materials obtained. Table 2.3 provides information of individual components on zeolite synthesis.

Table 2.3 Selected variables of gross composition on the final crystalline product in zeolite synthesis. [43]

Variables	Primary influence
$\text{SiO}_2/\text{Al}_2\text{O}_3$	Framework composition
$\text{H}_2\text{O}/\text{SiO}_2$	Rate, crystallization mechanism
OH^-/SiO_2	Silicate molecular weight, OH^- concentration
Inorganic cation(s)/ SiO_2	Structure, cation distribution
Organic additives/ SiO_2	Structure, framework aluminum content

The $\text{SiO}_2/\text{Al}_2\text{O}_3$ mole ratio, the hydroxide content, and the presence of inorganic cations in the gel composition are mainly contributed to final crystal structure besides the organic additives as a crystal-directing agent or template.[43] Thus, the crystallization of a particular zeolite structure contains these four components as the starting gel mixture.

2.2.4.2 Temperature

Temperature [43] can alter the zeolite phase obtained as well as the change in inductive period before starting crystallization. For any mixture as the temperature increases, the rate of crystallization increases. The solubilities of aluminate and silicate species also increase, causing a change in the concentration of liquid phase. Loosen zeolites prefer crystallization at low temperature while denser zeolites do at high temperature.

2.2.4.3 Time

Time, [43] can be optimized in the synthesis process. The complete crystallization over a short span of time is important. Crystallization parameters must be adjusted to minimize the production of the other phase while also minimizing the time needed to obtain the desired crystalline phase.

2.2.5 ZSM-5

ZSM-5, an important type of high silica zeolites. Its building blocks are formed from pentasil units linked through edges to form chains and these chains are connected to form corrugated sheets. These sheets are linked in three-dimensional framework. Unlike others, t zeolites have pores of uniform dimension and have no large super cages.

ZSM-5 consists of two intersecting channels formed by rings of 10-oxygen atoms as Figure 2.6 [45-47]. These two channels have slightly different pore dimensions. One runs parallel to the a-axis of the unit cell, which is sinusoidal and nearly of circular dimension (5.4 x 5.6 Å). The other runs parallel to the b-axis and has a straight body but elliptical opening with dimensions of 5.1 x 5.5 Å. These channels intersect and form a three dimensional 10 ring channel system. As the pore opening of ZSM-5 is different compared to large pore zeolites (FAU and Beta), a shape selectivity, a sorption capacity and a catalytic activities are distinctly different. The less deactivating characteristic of ZSM-5 is one of the important factors useful in industrial applications.

STRUCTURE OF ZSM-5 (MFI)

Chemical Composition	$\text{Na}_n[\text{Al}_n\text{Si}_{96-n}\text{O}_{192}] \sim 16 \text{ H}_2\text{O}$
Symmetry	Orthorhombic
Unit cell constants	$a = 20.1, b = 19.9$ and $c = 13.4 \text{ \AA}$
Space Group	$Pnma$
Pore Structure	10 membered ring structure ; $5.1 \times 5.5 \text{ \AA}$ [100] $5.6 \times 5.3 \text{ \AA}$ [010]

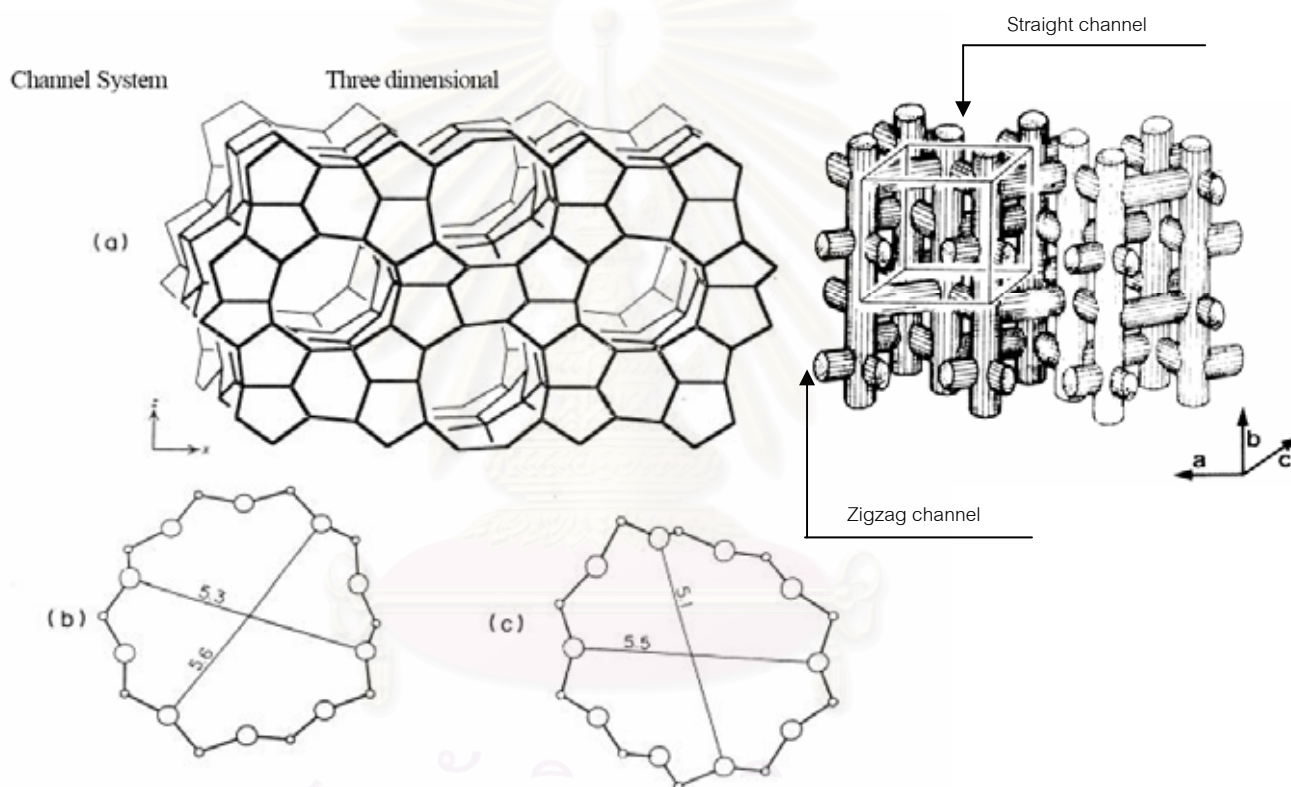


Figure 2.6 Structure of ZSM-5 a) The MFI framework topology b) 10-ring viewed along [010] (Straight channel) and c) 10-ring viewed along [100] Zigzag Channel.

2.3 Mesoporous Materials

Two classes of materials that are used extensively as heterogeneous catalysts and adsorption media are microporous and mesoporous materials. Well-known members of the microporous class are zeolites. Although zeolites exhibit excellent

catalytic properties, their applications are limited by the relatively small pore openings, which constraint pore-size ($<15 \text{ \AA}$) of microporous zeolites. Until 1992, Mobil corporation researchers [48] discovered a new family of mesoporous silicate molecular sieves called M41S. These mesoporous silicate materials have well-defined pore sizes of 15-100 \AA . The extremely high surface areas of greater than $1,000 \text{ m}^2/\text{g}$ and the ability to precisely tune the pore sizes are among the many desirable properties that have made such materials the focus of great interest. The M41S family is classified into several members. The most useful one is MCM-41 with hexagonal structure. Since the synthesis of M41S was reported, there is a considerable development to search for new mesoporous materials and to investigate their properties. Many families of mesoporous materials [48-53] with hexagonal structure were discovered, such as HMS [50, 53] (Hexagonal Mesoporous Silica), FSM-16 (Folded Sheets Mesoporous Materials)[49] and SBA-15 with straight hexagonal structure.[51] Because different types of templates can be used for synthesizing hexagonal mesoporous materials at various pH of gel, the new hexagonal materials can be obtained.[54] The interaction of various types of template with organic or inorganic species for assembling these materials are different as summarized in Table 2.4, together with the condition typically employed for a synthesis.

Table 2.4 Various synthesis conditions of hexagonal mesoporous materials and the type of interaction between template and inorganic species

Material	Template	Assembly	Media (pH)
MCM-41	Quaternary ammonium salt	Electrostatic	Basic or Acid
FSM-16	Quaternary ammonium salt	Electrostatic	Basic (pH = 8.5)
SBA-15	Amphiphilic triblock copolymer	Hydrogen bonding	Acidic (pH = 1-2)
HMS	Primary amine	Hydrogen bonding	Neutral

MCM-41 and FSM-16 can be synthesized using quaternary ammonium salt as a template. In case of SBA-15, amphiphilic triblock copolymer can be modified as a template and must be synthesized in acid condition of hydrochloric acid. On the other hand, HMS can be prepared in neutral and environmentally benign condition using primary amine as a template. Although these materials have the same hexagonal structure, some properties are different as shown in Table 2.5.

Table 2.5 Properties of some hexagonal mesoporous materials [48, 53, 55-57]

Material	Pore size (Å)	Wall thickness (nm)	BET specific surface area (m ² /g)	Framework structure
MCM-41	15-100	1	>1000	Honey comb
FSM-16	15-32	-	680-1000	Folded sheet
SBA-15	46-300	3-6	630-1000	Rope-like
HMS	29-41	1-2	640-1000	Wormhole

2.3.1 Mechanism of Mesostructure Formation

A number of models have been proposed to explain the formation of mesoporous materials and to provide a rational basis for the various synthesis routes. [54] On the most common level, these models are predicted upon the presence of surfactants in a solution to direct the formation of the inorganic mesostructure from the solubilized inorganic precursors. The type of interaction between the surfactant and the inorganic species is significantly different depending on the various synthesis routes as shown in Figure 2.7.

In case of MCM-41 and FSM-16, the interaction between template and inorganic species is electrostatic interaction while hydrogen bonding interaction occurs in HMS and SBA-15 synthesis.[58] The pore diameter of these materials are controlled by alkyl chain length of surfactant. Mechanisms of mesoporous formation are different depending on synthesis route for each material.

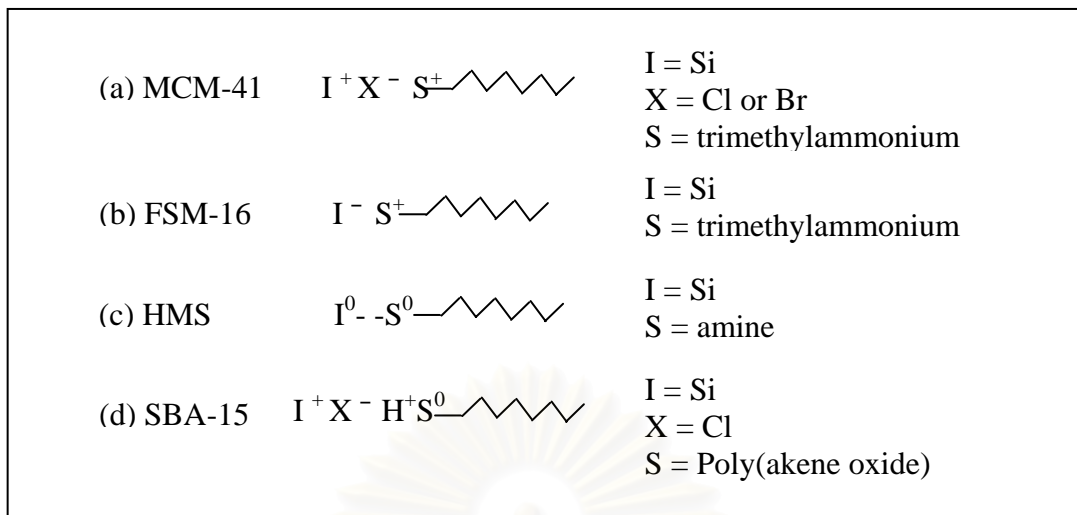


Figure 2.7 Schematic representations of various types of interaction of surfactant head group with inorganic species: electrostatic in MCM-41 (a) $I^+ X^- S^+$ and FSM-16 (b) $S^+ I^-$, hydrogen bonding in HMS (c) $S^0 I^0$ and SBA-15 (d) $I^+ X^- H^+ S^0$.

2.3.2 Hexagonal Mesoporous Silica (HMS)

HMS was discovered in 1994 by Pinnavia *et al.*[50] This material can be synthesized at room temperature by neutral templating route. In this case, primary amine can be used as a template, alcohol such as ethanol or propanol is used as a cosolvent. [53] Although alcohol behaves as a cosolvent in HMS synthesis, it makes a difference in polarity of mixed solvent, resulting different hydrolysis rate and nucleation rate. Pinnavaia and coworker revealed the different properties of HMS between the water rich system (water : ethanol = 90 : 10 v/v) and ethanol rich system (water : ethanol = 35 : 65 v/v). The textural mesoporosity or porosity arising from intraaggregate void and spaces formed by interparticle contacts of HMS using water rich system was higher. In the ethanol rich system, HMS with low textural porosity was obtained and the particles were composed of macroscale spheroid particles aggregate into the larger particles. On the other hand the water rich system yields mesoscale particles aggregated into larger particles.[59]

The pore size of HMS can be controlled by alkyl chain length between C₈-C₁₈ in primary amine templates[53] and also modified with auxiliary structure modifier such as mesitylene to expansion the pore of HMS.[59] Due to the interaction between template and inorganic species is hydrogen bonding, the organic phase can be totally

removed from as-synthesized samples by solvent extraction, which is not possible in the case of the other pathways where strong electrostatic interactions exist between organic and inorganic phase. The solvent extraction can be prevents the partial degradation of the mesoporous structure that could occur during calcination in air at relatively high temperature. Additionally, the environmentally synthesis condition make many resercher focused on HMS synthesis and its potential application.[52]

Pure silica HMS was limited its application to catalysis, supports or adsorbents. In order to provide HMS with potential catalytic application, it was possible to modify the nature of framework by incorporation of heteroelement. [52]When trivalent metal cations like Al^{3+} , B^{3+} , Ga^{3+} , Fe^{3+} were incorporated to framework of silica, negative charges were occurred that can be balanced with proton. These solid catalysts can be used as acid catalyst or acid support. Acidity adsorption of pyridine results in Al-HMS reported by Tuel *et al*[52] showed that Al-HMS contain both Lewis and Brønsted acid sites. The Brønsted acid sites in Al-HMS are weaker and their strength is approximately the same as that of amorphous silica-alumina. In addition, Mokaya and Jones[34] was found that directly calcined Al-HMS with Si/Al of 5 possessed acid sites very similar in strength to HY zeolite. To be function as support material, Al-HMS was used as a support in cracking, dehydrogenation, hydrodesulfurization[60], selective catalytic reduction of NO with NH_3 [61], Fischer-Tropsch[62], etc. When other cations like Ti^{4+} , V^{4+} , Sn^{4+} , Zr^{4+} substituted for silicon in the framework, the electroneutrally was maintained and the metal-containing can be used as oxidation catalyst.

2.3.2.1 Hydrogen Bonding Interaction

Tanev and Pinnavaia[53] showed that mesoporous silica could be prepared by the hydrogen-bonding interaction of alkylamine (S^0) head group and hydroxylated tetraethylorthosilicate (I^0) as shown in Figure 2.8. The materials lacked long-range order of pore, but had higher amounts of interparticle of mesoporosity because the long-range effects of the electrostatic interaction, controll in packing of micellar rods were absent. This neutral templating synthesis route produced mesoporous silicates with thicker walls and higher thermal stability compared to the LCT-derived silicates. The silicate framework in the resulting mesophase was

neutrally charged. From this reason, the surfactant can be easily removed by solvent extraction.

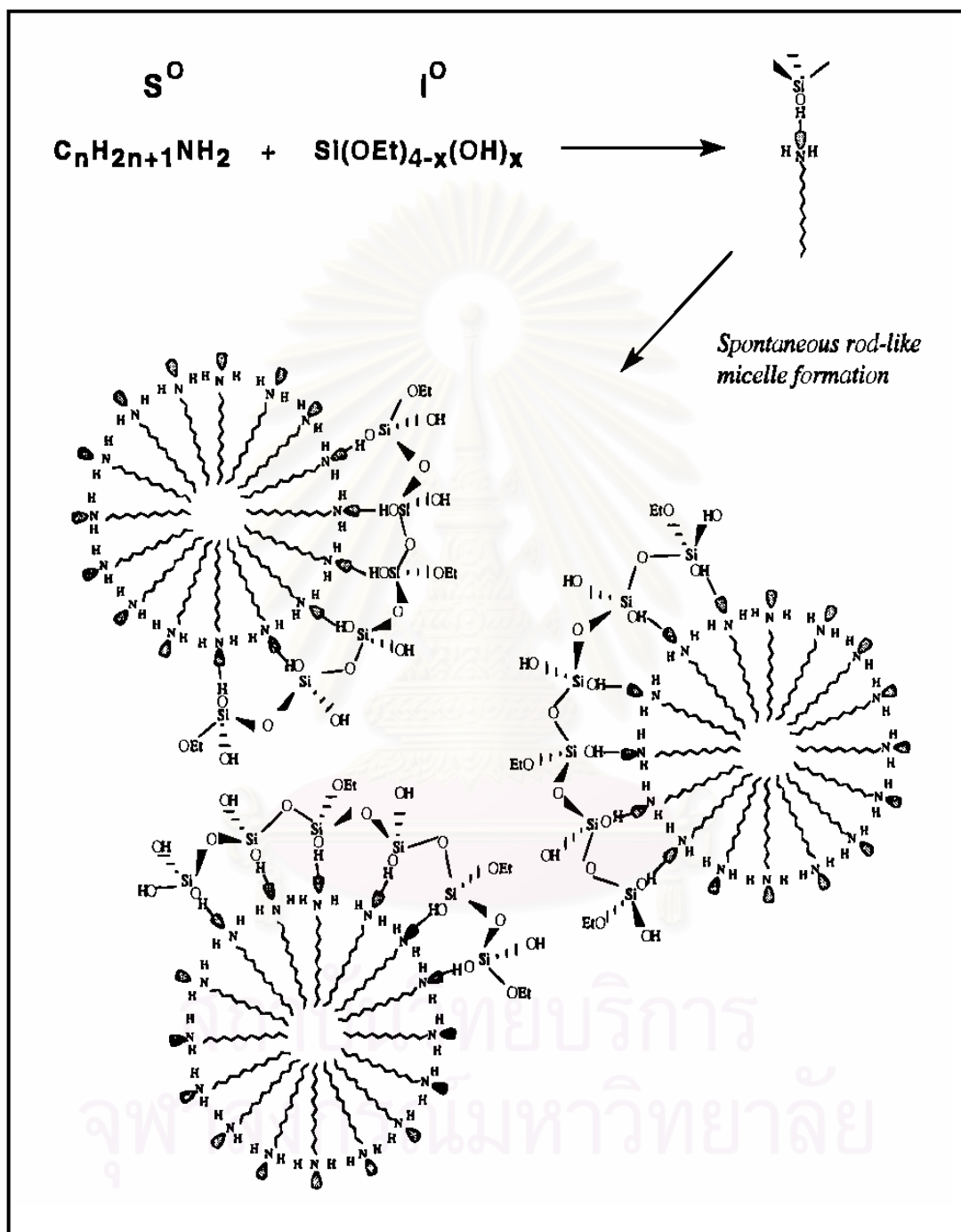


Figure 2. 8 Schematic representation of the S^0I^0 templating mechanism of formation of HMS. [53]

2.4 Composite material

A composite material is composed of at least two elements working together to produce a material whose properties are different from the properties of on their own. In order to overcome the limitations of single element (micro- or mesoporous materials) and to combine the advantages of these two types of molecular sieves, a new type of materials containing both types porosity is expected to offer attractive features. The type of composite can be separated to physical-composite and chemical-composite. Recently, the higher catalytic activity of micro/mesoporous composite materials in comparison to conventional Al-MCM-41 was demonstrated in cumene cracking reaction.[63] The better catalytic behaviour of these composite materials have arisen from zeolite-like connectivity of AlO_4 and SiO_4 tetrahedral in the framework walls, and the high thermal stability of the resulted mesostructures.

For example, Kloetstra *et al.*[26] prepared zeolite faujasite overgrown with a thin layer of mesoporous MCM-41, by adding FAU crystals to MCM-41 synthesis gel. The composite MCM-41/FAU showed good results in cracking of vacuum gasoil. Karlsson *et al.* also prepared composite materials by simultaneous synthesis of MFI/MCM-41 phases using a two-template approach [$\text{C}_6\text{H}_{13}(\text{CH}_3)_3\text{NBr}$ and $\text{C}_{14}\text{H}_{29}(\text{CH}_3)_3\text{NBr}$] at optimized template concentrations and reaction temperatures.[29] Bhatia *et al.*[35] reported that physical composite Beta/MCM-41 showed a higher conversion in the cracking of used palm oil for the production of liquid hydrocarbons compared to the chemical composite.

2.5 Characterization methods

There are several different characterization methods that have been used throughout the work in this thesis, and it would be beyond the scope of this section to provide a theoretical background for all of these methods. In this section, an emphasis has therefore been put the most important of the characterization methods that have been used in the research.

2.5.1 X-ray diffraction (XRD)

XRD is one of the most widely used methods for routine characterization of microporous and mesoporous materials. The method was developed and used in

material science for characterization of crystal structures[64-65] based upon the diffraction of x-rays in crystal lattices.

2.5.1.1 The Bragg equation

Figure 2.9 shows the principle of XRD method, where monochromatic x-rays with wavelength λ are reflected from parallel crystal planes, with an incident angle θ between the beam direction and the planes.

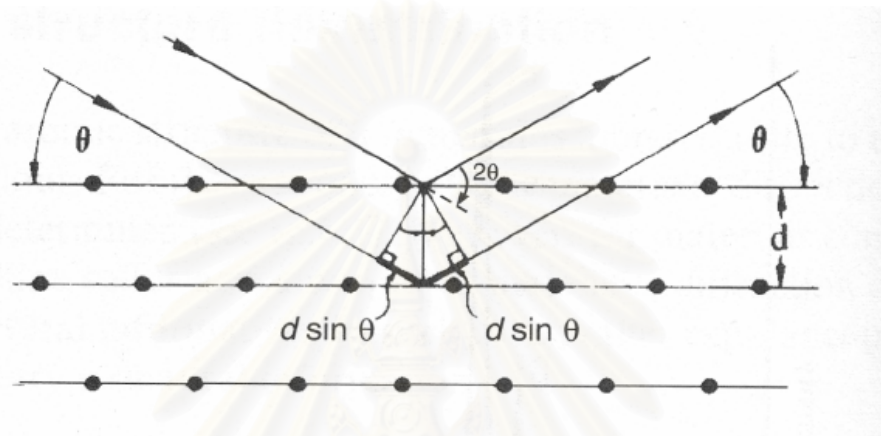


Figure 2.9 The diffraction of X-ray from the parallel crystal planes with interplanar spacing d . [65]

From geometrical considerations (Figure 2.9) it can be shown that x-rays reflected from two adjacent parallel planes will be in the same phase and thus interfere constructively when the following condition is met, which is known as the Bragg equation: [64]

$$n \lambda = 2 d \sin \theta \quad (1)$$

where n is an integer (the reflection order) and d is the interplanar spacing.

The intensity of the diffracted x-ray beam is dependent upon θ and d ; therefore, by measuring the diffraction intensity at different values of 2θ , the interplanar distances in the crystal may be elucidated. Since mesoporous materials have amorphous structure in the pore walls, there are no diffraction peaks due to the ordered crystal structure at high theta value. However, as there is a long-range order in the pore structure, at low 2θ values which corresponds to the d -values in the pore size range.

The “ d ” value is often expressed in terms of “ d_{hkl} ”, where h , k and l are the Miller indices for the crystal planes in three dimensional spaces. The (hkl) values may be expressed as a direction vector that is orthogonal to the plane.[65] The values of h , k and l then correspond to the x , y and z values of the vector, respectively.

2.5.2 N₂-sorption

Adsorption-desorption of molecules on surfaces of solid materials is a common method for characterization of porous materials.[66] Due to its inertness, N₂ is often used as an adsorbate. Much information about porosity of materials can be obtained from the shape of adsorption-desorption isotherms, and the total surface area of the sample can also be calculated.

2.5.2.1 Isotherms and hysteresis loops

IUPAC has classified the different shapes of isotherms into six types, and the different types of hysteresis loops into four categories, as seen in Figures 2.10 and 2.11, respectively.[66] Type I isotherm is typical for microporous materials such as zeolites, where the steep slope of the curve at low partial pressures indicates a high surface area. Type II isotherm is typical for aggregated powders with no ordered pore-structure such as clays, pigments and cements. This isotherm type is often seen with a H3 hysteresis loop. Type III and Type V isotherms are very rare, but may be seen in water/graphite systems. Type IV isotherms are typical materials containing mesopores. The distinctive form of Type VI isotherms is a stepwise layer-by-layer adsorption process, usually by non-polar molecules such as argon, krypton or xenon on uniform surfaces.

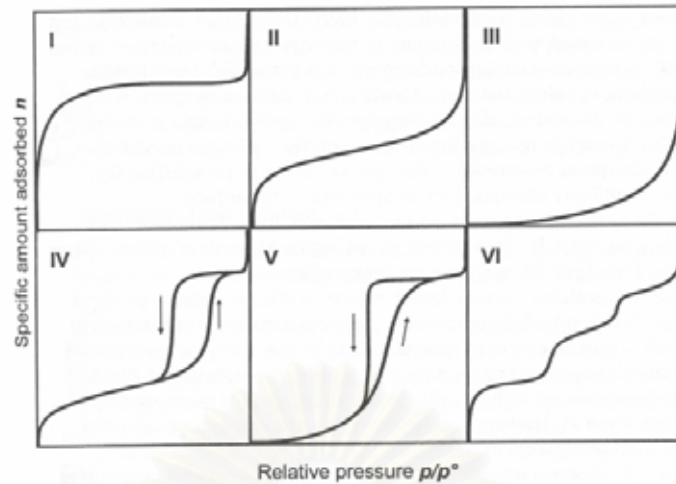


Figure 2.10 Adsorption-desorption isotherms according to the IUPAC classification.

Type H1 hysteresis loop is typical for adsorbents with well-defined structures and narrow pore size distributions, while the H2 loop is typical for materials with complex structures containing interconnected networks of pores with different size and shape. Type H3 loop is usually given by aggregates of plate-like particles or adsorbents containing slit-shaped pores. The H4 loop is also given by materials with slit-shaped pores, when the pore size distribution is in the micropore range.[66]

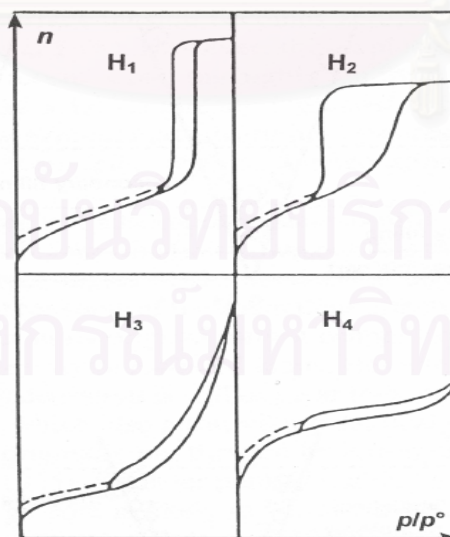


Figure 2.11 Hysteresis loops according to the IUPAC classification.

In case of ordered mesoporous materials, adsorption-desorption isotherm of Type IV is usually observed with a steep slope of the curve at intermediate partial pressures due to the filling of the mesopores. The slope of the curve at lower pressures is due to the monolayer adsorption at high internal surface area, and the plateau above the steep slope is due to the adsorption at external surface. Materials such as MCM-41 and MCM-48 usually have isotherms containing no hysteresis loop, called type IVa due to the very narrow pore size distribution in these materials. On the other hand, SBA-15 has a slightly broader pore size distribution which gives a H3 hysteresis loop in the isotherm. This isotherm shape is then called Type IVc.[66]

2.5.2.2 The BET equation

The specific surface area of porous materials may be estimated from the theory by Brunauer, Emmett and Teller, (BET) which may be expressed by the BET equation:[66]

$$\frac{p/p^0}{n(1-p/p^0)} = \frac{1}{n_m C} + \frac{C-1}{n_m C} (p/p^0) \quad (1)$$

where p/p^0 is the relative pressure, n is the amount adsorbed, n_m is the monolayer capacity, i.e. the maximum amount adsorbed, and C is a constant.

The plot of $(p/p^0)/[n(1-p/p^0)]$ versus p/p^0 gives a straight line with a slope, $s = (C-1)/n_m C$.

The specific surface area, $a(BET)$, may then be calculated from the relation:

$$a(BET) = n_m N_a \sigma \quad (2)$$

where N_a is Avagadro's constant and σ is the average area occupied by one molecule.

2.5.3 Scanning electron microscopy (SEM) [67]

Scanning electron microscopy is a powerful technique employed by diverse scientific disciplines, including chemistry, materials science, biology, and geology. By focusing a beam of electrons into a tight spot on the surface of a sample, this

produces secondary electrons, Auger electrons, backscattered electrons, and or even X-Rays from the sample. These signals are then collected to generate an image of the sample. The resultant image can be obtained with as much as a 25 Angstrom (2.5 nm) resolution. This resolution is two orders of magnitude greater than optical microscopy, which is limited by the wavelengths of visible light. These signals, in conjunction with specialized detectors can also collect information about elemental composition and crystallinity at various points within that image.

2.5.4 Solid state ^{27}Al -NMR [68]

The impact of solid-state NMR as a powerful tool for studies of micro- and mesoporous molecular sieves has been dramatic during recent years. Tremendous progress has been made, aiming towards enhanced resolution, sensitivity and improved multinuclear capabilities. Solid-state NMR is nowadays a well established technique for characterization of zeolites and related materials with respect to structure elucidation, catalytic behavior and mobility properties. Solid state ^{27}Al -NMR spectroscopy is another important characterization technique for microporous and mesoporous materials to distinguish between tetrahedrally and octahedrally coordinated aluminum in the framework at approximately 50 and 0 ppm, respectively. Hence, the amount of framework aluminum can be determined.

2.5.5 Temperature-programmed desorption of ammonia (TPD) [69]

Ammonia TPD is a method to measure the acidic property of solid. On widely various solid acid catalysts, it was clarified that the desorption was controlled by the equilibrium between the gaseous and adsorbed ammonia under usually utilized experimental conditions. A theoretical analysis method - Curve-Fitting Method - was proposed based on the theory expressing the desorption process. On the other hand, the introduction of water vapor after the adsorption of ammonia selectively removed the unnecessary ammonia species hydrogen-bonded and that adsorbed on Lewis acid site which had been generated on basic oxide surface, and the ammonia or ammonium cation adsorbed on simply acidic site was preferentially detected -- Water Vapor Treatment Method --. By these new methods, one can precisely determine the number of acid sites, the acid strength and its distribution on almost all of the solid samples. The amount of ammonia desorbing above some characteristic temperature is taken as

the acid-site concentration, and the peak desorption temperatures have been used to calculate heats of adsorption.

The acidity of Al-MCM41 samples has been measured by adsorption-desorption of ammonia. The amount of Brønsted acidity increases with the aluminum content of the sample. When the acidity of Al-MCM41 was compared with that of zeolite and an amorphous silica-alumina, it was found that the acid strength of the MCM-41 is weaker than in the zeolite and appears more similar to that of an amorphous silica-alumina.

2.5.6 Inductively coupled plasma atomic emission spectroscopy (ICP-AES) [70]

Being a powerful tool for elemental analysis, inductively coupled plasma atomic emission spectroscopy (ICP-AES) plays an important role in the purity analysis of rare earth elements (REEs) owing to its high performance, such as: low detection limits ($< 0.0x \mu\text{g ml}^{-1}$), good precision, wide linear dynamic range, simple sample treatment, *etc.* As shown in many papers, ICP-AES has the potential to determine individual REEs directly without mutual separation, and provided the spectrometer an adequate resolution and dispersion.

ICP-AES has been widely used since the 1970's for the simultaneous multi-element analysis of environmental and biological samples after dissolution. The excellent sensitivity and wide working range for many elements- together with the low level of interferences, make ICP-AES a nearly ideal method so long as sample throughput is high enough to justify the initial capital outlay. Laser sampling, in conjunction with ICP is a way to avoid dissolution procedures of solid samples prior to the determination of the elements.

ICP-AES has been approved for the determination of metals by the EPA under Method 6010. Method 6010 describes the simultaneous, or sequential, multielemental determination of elements by ICP-AES. This method is approved for a large number of metals and wastes. All matrices, including ground water, aqueous samples, EP extracts, industrial wastes, soils, sludges, sediments, and other solid wastes, require digestion prior to analysis. The following table lists the elements for which Method 6010 is applicable. Detection limits, sensitivity, and optimum ranges of the metals will vary with the matrices and model of spectrometer. The data shown in the

following table provide concentration ranges for clean aqueous samples. Use of this method is restricted to spectroscopists who are knowledgeable in the correction of spectral, chemical, and physical interferences.

Table 2.6 Recommended wavelengths and estimated instrumental detection limits.

Element	Wavelength (nm)	Estimated Detection Limit (?g/L)
Aluminum	308.215	45
Antimony	206.833	32
Arsenic	193.696	53
Barium	455.403	2
Beryllium	313.042	0.3
Boron	249.773	5
Cadmium	226.502	4
Calcium	317.933	10
Chromium	267.716	7
Cobalt	228.616	7
Copper	324.754	6
Iron	259.940	7
Lead	220.353	42
Magnesium	279.079	30
Manganese	257.610	2
Molybdenum	202.030	8
Nickel	231.604	15
Potassium	766.491	See note *
Selenium	196.026	75
Silicon	288.158	58
Silver	328.068	7
Sodium	588.995	29
Thallium	190.864	40
Vanadium	292.402	8
Zinc	213.856	2

* Highly dependent on operating conditions and plasma position.

The wavelengths listed are recommended because of their sensitivity and overall acceptance. Other wavelengths may be substituted if they can provide the needed sensitivity and are treated with the same corrective techniques for spectral

interference. In time, other elements may be added as more information becomes available and as required. The estimated instrumental detection limits shown are given as a guide for an instrumental limit. The actual method detection limits are sample dependent and may vary as the sample matrix varies.

2.6 Cracking reaction

Cracking reaction is a petroleum refining process in which heavy-molecular weight hydrocarbons are broken up into light hydrocarbon molecules by the application of heat and pressure, with or without the use of catalysts, to derive a variety of fuel products. Cracking reaction is one of the principal ways in which crude oil is converted into useful fuels such as motor gasoline, jet fuel, and home heating oil.

2.6.1 Thermal cracking[71]

Thermal cracking reaction is a refining process in which heat (~800°C) and pressure (~700kPa) are used to break down, rearrange, or combine hydrocarbon molecules. The first thermal cracking process was developed around 1913. Distillate fuels and heavy oils were heated under pressure in large drums until they cracked into smaller molecules with better antiknock characteristics. However, this method produced large amounts of solid, unwanted coke. This early process has evolved into the following applications of thermal cracking: visbreaking, steam cracking, and coking.

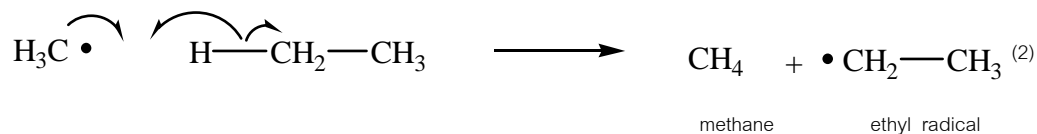
In the cracking of ethane, ethylene and hydrogen are formed at very high temperature. In cracking, the temperatures used are so high that initiating radicals are formed by spontaneous bond rupture. Only two types of bonds in ethane can be broken: the C-C bond and the C-H bonds. The bond dissociation energies of the C-C bond require somewhat less energy. Hence, fragmentation of a few ethane molecules into two methyl radicals takes place.

First initiation step:



In a second initiation step, a methyl radical abstracts a hydrogen atom from another ethane molecule:

Second initiation step:

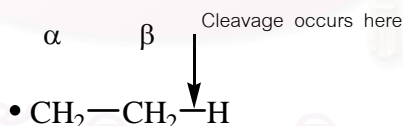


This step accounts for small amounts of methane formed in the cracking process. The ethyl radical is the chain-propagating radical. It first undergoes an interesting reaction in which it “unzips” to yield ethylene and a hydrogen atom in a process called β -scission:

First propagation step:



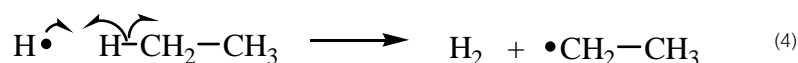
β -scission is another typical reaction of free radicals. The word “scission” means “cleavage” (it is derived from the same root as “scissors”). The Greek letter beta (β) refers to the fact that the cleavage occurs on carbon away from the radical site. (The Greek letters α , alpha; β , beta; γ , gamma; and so on are sometimes used to indicate the relative positions of groups on carbon chains.)



Although β -scission might look like a new reaction, actually it is simply the reverse of an addition; in this case it is the reverse of the addition of a hydrogen atom to ethylene.

The hydrogen atom produced in the first propagation step then abstracts a hydrogen atom from another molecule of ethane to give a new ethyl radical:

Second propagation step:



The ethyl radical enters into the first propagation reaction, equation (3), thus continuing the free-radical chain. The hydrogen that is a by-product of equation (4) is

collected and used to produce ammonia by hydrogenation of nitrogen. The ammonia finds important use in agriculture as a fertilizer.

It can be seen that there are four types of reactions that free radicals can undergo. Three of these are reactions that produce other radicals:

1. Addition to a double bond
2. Atom abstraction
3. β -Scission.

The other reaction destroys free radicals:

4. Recombination of two free radicals to form a covalent bond.

These reactions constitute a “toolbox” of fundamental free-radical process. Most free-radical processes are examples of these reactions or combinations of them. The low-molecular weight alkanes obtained from these cracking processes can be separated and purified, and are the most important raw materials for the large-scale synthesis of aliphatic compounds.[72]

2.6.2 Catalytic cracking[73]

Catalytic cracking breaks complex hydrocarbons into simpler molecules in order to increase the quality and quantity of lighter, more desirable products and decrease the amount of residuals. This process rearranges the molecular structure of hydrocarbon compounds to convert heavy hydrocarbon feedstock into lighter fractions such as kerosene, gasoline, liquified petroleum gas (LPG), heating oil, and petrochemical feedstock.

Catalytic cracking is similar to thermal cracking except that catalysts facilitate the conversion of the heavier molecules into lighter products. Use of a catalyst (a material that assists a chemical reaction but does not take part in it) in the cracking reaction increases the yield of improved-quality products under much less severe operating conditions than in thermal cracking. Typical temperatures are from 850°-950° F at much lower pressures of 10-20 psi. The catalysts used in refinery cracking units are usually solid materials (zeolite, aluminum hydrosilicate, treated bentonite clay, fuller's earth, bauxite, and silica-alumina) that come in the form of powders, beads, pellets or shaped materials called extrudites.

General cracking mechanisms[74]

In general, for components with equal carbon numbers, the rate of cracking decreases in the order: *i*-olefins > *n*-olefins > *i*-paraffins \approx naphthenes > *n*-paraffins > aromatics. The cracking mechanism can be seen as a chain mechanism that involves the intermediate formation of carbocations, positively charged hydrocarbon species.

Carbocations include both carbenium ions (e.g. R1-CH₂-C⁺H-R2, R1-CH=C⁺-R2) and carbonium ions (e.g. R1-CH₂-C⁺H₃-R2, R1-CH=C⁺H₂-R2). In carbenium ions, the charge carrying carbon atom can be di- or tri-coordinated, while in carbonium ions, the charge carrying carbon atom is tetra- or pentacoordinated.

The stability of the carbocations decreases in the order tertiary > secondary > primary [75]. Cracking of hydrocarbons is primary a reaction that proceeds through adsorbed carbenium ion intermediates.

Reactions of olefins

The formation of carbenium ions from olefins can easily proceed by addition of proton from a Brønsted acid site of the catalyst to the carbon-carbon double bond. Cracking of the adsorbed carbenium ion proceeds through the β -scission mechanism[76-77] or through the protonated cyclopropane mechanism[78]. An illustration is given in Fig. 2.12.

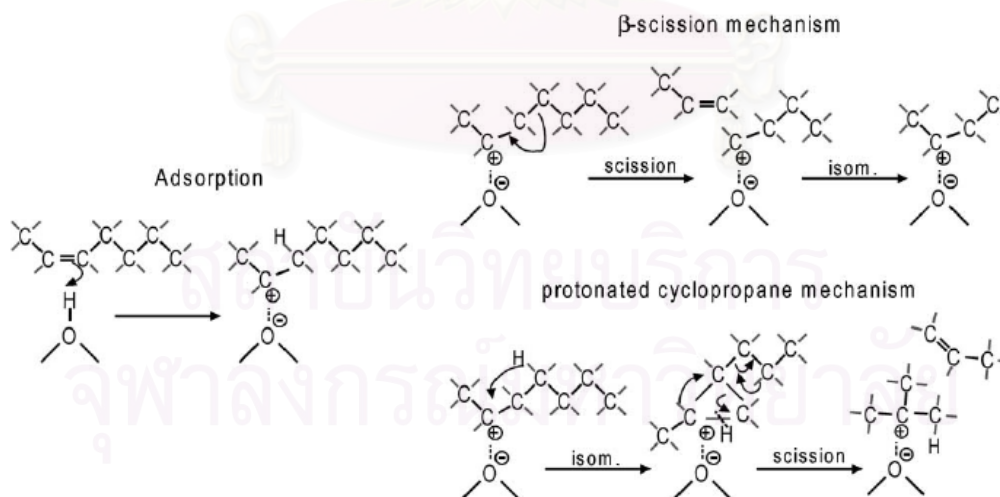
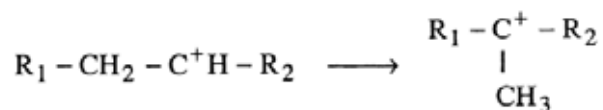


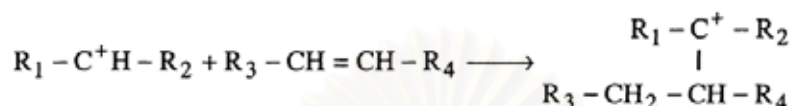
Figure 2.12 Cracking mechanisms illustrated by the reaction of *n*-heptene; adsorption at a Brønsted acid site leads to formation of an adsorbed carbenium ion that can be cracked. Both the β -scission mechanism[76-77] and the protonated cyclopropane mechanism[78] are shown.

Other reactions of the adsorbed carbenium ion are[79-80]:

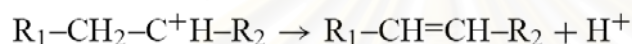
1. Isomerization to a more stable carbenium ion, for example, through a methyl shift:



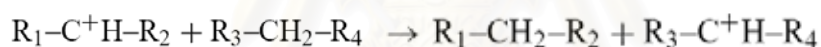
2. Oligomerization with olefin in a bimolecular reaction to form a larger adsorbed carbenium ion:



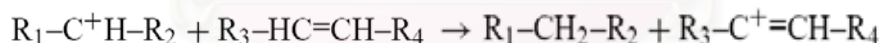
3. Desorption with deprotonation to form an olefin (the opposite of adsorption):



4. Desorption with hydride abstraction from a paraffin to form new paraffin from the carbenium ion and new carbenium ion from the paraffin (H-transfer reaction):



5. Desorption with hydride abstraction from (cyclic) olefins or coke (precursors) to form paraffin and a more aromatic compound (H-transfer reaction):



The bimolecular reactions (2), (4) and (5) can occur if the pore size of the catalyst is large enough to accommodate the reactive intermediates, or they should occur on the outer surface of the zeolite particles. If the pores are too small, as in the case of ZSM-5 (0.53 nm × 0.56 nm), these reactions cannot take place with the larger (gasoline) components, although oligomerization or dimerization of small (C₂–C₄) olefins could be possible. For example, in the mobile olefins to gasoline and distillates process (MOGD) coupling of light hydrocarbons is catalyzed by ZSM-5.

With ZSM-5, cracking through dimeric intermediates has been reported in the reactions of small *n*-olefins (C₄–C₆). Abbot and Wojciechowski[79] have studied cracking of *n*-olefins from C₅ to C₉ at 678K with ZSM-5 and found that cracking of pentene solely took place through a dimeric/disproportionation mechanism[81-82].

Cracking of heptene and larger molecules proceeded mainly through monomolecular cracking and at 678 K; hexene represented the transition case of the two mechanisms and was cracked by both monomolecular cracking and through dimeric intermediates.

With Y-type zeolites, the dimeric mechanism is a more important reaction route; for example, it has been found that cracking of C_7 took place for 25% via a dimeric disproportionation reaction at 746K and for 32% at 673K.

2.6.3. Proposed Cracking Mechanisms of Polymer[83]

Based on the literature cited above, it is to be expected that with ZSM-5, the cracking reactions of larger, C_7^+ , olefins are restricted to simple β -scission reactions; relatively straight chains (or parts of it) can enter the pores, are adsorbed, split-off small olefins, and desorbed. As an example, the reaction of n-heptene with β -scission mechanism over ZSM-5 is shown in Fig.2.13. The adsorbed C_7 -carbenium ion is cracked to propene and produced C_4 -carbenium ion. The latter can desorb as butene or be cracked into two ethene molecules.



Figure 2.13 Monomolecular cracking mechanisms with ZSM-5.

Generally, the second reaction, formation of ethene, is energetically less favorable because it involves the formation of two primary carbenium ions. However, due to the small pores of ZSM-5, the electrical field in the pores is larger and a large interaction between the catalyst and the adsorbed carbenium ions shall exist. It is believed that the oxygen atoms of zeolite structure play a role in solvating carbocations, delocalizing the positive charge into the framework. The smaller the size of the pores of zeolite, the closer the different oxygen atoms are to be adsorbed and the higher the possible interaction. As a result of increasing stabilization of

intermediates, the formation of ethene is enhanced when small pore-zeolites such as ZSM-5 are involved.

For the base catalyst, zeolite Y, as active species (pore size 0.74 nm) the adsorbed C_4 -carbenium species can, in addition to the reactions possible on ZSM-5, relatively easily oligomerize with, e.g. a new heptene molecule to form an adsorbed C_{11} -carbenium ion that can be cracked, e.g. to hexene and adsorbed C_5 -carbenium that can oligomerize with a new olefin, and so on. This bimolecular cracking mechanism is illustrated in Fig. 2.14. Also, the adsorbed heptene carbenium ion could have oligomerized before cracking. The occurrence of a bimolecular cracking mechanism was also proposed by Williams *et al.*[79] to explain the enhanced activity of ultra-stable zeolites Y.

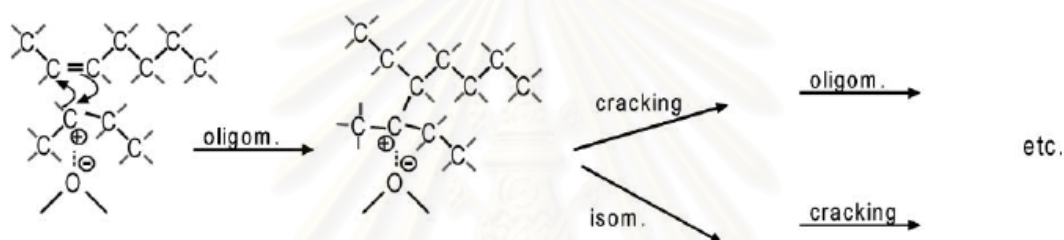


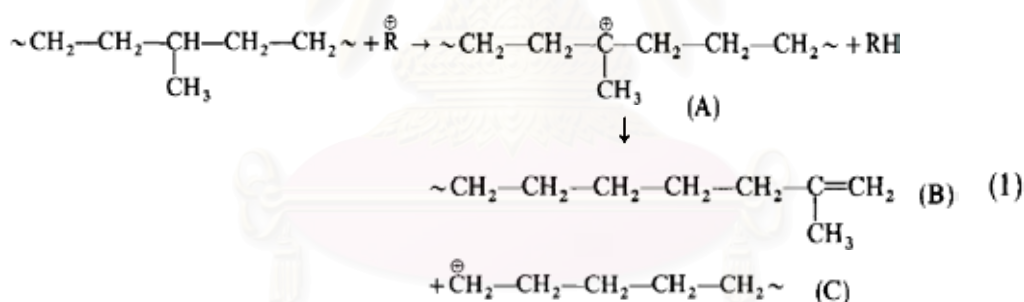
Figure 2.14 Bimolecular cracking mechanism of zeolite Y in addition to the monomolecular mechanism.

Because of the larger adsorption strength of larger hydrocarbons, the bimolecular mechanism have an important contribution in the cracking mechanism of heavier gasoline-range olefins, provided that the catalyst pore size is large enough to accommodate the reaction intermediates. Aromatics and highly branched components, therefore, are too large to react through bimolecular mechanisms. Linear components are the most likely ones to react through this mechanism.

According to this proposed mechanism, the active site of ZSM-5 is the acid site itself, while the active site in zeolite Y can be represented by the adsorbed carbenium ion. The reaction intermediates with ZSM-5 contain the maximum number of carbon atoms in the feedstock (C_5 – C_{11}), while the (surface) intermediates with the base catalyst can be much larger. As a result, the cracking products from ZSM-5 will be mainly C_3 , C_4 , and to some extent also C_2 olefins, while with the zeolite Y base catalyst larger fragments can be formed.

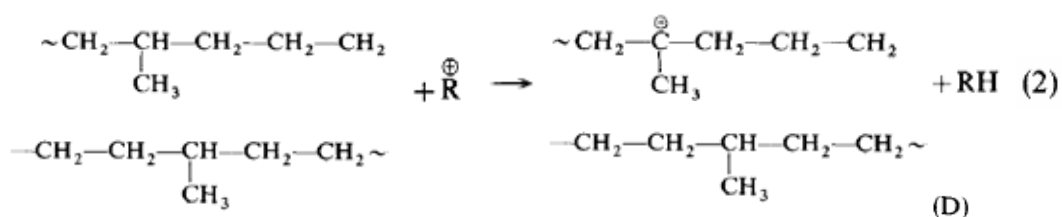
This agrees with the results that can be found in literature; the main products from *n*-olefins and *i*-olefins cracking on ZSM-5 are light olefins with a high selectivity for propene, *i*-butene, and in some cases also increased yields of ethene are reported.

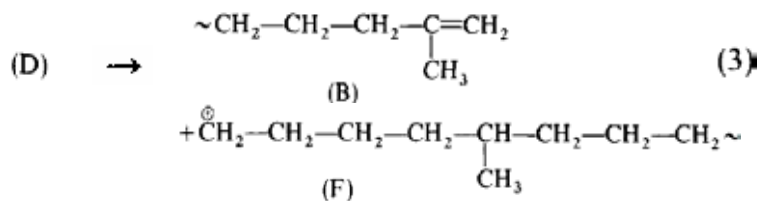
A mechanism for the catalytic cracking of PE and PP using mesoporous Al-MCM-41 as catalyst is proposed by Ishihara *et.al.*[81-82] As described, branched polyethylene components that have short chains (C₁-C₅) and consisting mainly of methyl groups. Branching of the main fraction was at a frequency of one branch per three ethylene monomer units $\sim\text{CH}_2-\text{CH}_2-\text{CH}_2-\text{CH}_2-\underset{\text{CH}_3}{\text{CH}}-\text{CH}_3$. The typical oligomer structure was found to be virtually the same as that of polyisooheptyl based on branching frequency. Moreover, oligomer chains showed random branching in an ethylene sequence in regular structures of polyisooheptyl. The catalytic cracking of PE is initiated by attack of low molecular weight carbonium ion (R⁺) on a very small number of on-chain hydrogen atoms attached to tertiary carbon atoms in polymer chains. The initial reaction of molecular weight reduction is shown in equations (1). β -scission of on-chain carbonium ions (A) occurs to produce chain-ends (B) and (C):



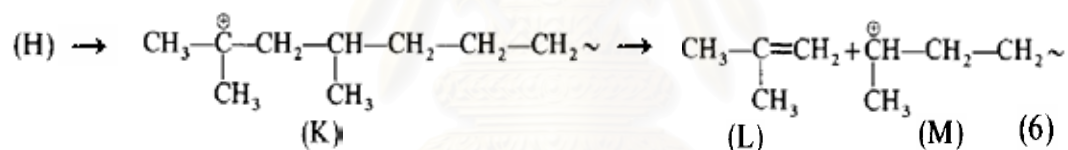
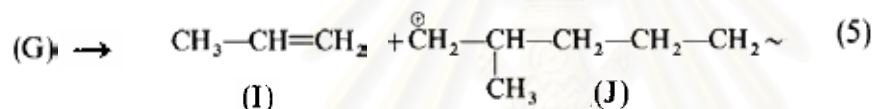
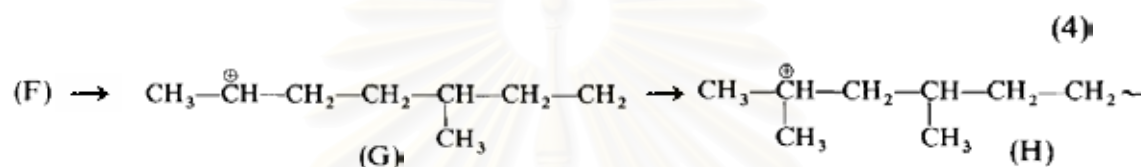
Mechanism of gas formation.

Gaseous products are produced from the liquid fraction produced by decomposition of oilgomers and reaction with typical oilgomers is shown in the following scheme. (where R⁺ represents the volatile carbonium ion, $\sim\text{CH}_2-\overset{\oplus}{\text{C}}\text{H}-\text{CH}_2$)



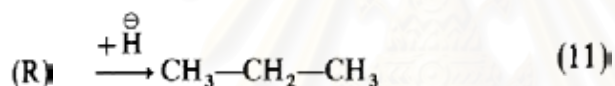
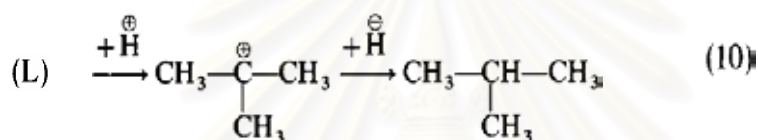
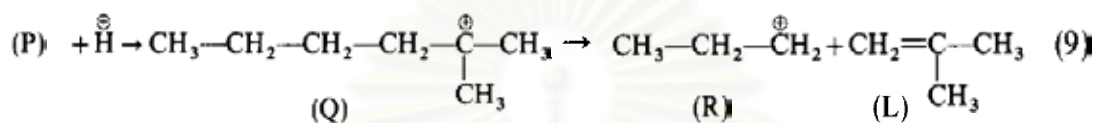
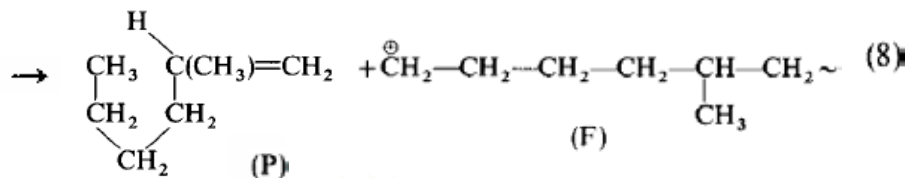
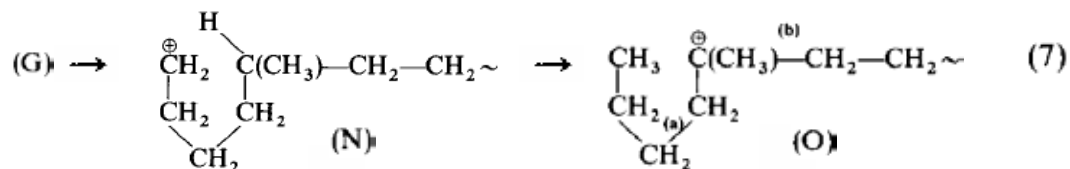


Gas formation takes place by way of the decomposition of these fractions. The unstable reaction intermediate (F) is isomerized to secondary (G) or tertiary carbonium ions (H) as shown by equation (4).



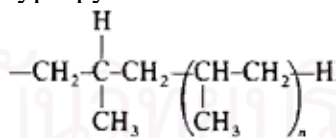
Ions (G) and (H) are essential to gaseous product formation and are mainly produced by β -scission of these carbonium ions (H). Isobutene is converted to isobutene through hydrogen transfer by the catalyst so that its yield is remarkably high. Propylene is produced in high yield by direct β -scission of other important ions (G) at high temperature.

The propane component is independent of propylene yield and is not produced by hydrogenation of propylene. The propane component is probably produced from propyl carbonium ions produced by β -scission of volatile tertiary carbonium ions without hydrogenation of propylene. For instance, stabilization of (F) ions takes place with lower activation energy of isomerization and thus intramolecular rearrangement to inner tertiary carbon atoms occurs. (F) ions cause intermolecular rearrangement by back biting reactions:



The stabilization of tertiary carbonium ions (O) proceeds by β -scission at the (b) position to give rise to a more stable fraction (P) than propyl ions ((a) position). Equations (7)-(11) show isobutene and propane are produced. Propane is not produced by the hydrogenation of propylene.

The mechanism of polypropylene is similar to polyethylene but the typical oligomer of polypropylene is



2.6.4 Reactions of Paraffins

Compared to olefins, paraffins have lower reactivity towards cracking due to a difficult formation of carbenium ions. Direct formation of carbenium ions requires the abstraction of hydride ions. At Lewis acid sites or adsorbed carbenium ions can react with paraffins in a bimolecular-type of mechanism. The latter mechanism requires the presence of the adsorbed carbenium ions and can take place if the pore size of the

catalyst is large enough to accommodate the necessary transition state (as is the case in zeolite Y and not in ZSM-5).

Indirect formation of carbenium ions is proposed to proceed through the formation of carbonium ions; paraffin reacts with a proton from a Brønsted acid site and the resulting adsorbed carbonium ion is cracked to an adsorbed carbenium ion and hydrogen or a small olefin. The formation of a carbonium ion requires an energetically unfavorable transition state and has high activation energy. This mechanism for activation of paraffins will only be significant in the absence of olefins and is favored by high temperatures, low hydrocarbon partial pressures and low conversions of the paraffins. The occurrence is not expected to be significant when cracking a gasoline mixture that contains olefins. The olefin can easily form carbenium ions and cause cracking of paraffins through the bimolecular cracking mechanisms as discussed above.



CHAPTER III

EXPERIMENTS

3.1 Instruments and Apparatus

Ovens and Furnaces

During the synthesis course, crystallization of ZSM-5 was performed using a Memmert UM-500 oven as a heater. Heating of any solid sample at 100°C was carried out using the same oven. Organic templates of ZSM-5 and Al-HMS were removed by calcination at 540 and 550°C, respectively, using a Carbolite RHF 1600 muffle furnace with programmable heating rate of 1°C.

X-ray Powder Diffractometer (XRD)

Characteristic structure of synthesized catalysts was identified using a Rigaku D/MAX-2200 X-ray diffractometer (XRD) with a monochromator and Cu K_α radiation (40 kv, 30 mA). The two-theta angle was ranged from 1.2 to 10° for Al-HMS samples and 5 to 50° for ZSM-5 samples. In case of Al-HMS, the scan speed was 2°/min while that of 5°/min was applied for ZSM-5. The scan step was fixed at 0.02°. The three slits setting (scattering, divergent and receiving slits) for Al-HMS were fixed at 0.5°, 0.5° and 0.15 mm, respectively and the values of 0.5°, 0.5°, 0.30 mm were applied for ZSM-5.

Inductively Coupled Plasma-Atomic Emission Spectrometer (ICP-AES)

Aluminum content in the catalysts was analyzed by a Perkin Elmer Plasma-1000 inductively coupled plasma-atomic emission spectrometer (ICP-AES) at the Scientific and Technological Research Equipment Center of Chulalongkorn University.

Scanning Electron Microscope (SEM)

SEM image was done to determine the crystal size and morphology of ZSM-5 and Al-HMS using a JEOL JSM-5410LV scanning electron microscope at the Scientific and Technological Research Equipment Center of Chulalongkorn University.

Nuclear Magnetic Resonance Spectrometer (NMR)

Solid state ^{27}Al -MAS-NMR spectra were performed using a Bruker Advance DPX 300 MHz NMR spectrometer at the National Metal and Materials Technology Center (MTEC), National Science and Technology Development Agency.

Nitrogen Adsorptometer

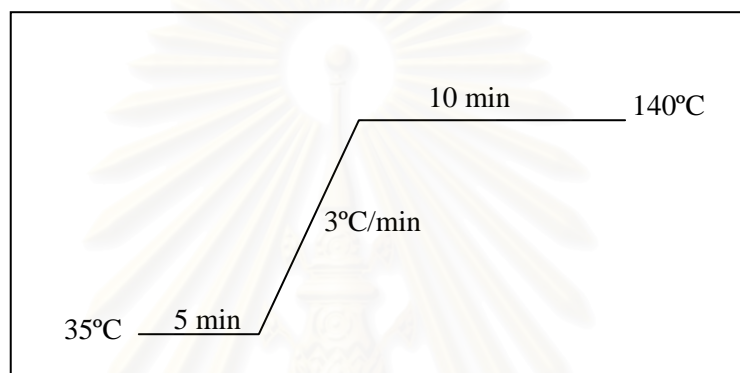
Characterization of catalyst porosity in terms of nitrogen adsorption-desorption isotherms, BET specific area, external surface area and pore size distribution of catalysts were determined by a BEL Japan BELSORP-mini 28SP adsorptometer. The sample weight was approximately 40 mg and pretreated at 400°C for 3 h. Nitrogen gas was used as an adsorbate at 77 K in measurement step at the department of Chemistry, Faculty of Science, Chulalongkorn university.

Ammonia Temperature Program Desorptometer (NH₃-TPD)

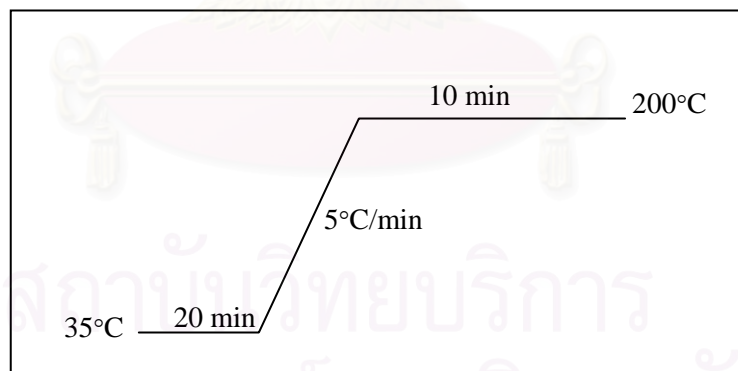
Acidity and acid strength of catalysts were determined using a BEL Japan, BELCAT with the sample weight about 100 mg. The desorbed ammonia was monitored by a thermal conductivity-type detector. The pretreatment was as follows: the catalyst sample was heated up to and kept for 10 min at 610 °C under a flow of helium. After replacing the He flow by a flow of synthetic air and keeping for 20 min at the same temperature, the sample was cooled down to room temperature. The samples were analyzed at the department of Chemistry, Faculty of Science, Chulalongkorn university.

Gas Chromatograph (GC)

Hydrocarbon gases were analyzed using a Varian CP-3800 gas chromatograph equipped with a 50-m long and 0.53-mm inner diameter Alumina-PLOT column. Liquid samples were analyzed using a Varian CP-3800 gas chromatograph equipped with a 30-m long and 0.25-mm inner diameter CP-sil 5 (0.25 μm film thickness) column. All GC detectors are flame ionization detectors (FID). The GC heating programs for 3- μl gas and 1- μl liquid analysis are shown in Schemes 3.1 and 3.2, respectively.



Scheme 3.1 The GC heating program for gas analysis.



Scheme 3.2 The GC heating program for liquid analysis.

3.2 Chemicals and Gases

Tetraethyl orthosilicate (98% TEOS), ammonium chloride (NH_4Cl) and tetrapropyl ammonium bromide (TPABr) were commercially available from Fluka. Colloidal silica (Ludox AS 40%) was purchased from Aldrich. Hexadecylamine (HDA) and Aluminum isopropoxide (AIP) were obtained from TCI Japan. Sodium

aluminate (NaAlO_2) was supplied from Riedel-de Haën. Glacial acetic acid (CH_3COOH) and sodium hydroxide (NaOH) were supplied from Lab-scan. Highly pure grade nitrogen was purchased from Thai Industrial Gases (TIG) and a trace amount of moisture in gas was removed by passing through a 40 cm x 2.5 cm tube of molecular sieve 4A. Ammonia gas (NH_3 , highly pure grade) was purchased from Linde Gas Thailand. Standard gas mixture and liquid mixture for GC analysis were kindly obtained from PTT CHEM. Other chemicals were purchased from Merck or Fluka, otherwise specifically identified.

3.3 Synthesis of Catalysts

3.3.1 Synthesis of Al-HMS with a Si/Al mole Ratio in gel of 20

Synthesis of Al-HMS was performed by the procedures reported by Metha S.[85]. The gel molar composition of 1.0SiO_2 : $0.025\text{Al}_2\text{O}_3$: 0.25HDA : 8.30EtOH : $100\text{H}_2\text{O}$ was prepared by dissolving 12.07 g of hexadecylamine (HDA) in the mixed solvent of ethanol and water (76.48 g ethanol and 198.40 g water) in a 250-cm^3 beaker. The mixture was stirred for 20 min until homogeneous solution was obtained. Then, 2.04 g of aluminum isopropoxide (AIP) was added to the mixture under vigorous stirring for 30 min. A portion of 41.67 g of tetraethyl orthosilicate (TEOS) and a portion of 162.0 g of water were then added dropwise in sequence into the mixture with stirring for 2 h. After aging with stirring the resulting gel for 20 h, the white solid product was filtered and washed several times until pH of filtrate was equal to 7. The solid was air-dried for 1 day. The as-synthesized Al-HMS was obtained. The hexadecylamine template was removed by calcination of the sample at the temperature of 550°C for 10 h. The procedure for preparing the Al-HMS support was shown in Scheme 3.3.

3.3.1.1 Preparation of Al-HMS with various Si/Al mole Ratios

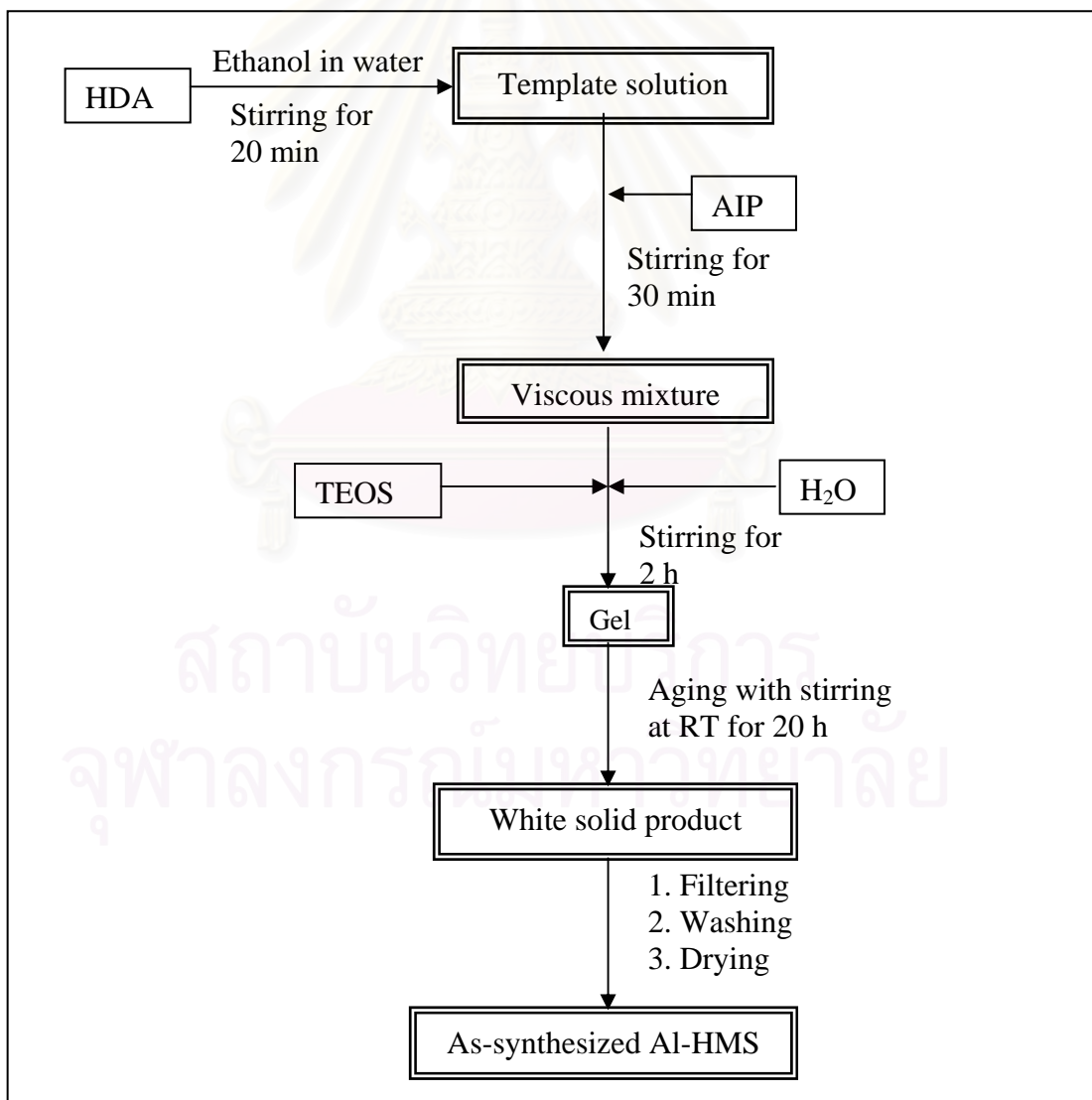
The Al-HMS samples with various Si/Al mole ratios in gel of 20, 60 and 200 were prepared using the similar method described in scheme 3.3. Different amounts of aluminum required for each sample were indicated in Table 3.1. The Al-HMS samples were characterized using XRD.

Table 3.1 Amounts of aluminum isopropoxide (AIP) in the preparation of Al-HMS with Si/Al mole ratios in gel of 20, 60 and 200

Si/Al mole ratio in gel	AIP (g)
20	2.04
60	1.02
200	0.204

3.3.2 Synthesis of Pure Silica HMS

Pure silica HMS was also synthesized using the procedure described in section 3.3.1 but no aluminum isopropoxide was added. The as-synthesized white solid product was obtained. The template removal process was carried out similar to the case of Al-HMS.



Scheme 3.3 Preparation diagram for Al-HMS catalyst.

3.3.3 Synthesis of ZSM-5 with a Si/Al mole ratio in gel of 40

Synthesis of ZSM-5 was performed by the procedure reported by Vorranutch J.[84]. This method was performed using 40% colloidal silica as silica sources. A mixture solution between 36.74 g of 40% colloidal silica and 20.37 g of a 32% sodium hydroxide solution into a 500-cm³ 4-necked round bottom flask containing 44.30 g of a 36.80% solution of tetrapropyl ammonium bromide in water was added dropwise. The apparatus for gel preparation was shown in Figure 3.1. The mixture was stirred vigorously at room temperature for 1 h to obtain a homogeneous milky suspension. Then, a solution of 0.50 g of sodium aluminate in 15.55 g distilled water was added dropwise to the suspension. The mixture with the mole ratio of SiO₂ : 0.36 Na₂O : 0.025 Al₂O₃ : 0.25 TPABr : 80 H₂O, was then aged at room temperature for 4 h under stirring. Acetic acid was used to lower the pH of gel from 13 to a range of 11-12. The milky suspension became viscous white slurry. The gel was transferred into a stainless steel vessel lined with Teflon and heated in an oven at 100°C for 2 days without pH adjustment. After that the gel was heated at 125°C for 6 days with pH adjustment every day. The schematic diagram of this whole procedure is shown in Scheme 3.4. The white solid sample was filtered, washed and dried. The as-synthesized white solid product was characterized using XRD.

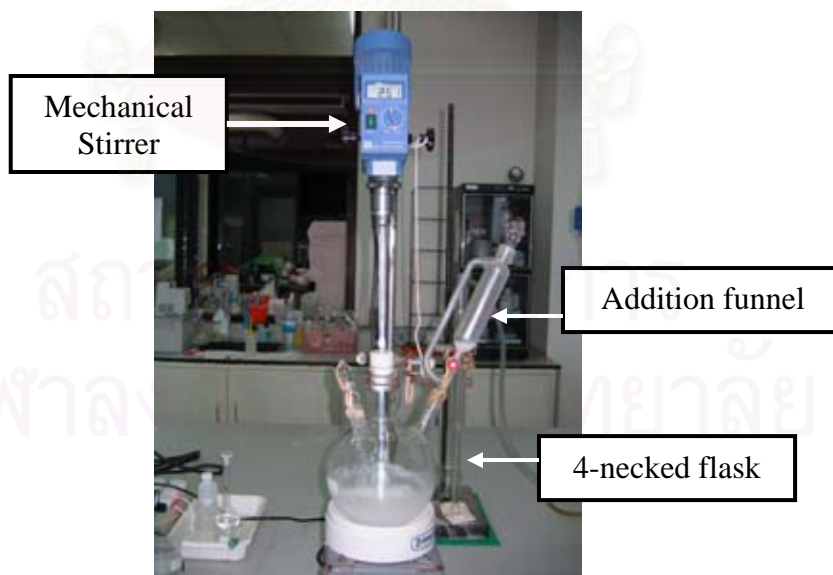
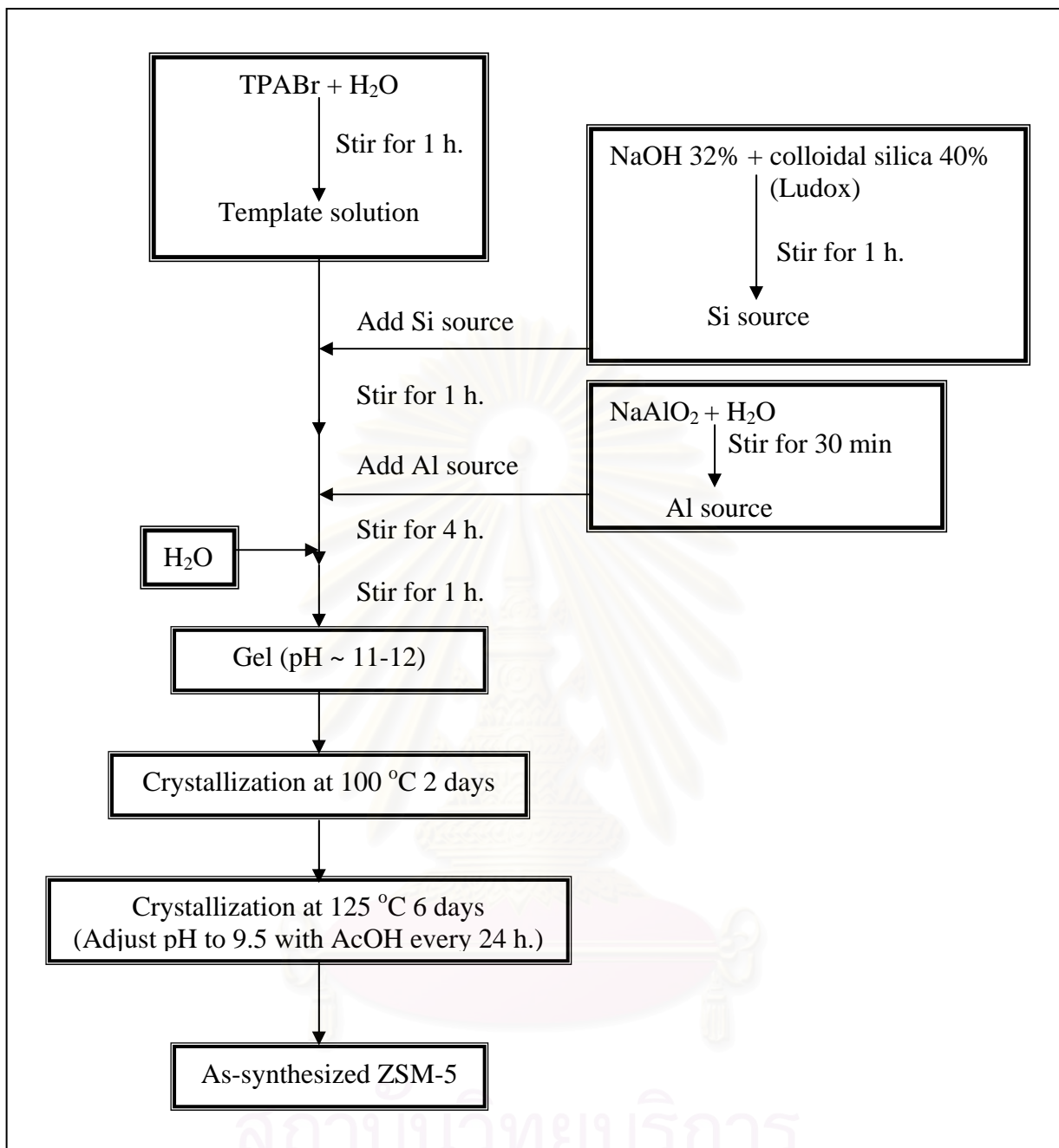


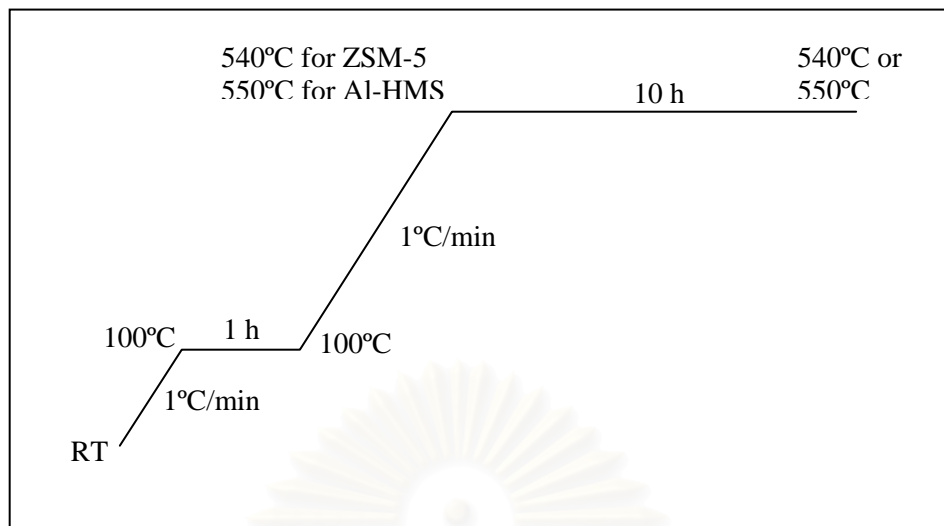
Figure 3.1 Apparatus for synthesis of ZSM-5.



Scheme 3.4 Preparation diagram for ZSM-5.

3.4 Removal of Organic Template from Catalysts

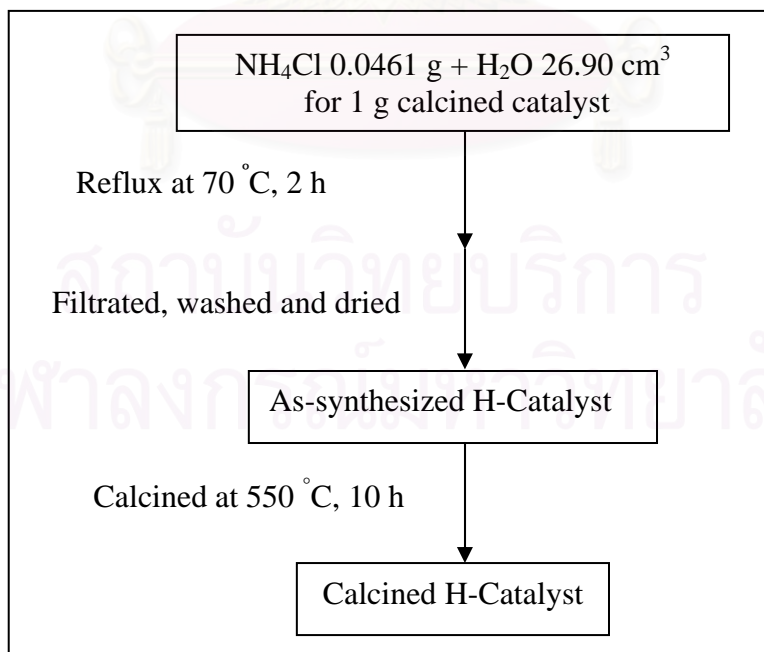
Organic template in the catalyst structure must be removed by oxidation to carbon dioxide at elevated temperature. As-synthesized catalysts were calcined in a muffle furnace using the heating program for the template removal as shown in Scheme 3. 5. The calcined sample was kept in a desiccator prior to use.



Scheme 3.5 A heating program for organic template removal.

3.5 Ion exchange of Catalysts

All calcined catalysts, Al-HMS and ZSM-5, were exchanged by NH_4^+ ion in 0.03M ammonium chloride solution. The ion exchanged catalysts were characterized using ICP-AES, solid-state ^{27}Al -NMR, NH_3 -TPD, and nitrogen adsorption instruments. The schematic diagram of this whole procedure is shown in Scheme 3.6.



Scheme 3.6 Ion exchange diagram for catalysts.

3.6 Sample Preparation for ICP Analysis

In a 100-cm³ Teflon beaker, 0.0400 g of a calcined sample was soaked with 20 cm³ of 6M HCl and subsequently 20 cm³ of 48% HF was added dropwise to remove silica in the form of volatile SiF₄ species. The sample was gently heated until dryness on a hot plate and the fluoride treatment was repeated twice more before a 10 cm³ mixture solution of 6M HCl : 6M HNO₃ at the ratio of 1 : 3 was added slowly and warmed until dryness again. After that the 10-cm³ of water was added. Then the solution was warmed until complete dissolution. The solution was transferred to a 50-cm³ polypropylene volumetric flask and made to the volume with deionized water. The flask was capped and shaken thoroughly before transferred to a plastic bottle with a threaded cap lined under with a polyethylene seal.

3.7 Preparing the composite of ZSM-5/Al-HMS

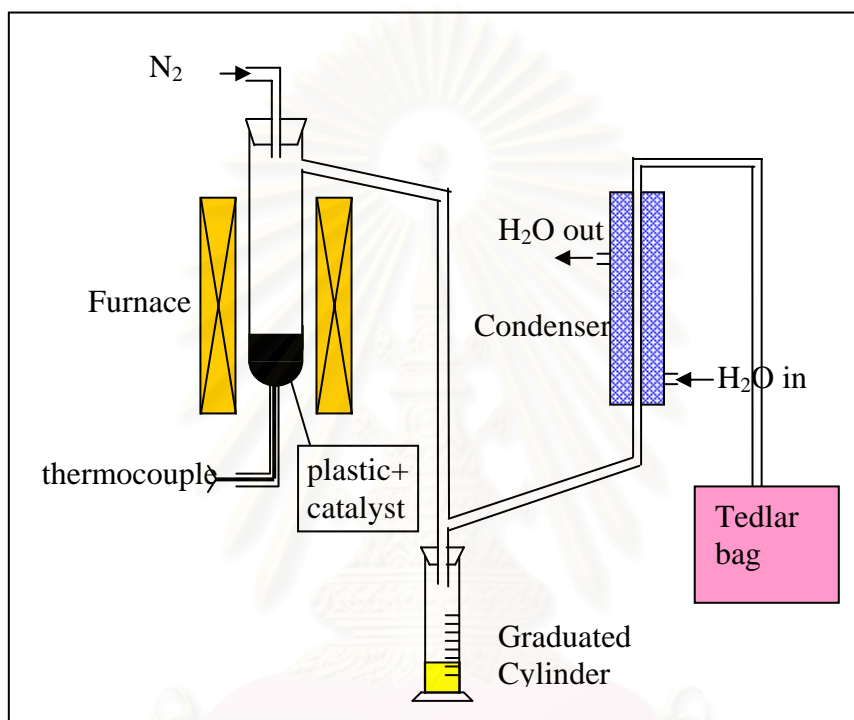
The composite catalyst was prepared by physical mixing of ionic exchanged ZSM-5 and Al-HMS at weight ratio of 1:2, 1:1, and 2:1 respectively. The composite was mixed by shaking by hand for 30 min.

3.8 Catalytic Cracking of HDPE and PP using ZSM-5/Al-HMS

3.8.1 Effect of Temperature on Activity of ZSM-5/Al-HMS

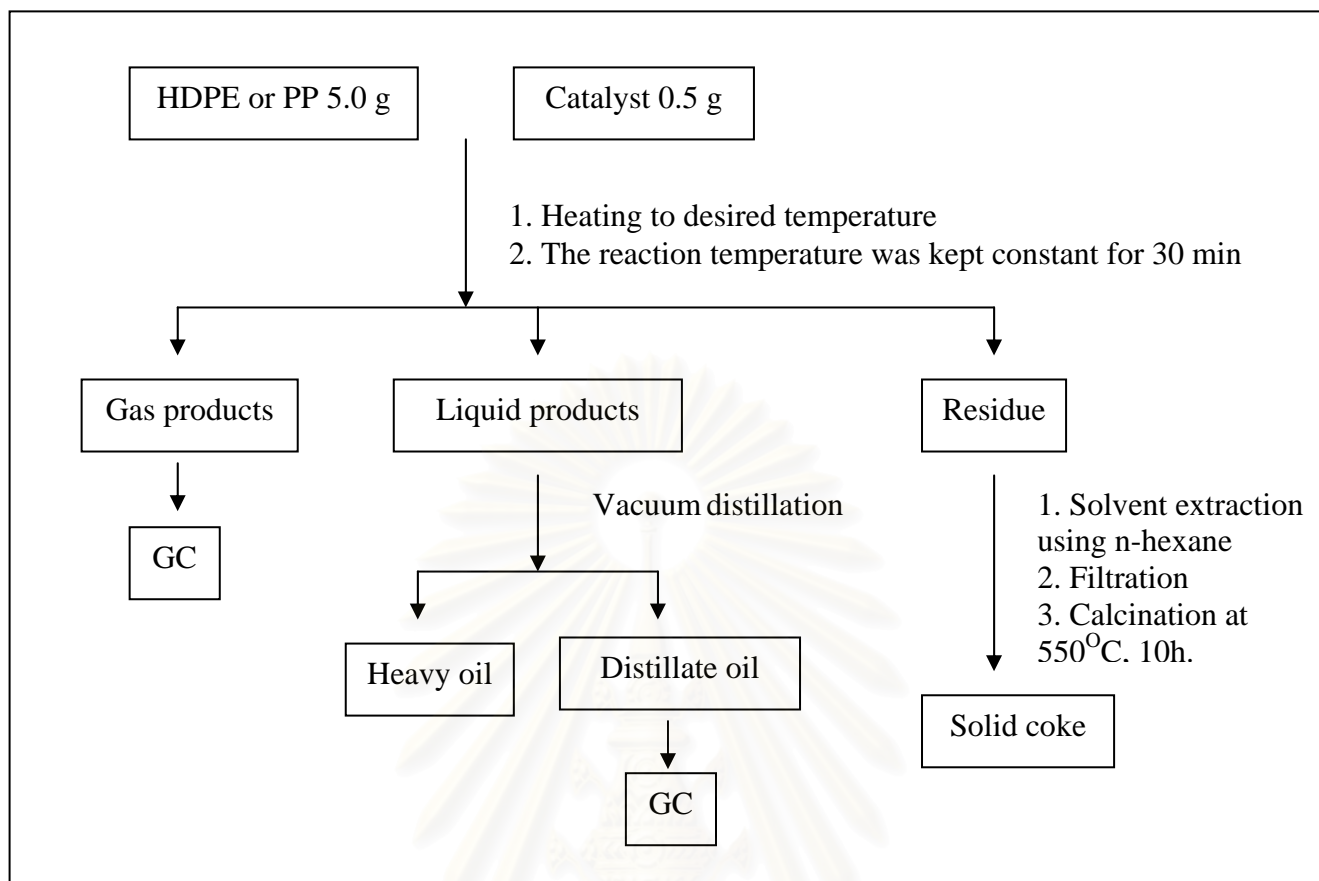
Degradation of plastic polymer was carried out in a glass reactor (4.4 cm. i.d. and 37 cm. in length) under atmospheric pressure by batch operation as shown in Figure 3.2. A 5.0 g of plastic (HDPE or PP) and 0.5 g of catalyst were loaded into the reactor. In a typical run, the reactor was purged with N₂ at a flow rate of 20 ml/min to remove air. The reactor was heated to a desired temperature (350°C, 400°C and 450°C) with a heating rate of 20°C/min using a split-tube furnace equipped with a programmable temperature controller and a K-type thermocouple. The reaction temperature was kept constant for 30 min. The gaseous products flew from the reactor with the nitrogen stream and passed through a cooled condenser. The gaseous products were collected in a Tedlar bag since the start of heating while the liquid products were condensed and collected in a cylinder. After completion of the reaction, the reactor was cooled down to room temperature and weighed. The degradation products were classified into three groups identified as gases (products which were not condensable at water cooling temperature), liquid hydrocarbons and residue. The

gaseous products were analyzed by a gas chromatography. The liquid products were distilled under vacuum using a controlled heating block at 200 °C. The distilled oil was analyzed by GC. The chromatogram is a distribution of hydrocarbons derived from GC on the basis of boiling points of normal paraffin. The coke formation was determined by the weight loss upon calcination of the used catalyst after extraction of waxes. The heating program for calcination of used catalyst is shown in Scheme 3.5.



Scheme 3.7 Catalytic cracking apparatus.

สถาบันวิทยบริการ
จุฬาลงกรณ์มหาวิทยาลัย



Scheme 3.8 Catalytic cracking Scheme for HDPE and PP.

3.8.2 Effect of catalytic to plastic ratio

The catalytic cracking reaction was carried out according to the procedure in section 3.8.1, but the amount of catalyst to plastic was changed to 2 wt%, 5 wt%, 10 wt%, and 20 wt% respectively using the optimal temperature.

3.8.3 Effect of ZSM-5 : Al-HMS ratio in composite catalyst

The effect of ZSM-5 : Al-HMS ratio in composite catalyst on cracking of HDPE and PP was studied in the same way as general procedure, but the ratio between ZSM-5 and Al-HMS was varied to 1:2, 1:1, and 2:1 respectively under the optimal condition.

3.8.4 Effect of aluminium content in catalyst

The effect of aluminium in Al-HMS catalyst was investigated by varying the Si/Al mole ratios in gel of 20, 60 and 200. The reaction was performed in the optimal condition obtained from section 3.8.3.

3.8.5 Thermal cracking and catalytic cracking over pure catalysts

In this study, thermal cracking of HDPE and PP was investigated and compared with catalytic cracking reactions over pure ZSM-5, Al-HMS (Si/Al = 20, 60 and 200) and HMS at the optimal condition.

3.9 Recycle of catalyst

The catalyst was reused by calcination in air at 550°C for 10 h, characterized by XRD and surface area analysis before testing its activity.



CHAPTER IV

RESULTS AND DISCUSSION

4.1 Characterization of catalysts

4.1.1 The physico-chemical properties of ZSM-5 (Si/Al = 40)

4.1.1.1 XRD Results

Synthesis of ZSM-5 (Si/Al = 40) with the mole ratio in gel of SiO_2 : 0.36 Na_2O : 0.025 Al_2O_3 : 0.25 TPABr : 80 H_2O was performed by the procedure reported by Vorranutch J.[84]. XRD patterns of as-synthesized and calcined ZSM-5 are shown in Figure 4.1 and Figure 4.2. Both as-synthesized and calcined ZSM-5 showed the characteristic pattern of MFI structure without any phase of other materials. The as-synthesized ZSM-5 showed the characteristic peaks at low angle around $8-9^\circ$ and the characteristic peaks at high angle range of $22-24^\circ$. After calcination, the peak intensities at low angle increased while those peaks at high angle decreased because the template in pores of ZSM-5 was removed and aluminium in the framework might be transferred to non-framework aluminium.

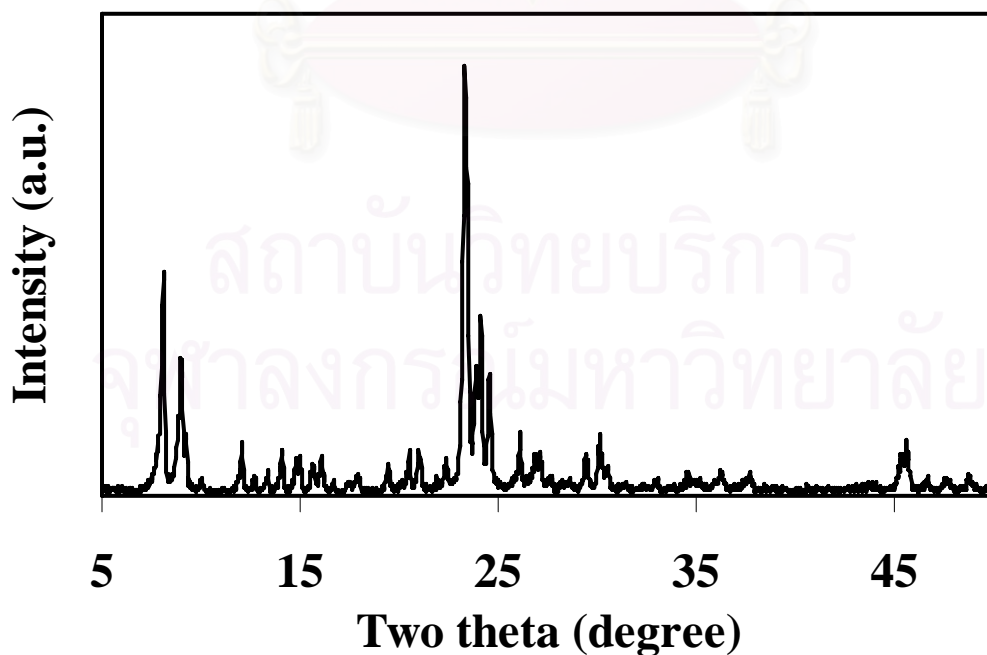


Figure 4.1 XRD patterns of as-synthesized of ZSM-5 B1.

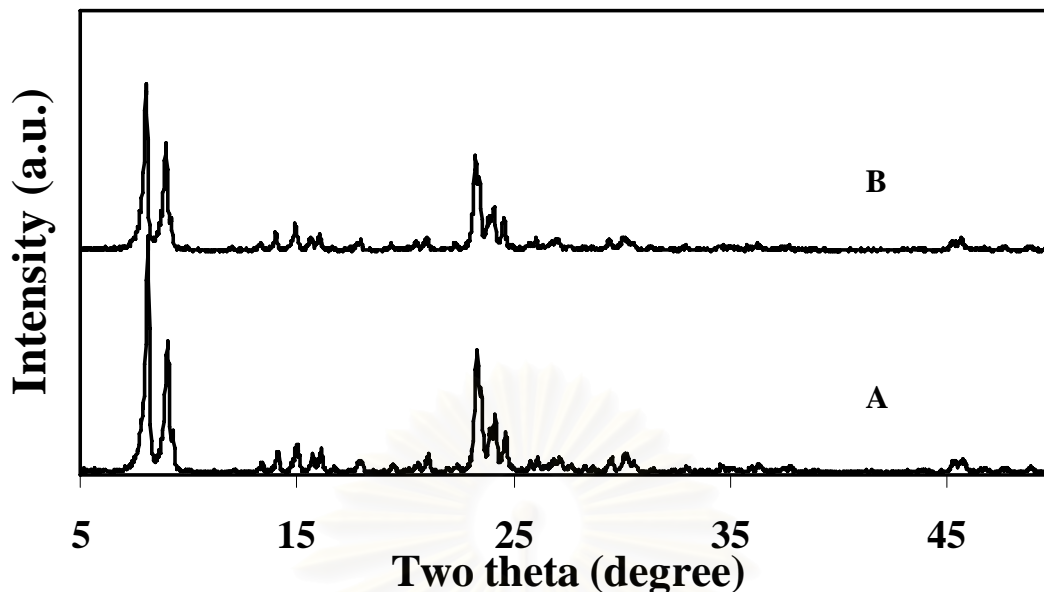


Figure 4.2 XRD patterns of calcined of ZSM-5: (A) ZSM-5 B1 and (B) mixed all batches of ZSM-5.

Because one batch of ZSM-5 yielded 5 g of calcined catalyst, 5 batches were synthesized and XRD patterns are shown in appendices section. All batches of ZSM-5 were mixed and shaken by hand for 30 min. The XRD patterns of mixed ZSM-5 shown in Figure 4.2 indicates the mixed samples were similar the characteristic peaks of ZSM-5 structure with the intensities were roughly close those of ZSM-5 in each batch.

4.1.1.2 Elemental Analysis

The Si/Al ratios in gel and in catalyst of all ZSM-5 batches are compared in Table 4.1. The Si/Al ratios in catalyst were slightly higher than the Si/Al ratios in gel. The result suggests that aluminium atoms have incorporated into the structure of catalyst. That is also in agreement with the Al-NMR spectra in section 4.1.1.4.

Table 4.1 Si/Al mole ratios in gel and in catalyst of calcined ZSM-5 (Si/Al = 40)

Sample	Si/Al mole ratio in gel ^a	Si/Al mole ratio in catalyst ^b
ZSM-5 B1	40	47.0
ZSM-5 B2	40	47.9
ZSM-5 B3	40	49.0
ZSM-5 B4	40	47.8
ZSM-5 B5	40	47.5
Mixed ZSM-5	40	47.8

a: Calculated from reagent quantities.

b: Aluminum (Al) was determined by ICP-AES and Si was calculated from the deduction of AlO₂ in the sample weight.

4.1.1.3 Nitrogen Adsorption-Desorption

Nitrogen adsorption-desorption isotherm of mixed ZSM-5 with Si/Al ratio in gel of 40 is shown in Figure 4.3. All ZSM-5 catalysts exhibited a hysteresis loop of type I adsorption isotherm which is a characteristic pattern of microporous materials. All BET specific surface area and pore diameter of ZSM-5 catalysts were in range of 400-415 m²/g and 2.0-2.4 nm, respectively, as summarized in Table 4.2.

Table 4.2 BET specific surface area and pore diameter of calcined ZSM-5 (Si/Al = 40)

Sample	a _{s, BET} (m ² /g)	Pore diameter (nm)
ZSM-5 B1	407	2.1
ZSM-5 B2	400	2.1
ZSM-5 B3	415	2.0
ZSM-5 B4	405	2.1
ZSM-5 B5	404	2.3
Mixed ZSM-5	411	2.4

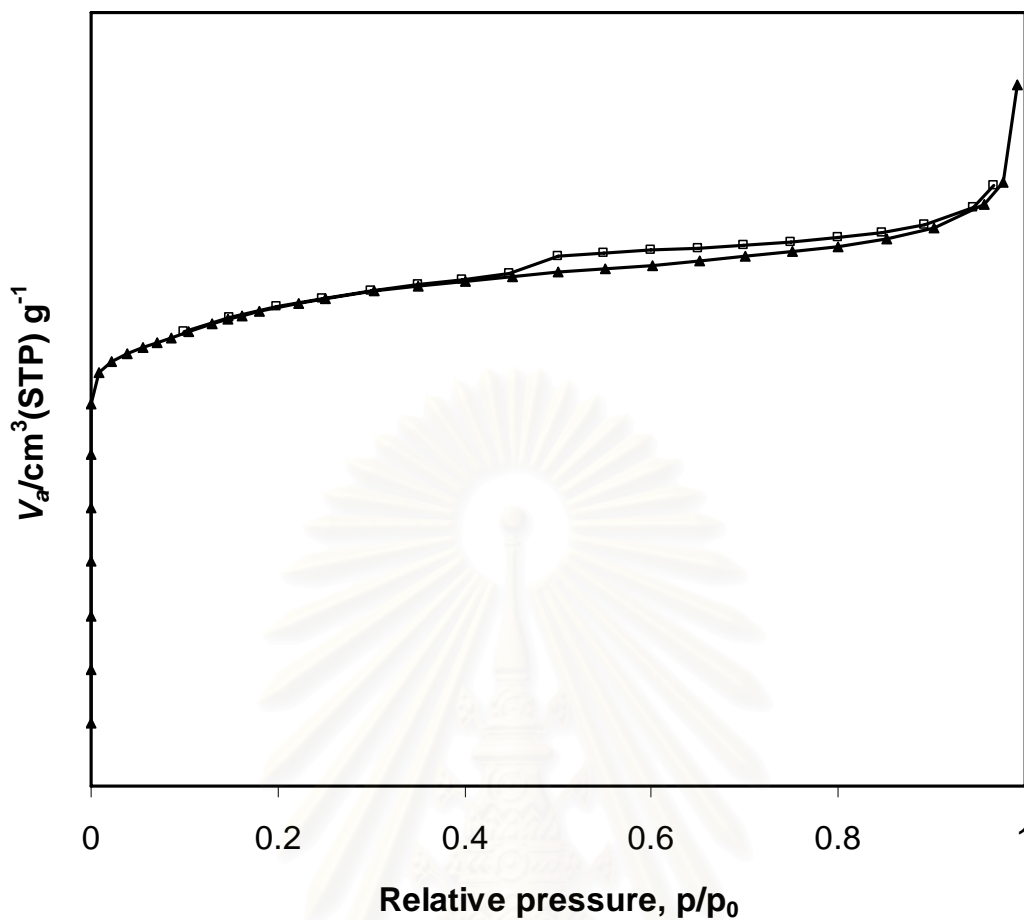


Figure 4.3 N₂ adsorption-desorption isotherms of mixed ZSM-5 (Si/Al = 40) catalyst.

4.1.1.4 ²⁷Al-MAS-NMR Spectra

To investigate the position of the incorporated aluminum atoms in the structure of aluminum containing catalyst, solid-state ²⁷Al-NMR spectra were performed. Generally, the presence of aluminum atoms in the framework or tetrahedral position is preferable due to the fact that non-framework aluminum oxides will cause the loss of surface area in porous catalysts.

²⁷Al-NMR spectra of exchanged mixed ZSM-5 catalyst is shown in Figure 4.4. Only one predominant peak was found at the chemical shift of 55 ppm which belongs to the tetrahedral aluminum atoms in the framework position. It suggests that all aluminium atoms in ZSM-5 were in tetrahedral framework.

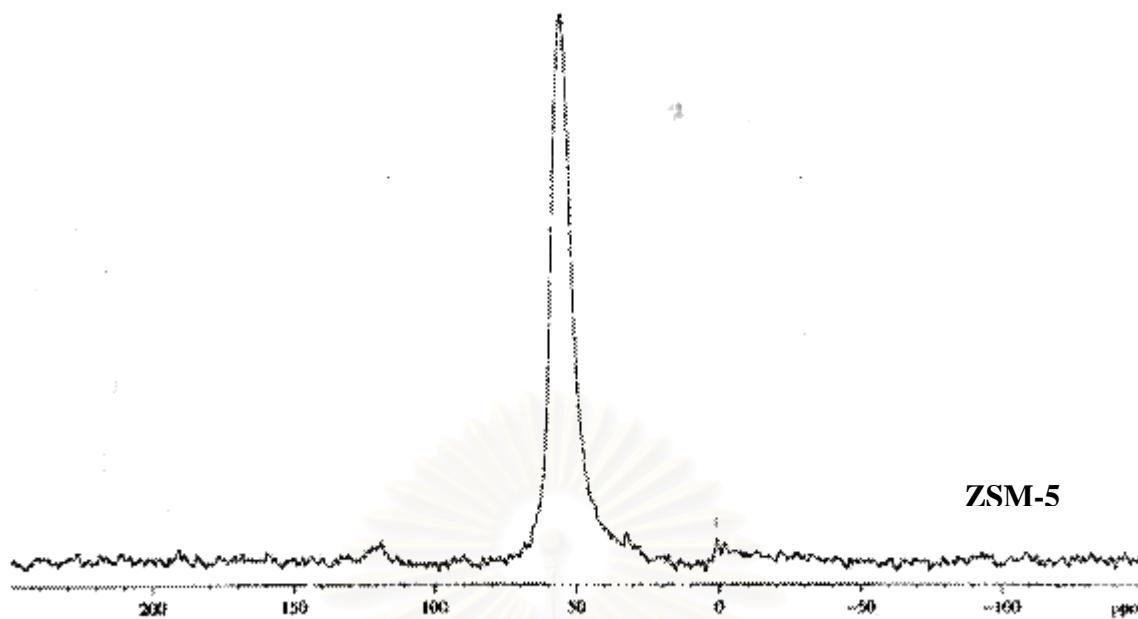


Figure 4.4 ^{27}Al -MAS-NMR spectrum of mixed calcined ZSM-5 catalyst (Si/Al = 40).

4.1.1.5 NH_3 -TPD Profile

The NH_3 -TPD profiles of mixed ZSM-5 catalyst with Si/Al ratio in gel of 40 is shown in Figure 4.5. The result shows ammonia desorption peaks at temperature around 150°C and 400°C . The peak at 150°C is due to the presence of Brønsted acid sites that interacts with basic ammonia molecules and the peak at 400°C is Lewis acid sites. The number of acid sites or acidity of the mixed ZSM-5 catalyst with Si/Al ratio in gel of 40 was calculated as 0.429 mmol/g . However, the active site for polymer degradation is known as Brønsted acid sites or protons. Thus the ZSM-5 catalyst is expected to exhibit their catalytic activity in polymer degradation.

สถาบันวิทยบริการ
จุฬาลงกรณ์มหาวิทยาลัย

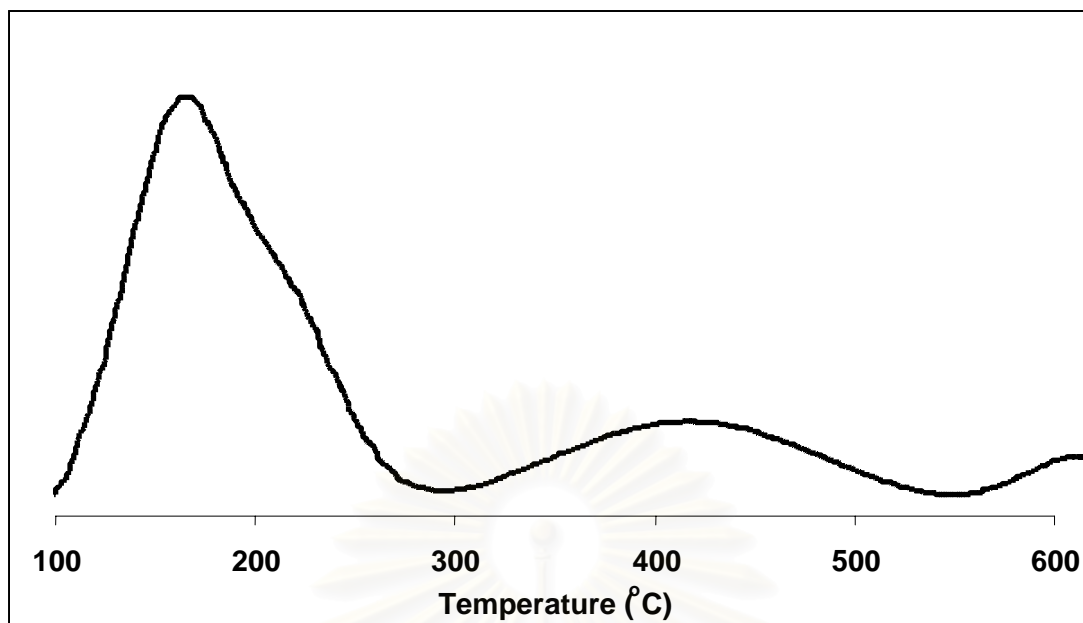


Figure 4.5 NH₃-TPD profiles of mixed ZSM-5 catalyst Si/Al ratio in gel of 40.

4.1.1.2 SEM Images

SEM images of mixed ZSM-5 are shown in Figure 4.6. Two different shapes were found. Rectangle morphology with the particle size of 1.95 x 1.4 μm were obtained from ZSM-5 B2 sample while the others were cross-formed particles with approximate size of 1.25 x 1.1 μm (See appendice section). This indicates that the mixed ZSM-5 is not homogeneous in morphology. However, other properties such as Si/Al ratio in catalyst and BET specific surface area were also considered.

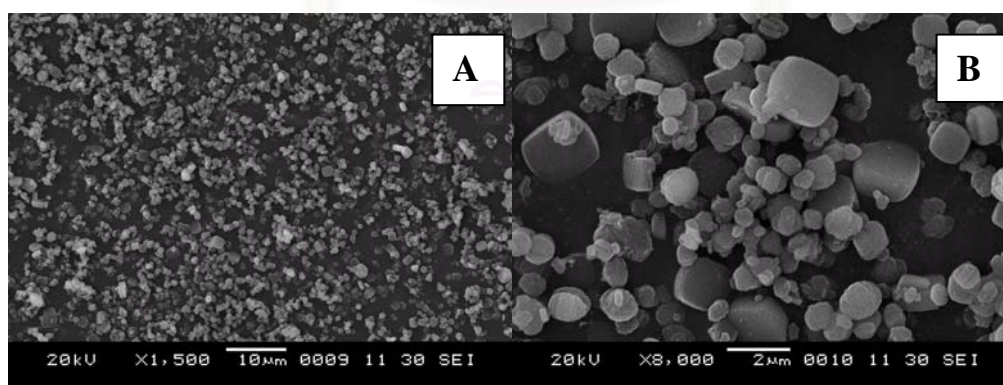


Figure 4.6 SEM images of mixed ZSM-5: (A) 1500x and (B) 8000x.

4.1.2 The physico-chemical properties of Al-HMS

4.1.2.1 XRD Results

Al-HMS was performed by the procedures reported by Metha S.[85]. XRD patterns of mesoporous Al-HMS catalyst with Si/Al mole ratio in gel of 20, 60 and 200 (Al-HMS 20, Al-HMS 60 and Al-HMS 200, respectively) are illustrated in Figure 4.7 and Figure 4.8. It indicates that all of as-synthesized materials showed typical long-range order hexagonal lattice corresponding to only one characteristic peak of HMS at the (100) lattice plane. After calcination the structure of each catalyst was remained with increasing peak intensity, resulting from the removal of template from the mesopores.

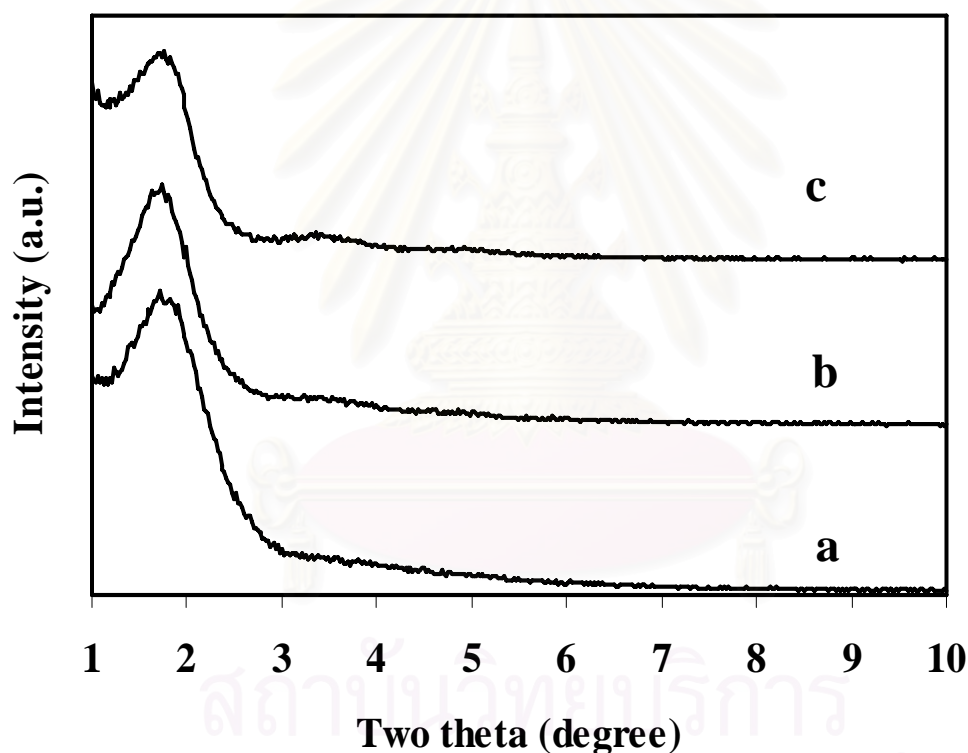


Figure 4.7 XRD patterns of as-synthesized of Al-HMS with various Si/Al ratios in gel: (a) Al-HMS 20 (Si/Al = 20), (b) Al-HMS 60 (Si/Al = 60) and (c) Al-HMS 200 (Si/Al = 200).

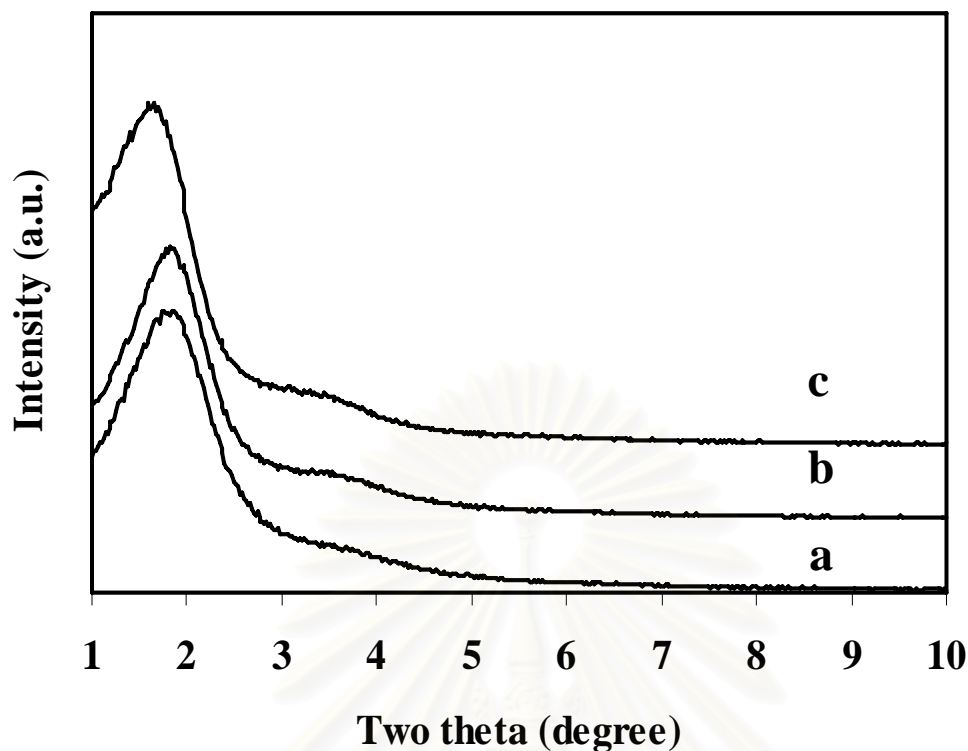


Figure 4.8 XRD patterns of calcined of Al-HMS with different Si/Al ratios in gel: (a) Al-HMS 20 (Si/Al = 20), (b) Al-HMS 60 (Si/Al = 60) and (c) Al-HMS 200 (Si/Al = 200).

4.1.2.2 Elemental Analysis

The Si/Al ratios in gel and in product of the Al-HMS are compared in Table 4.3. The Si/Al ratios in products of the Al-HMS were lower than those in gel. The results suggest that aluminium atoms have incorporated into the structure. The higher content of aluminium may be due to the loss of silica in framework. The agglomeration of silicon atoms is plausible for restriction silicon to access the framework.

However, the data from ICP-AES technique is not exhibit the position of aluminum atom, whether it located in framework or extra-framework, therefore ^{27}Al -NMR technique was required to exhibit the position of aluminum atom.

Table 4.3 Si/Al mole ratios in gel and in catalyst of exchanged Al-HMS with different Si/Al ratios

Sample	Si/Al mole ratio in gel ^a	Si/Al mole ratio in catalyst ^b
Al-HMS 20	20	11.8
Al-HMS 60	60	31.1
Al-HMS 200	200	99.2

a: Calculated from reagent quantities.

b: Aluminum (Al) was determined by ICP-AES and Si was calculated from the deduction of AlO₂ in the sample weight.

4.1.2.3 Nitrogen Adsorption-Desorption

Nitrogen adsorption-desorption isotherms of Al-HMS with different Si/Al ratio are shown in Figure 4.9. All Al-HMS catalysts exhibited hysteresis loop of type IV adsorption isotherm which is a characteristic pattern of mesoporous materials. The BET specific surface areas are listed in Table 4.4. All catalysts exhibited a narrow distribution with the pore size of 4.8 nm (48 Å) except Al-HMS-20 was 4.2 nm.

Although the mesostructures obtained from the Al-HMS have equivalent frameworks, the textural mesoporosity, as evidenced by the N₂ adsorption/desorption in the region $P/P_0 > 0.8$, Al-HMS-20 derivative with high textural porosity was composed of mesoscale fundamental particles that aggregate into larger particles. In contrast, Al-HMS-60 and Al-HMS-200 mesostructures with low textural porosity were assembled into much larger aggregates of macroscale fundamental particles [59].

Table 4.4 Textural properties of calcined Al-HMS with different Si/Al ratios

Sample	$a_{s, \text{BET}}$ (m ² /g)	Pore diameter (nm)	d_p (nm)
Al-HMS 20	759	8.5	4.2
Al-HMS 60	730	6.1	4.8
Al-HMS 200	693	6.8	4.8

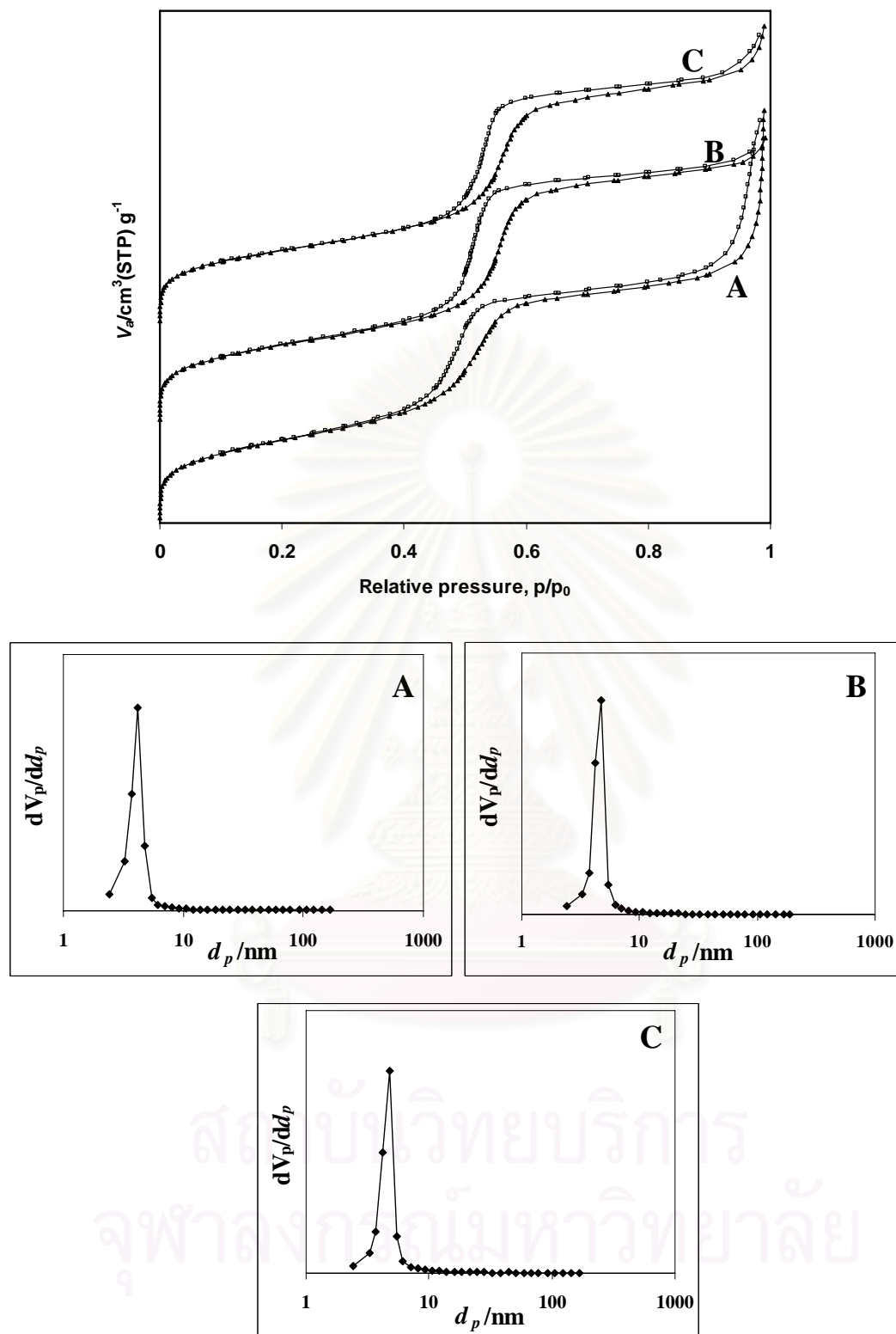


Figure 4.9 N_2 adsorption-desorption isotherms and pore size distribution of Al-HMS with various Si/Al ratios in gel of (A) Al-HMS 20 (Si/Al = 20), (B) Al-HMS 60 (Si/Al = 60) and (C) Al-HMS 200 (Si/Al = 200).

4.1.2.4 NH₃-TPD Profiles

Figure 4.10 shows NH₃-TPD profiles of Al-HMS catalyst with different Si/Al ratios. The NH₃-TPD profiles indicate that all catalysts exhibited two NH₃ desorption peaks. The peak position corresponds to acid strength while the peak area corresponds to number of acid site. The peak centered around 150-180°C is typically assigned to a weak acid site or Bronsted acid, and the other one around 350°C is assigned to a strong acid site or Lewis acid. The number of acid sites decreases when the Si/Al ratio increases due to the decrease in aluminum content in catalyst. These results are consistent with the ICP data in section 4.1.2.2. The number of acid site or acidity for Al-HMS 20, Al-HMS 60 and Al-HMS 200 were calculated as 0.409 mmol/g, 0.342 mmol/g, and 0.325 mmol/g, respectively.

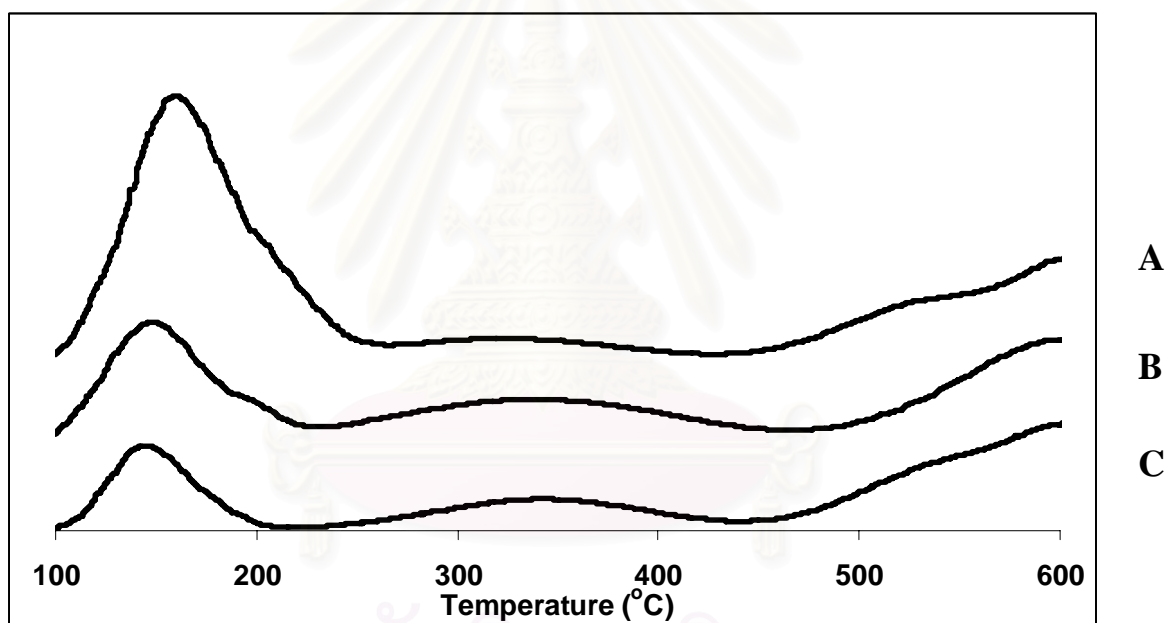


Figure 4.10 NH₃-TPD profiles of Al-HMS with various Si/Al ratios in gel: (A) Al-HMS 20 (Si/Al = 20), (B) Al-HMS 60 (Si/Al = 60) and (C) Al-HMS 200 (Si/Al = 200).

4.1.2.5 ²⁷Al-MAS-NMR Spectra

The ²⁷Al-NMR spectrum of the calcined Al-HMS in Figure 4.11 exhibits two signals at the chemical shifts of 55 and 0 ppm for Si/Al ratios of 20 and 60 whereas Al-HMS 200 shows only one peak at 55 ppm. The predominant peak at the chemical shift of 55 ppm typically belongs to the tetrahedral aluminum (T_d) and

the peak at chemical shift of 0 ppm can be assigned to octahedral non-framework aluminum(O_h). It can be concluded that aluminum atoms were incorporated into silica framework mainly in tetrahedral position and partially in octahedral position. In case of Al-HMS-20 and Al-HMS-60, aluminium atoms were in both tetrahedral and octahedral form whereas, all aluminium atoms in Al-HMS-200 were in tetrahedral framework. The more aluminium was added, the higher the peak height of tetrahedral and octahedral aluminium, the lower the ratio of peak area between tetrahedral aluminium and octahedral aluminium.

Table 4.5 Ratio of peak area between tetrahedral aluminium and octahedral aluminium of Al-HMS with various Si/Al ratios

Sample	T_d peak area/ O_h peak area ratio
Al-HMS 20	1.24
Al-HMS 60	1.85
Al-HMS 200	∞

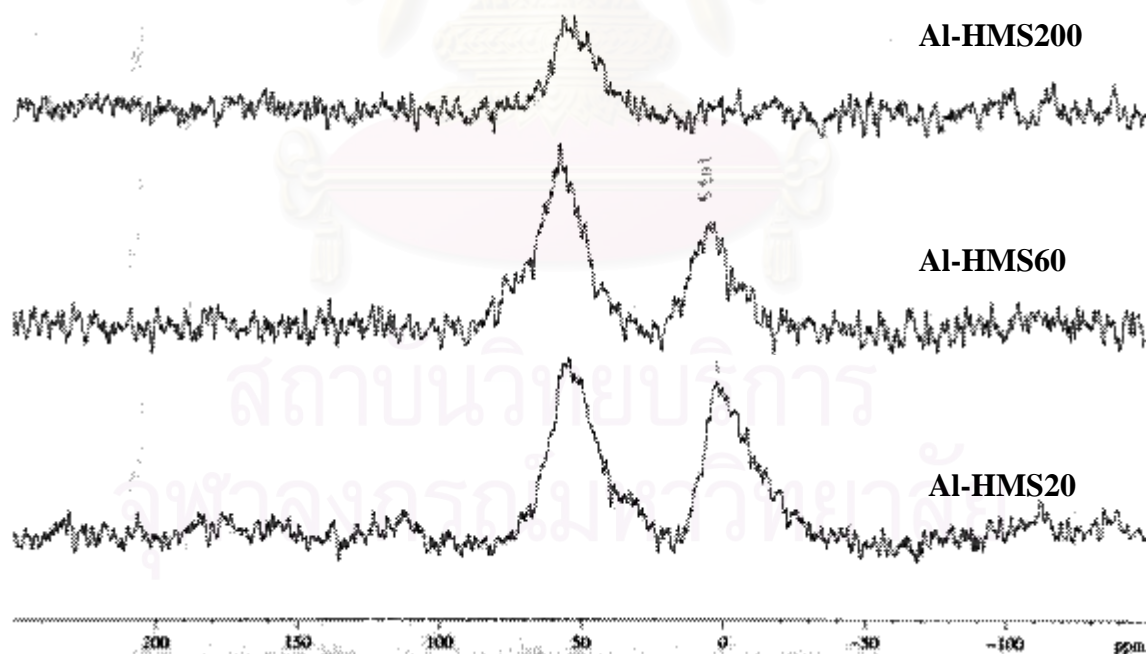


Figure 4.11 ^{27}Al -MAS-NMR spectra of calcined Sample Al-HMS with different Si/Al ratios in gel.

4.1.2.6 SEM Images

SEM images of Al-HMS with Si/Al mole ratio in gel of 20, 60 and 200 are shown in Figure 4.12. All Al-HMS samples exhibited an agglomeration of sphere particles with the particle size diameter in the range of 400-750 nm.

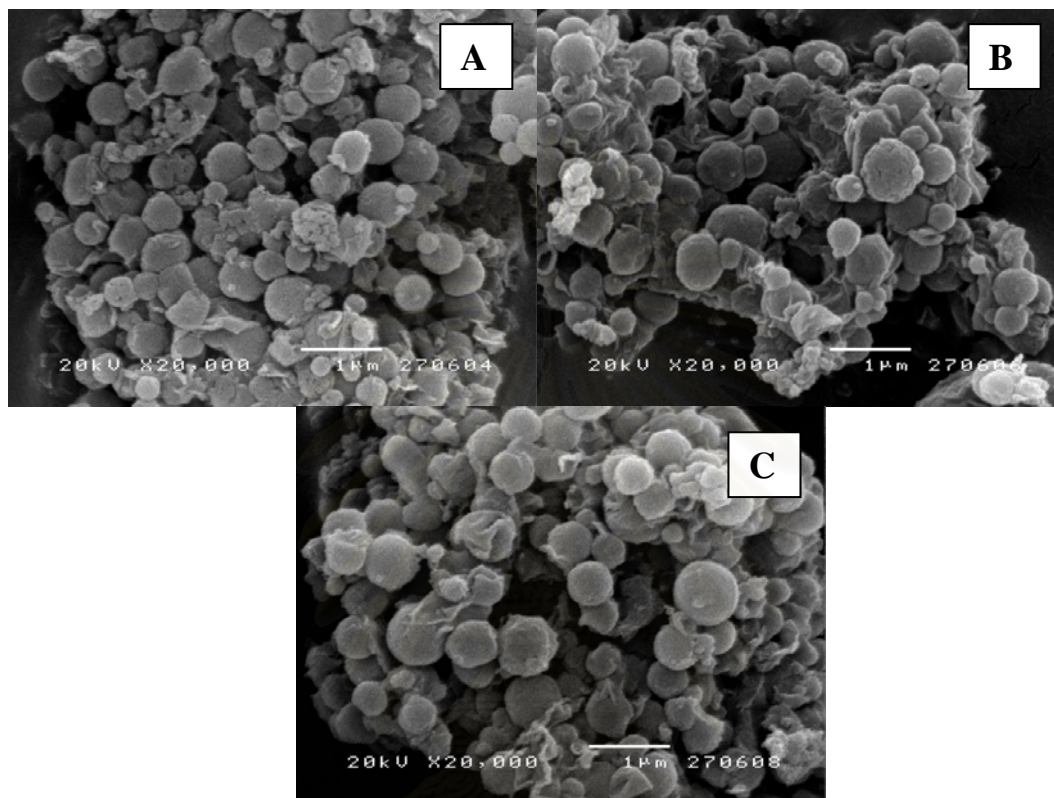


Figure 4.12 SEM images of calcined Al-HMS with different Si/Al ratios in gel: (A) Al-HMS 20 (Si/Al = 20), (B) Al-HMS 60 (Si/Al = 60) and (C) Al-HMS 200 (Si/Al = 200).

4.2 The characterization of ZSM-5/Al-HMS composite catalysts

4.2.1 XRD Results

From Soamwadee C. [86] reported, the conversion of PP degradation was maximum at Al-HMS with Si/Al mole ratio in gel of 60. Therefore, the initial study for this work was chosen for Al-HMS-60 in order to mix with ZSM-5 as composite catalyst. The physical composite catalyst was prepared by mixing weight ratio of ZSM-5 and Al-HMS as 1:1 and shaking by hand for 30 minutes. The XRD pattern of ZSM-5/Al-HMS-60 composite catalyst with weight ratio of 1:1 is shown in Figure

4.13. The composite catalyst showed the characteristic patterns of both ZSM-5 and Al-HMS structures.

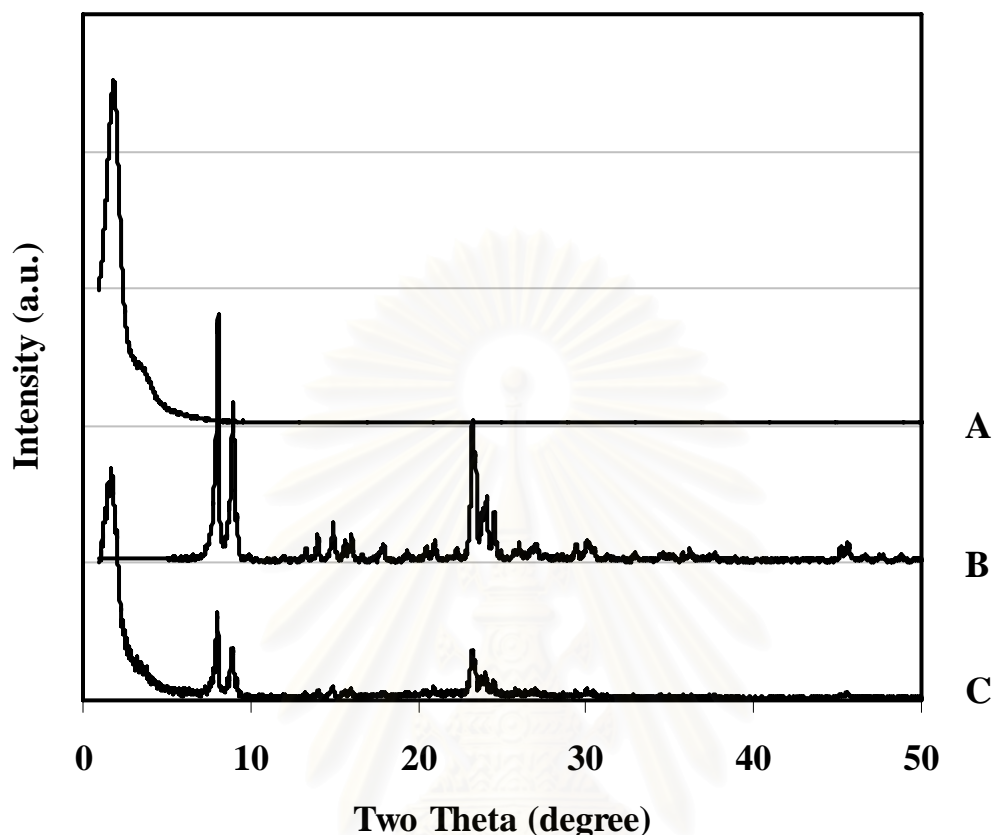


Figure 4.13 XRD patterns of catalysts: (A) Al-HMS-60, (B) ZSM-5 and (C) ZSM-5/Al-HMS-60 (1:1) composite catalyst.

4.2.2 Nitrogen Adsorption-Desorption

Nitrogen adsorption-desorption isotherm of ZSM-5/Al-HMS-60 composite catalyst with ratio of 1:1 is shown in Figure 4.14. The composite catalyst exhibited hysteresis loop of type IV adsorption isotherm which is a characteristic pattern of mesoporous materials while the pure of ZSM-5 and Al-HMS-60 catalyst showed hysteresis loops of type I and type IV, respectively. The BET specific surface area and pore diameter of composite were $539 \text{ m}^2/\text{g}$ and 4.9 nm , respectively which were between values of the pure of ZSM-5 and Al-HMS-60 catalyst.

Table 4.6 BET specific surface area and pore diameter of calcined catalysts

Sample	$a_{s, \text{BET}}$ (m^2/g)	Pore diameter (nm)
ZSM-5	411	2.4
ZSM-5/Al-HMS-60	539	4.9
Al-HMS-60	730	6.1

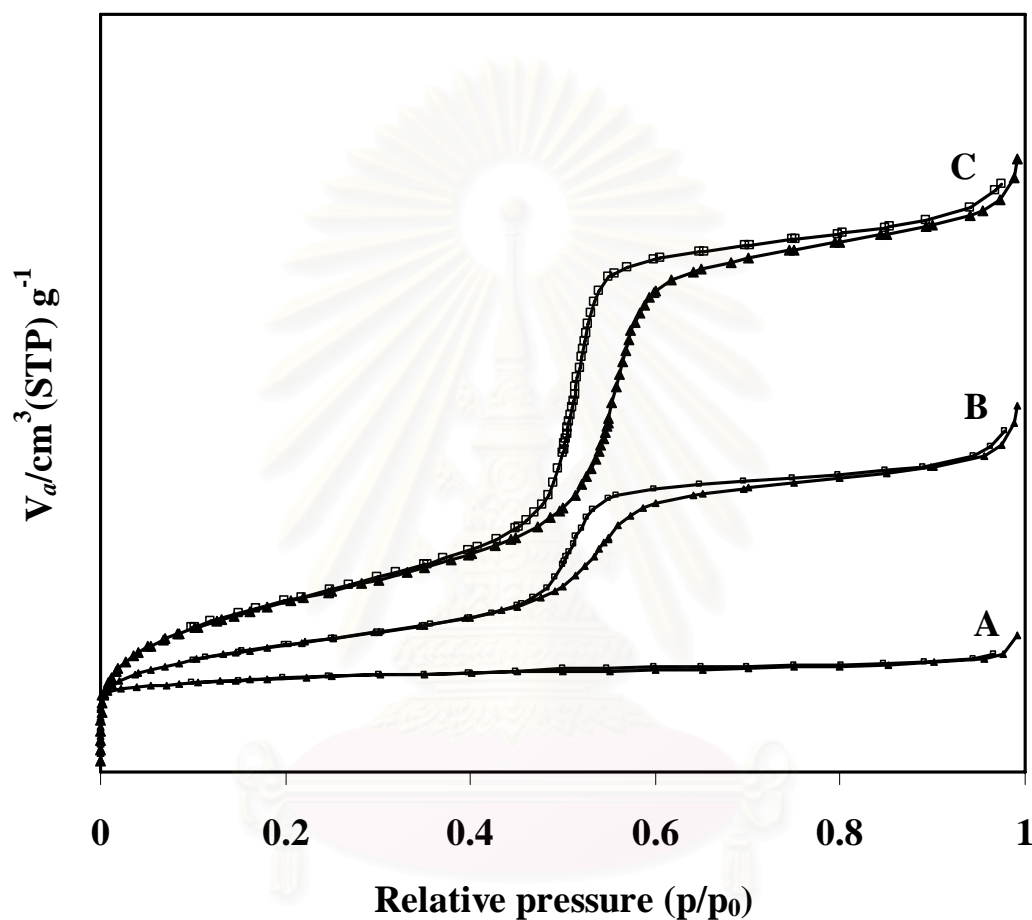


Figure 4.14 N_2 adsorption-desorption isotherms of ZSM-5/Al-HMS-60 ratio 1:1 composite catalyst compared with the pure of ZSM-5 and Al-HMS-60 catalyst: (A) ZSM-5, (B) ZSM-5/Al-HMS-60 (1:1) composite catalyst and (C) Al-HMS-60.

4.3 Activity of ZSM-5/Al-HMS composite catalysts in HDPE Cracking

4.3.1 Effect of Temperature

ZSM-5/Al-HMS-60 composite catalyst with ZSM-5:Al-HMS-60 weight ratio of 1:1 was used for studying effect of temperature on its activity. Conversion and the product yields for catalytic cracking of HDPE over ZSM-5/Al-HMS-60 (1:1) at 350°C, 400°C and 450°C are shown in Table 4.7. At 350°C, the reaction conversion was low and residue remained in the reactor was white candle wax. When the reaction temperature increased from 350°C to 450°C, conversion of HDPE increased from 10.5 wt% to more than 90 wt% and the products were mainly in gas fraction. The residues at 400°C and 450°C were less than at 350°C. The conversion of HDPE at 400°C and 450°C were not different but the yield of gas product was slightly higher at 450°C. This can be explained that with increasing reaction temperature, HDPE diffuses into the catalyst pore easier and generates more carbocation intermediates [77-80]. When increased temperature, carbocations can decompose through the so-called “ β scission” to form a smaller carbocation and an olefin which resulting light hydrocarbon products. A large difference in conversion between catalytic and thermal cracking indicating the efficiency of catalyst was obtained at 400°C as 91.8 wt%. With increasing reaction temperature, the efficiency of catalyst decreased because of the effect of thermal cracking. Thus, the optimal temperature for catalytic cracking of PE in this work was 400°C. With increasing reaction temperature, the initial rate of liquid fraction formation at 450°C was much faster than that at 400°C, as shown in figure 4.15.

Figure 4.16 shows distribution of gas fraction obtained by catalytic cracking of HDPE over ZSM-5/Al-HMS-60 (1:1) composite catalysts at 350°C, 400°C and 450°C. Considering only gases at ambient condition which are normally C_1 through C_5 , the major components for catalytic cracking at 400°C and 450°C were propene. However, the vapor of C_5+ (liquids at ambient condition) which had higher boiling point than that of C_5 (n-pentane) was obviously detected in a significant amount. Figure 4.17 shows distribution of gas fraction obtained by thermal cracking of HDPE at 400°C and 450°C. For thermal cracking, the main products were ethene, propene and C_5+ .

Table 4.7 Thermal and catalytic cracking of HDPE over ZSM-5/Al-HMS-60 (1:1) composite catalysts at various reaction temperatures

Reaction temperature	350°C		400°C		450°C	
Cracking	Thermal	Catalytic	Thermal	Catalytic	Thermal	Catalytic
Conversion (%)	0.0±0.0	10.5±0.3	4.6±0.2	96.4±0.0	87.7±0.1	95.4±0.0
Product yield (%)						
1. gas fraction	0.0±0.0	10.3±0.3	4.6±0.2	59.0±0.2	30.3±0.1	64.7±0.1
2. liquid fraction	0.0±0.0	0.2±0.0	0.0±0.0	37.4±0.2	57.4±0.0	30.7±0.1
- % heavy oil	-	-	-	21.7	46.3	13.7
- % distillate oil	-	-	-	15.7	11.1	17.0
3. residue	0.0±0.0	89.5±0.3	95.4±0.2	3.6±0.0	12.3±0.1	4.6±0.0
- wax	0.0	89.5	95.4	3.2	12.3	3.8
- solid coke	-	0.0	-	0.4	-	0.8
Total volume of liquid fraction (cm ³)	-	-	-	2.6	3.9	2.2
Liquid fraction density (g/cm ³)	-	-	-	0.71	0.74	0.72
Δ conversion (%)	10.5		91.8		7.7	

Reaction condition: 10 wt% of catalyst, 30 min, 20 cm³/min.N₂ flow.

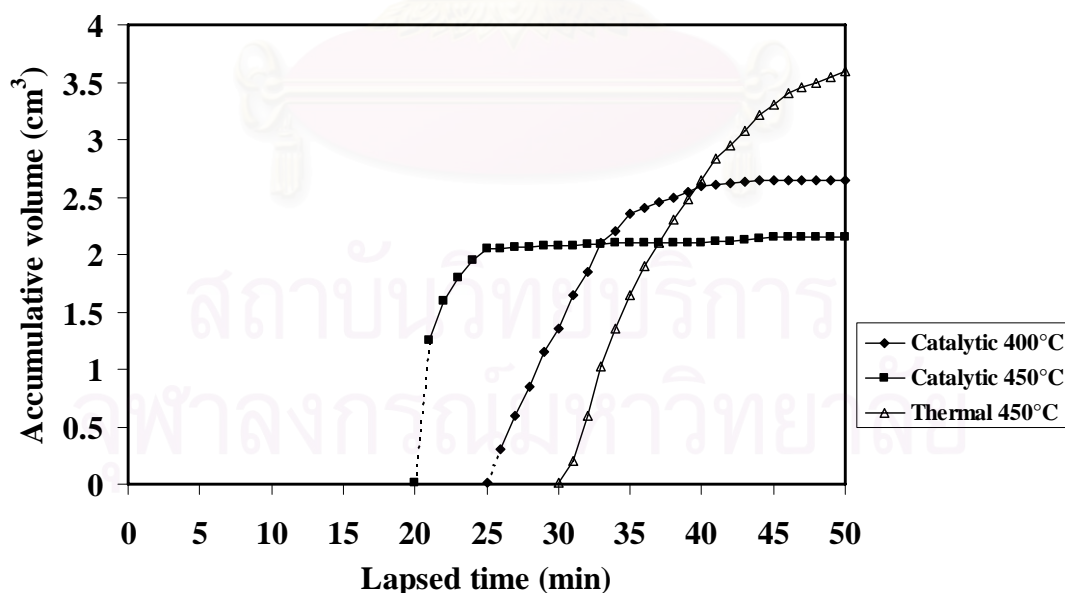


Figure 4.15 Accumulative liquid volume of liquid fractions obtained from thermal and catalytic cracking of HDPE over ZSM-5/Al-HMS-60 (1:1) composite catalysts at various reaction temperatures.

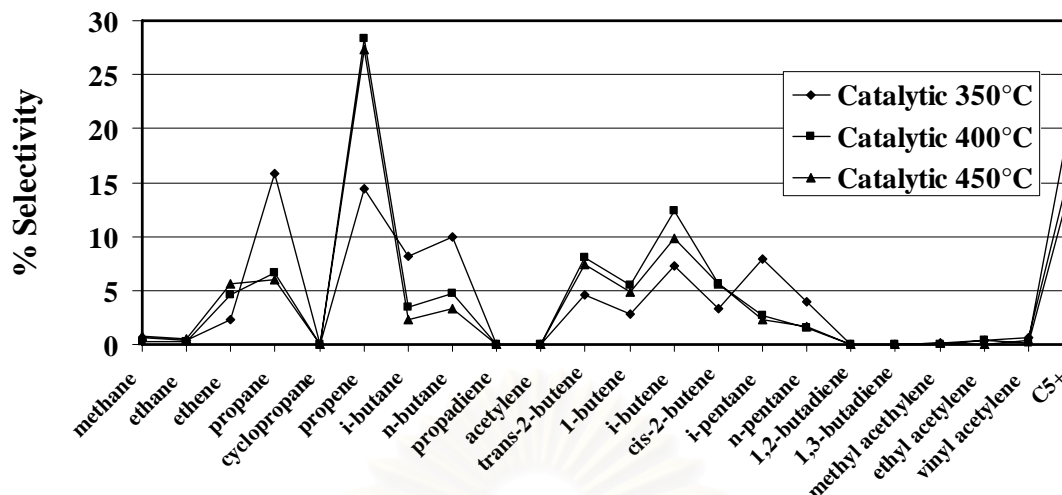


Figure 4.16 Gas product distributions from catalytic cracking of HDPE over ZSM-5/Al-HMS-60 (1:1) composite catalysts at various reaction temperatures.

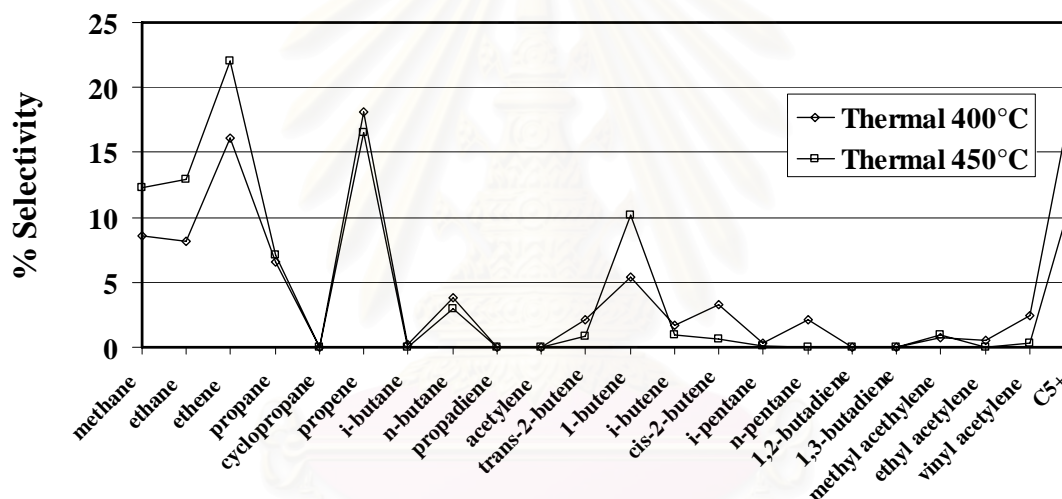


Figure 4.17 Gas product distributions from thermal cracking of HDPE at various reaction temperatures.

Figure 4.18 shows product distribution of distillate oils obtained by catalytic cracking of HDPE over ZSM-5/Al-HMS-60 (1:1) composite catalysts at 400°C and 450°C. The distillate oils were mainly composed of hydrocarbons in the range of C₇ to C₈ which is similar to the standard gasoline oil, while thermal cracking produced wide hydrocarbon products in range of C₆-C₈. For catalytic cracking, with increasing reaction temperature, the liquid compositions were not significantly changed.

Therefore, it has been concluded that with increasing the reaction temperature, HDPE diffuses into the catalyst pore easier and generates more carbocation intermediates. That results in faster rate of reaction, high conversion and product

yields. However, there was no effect on product distribution in both gas and liquid phase. Thus, the reaction temperature at 400°C was chosen for further study due to the high conversion, high liquid fraction, and low coke.

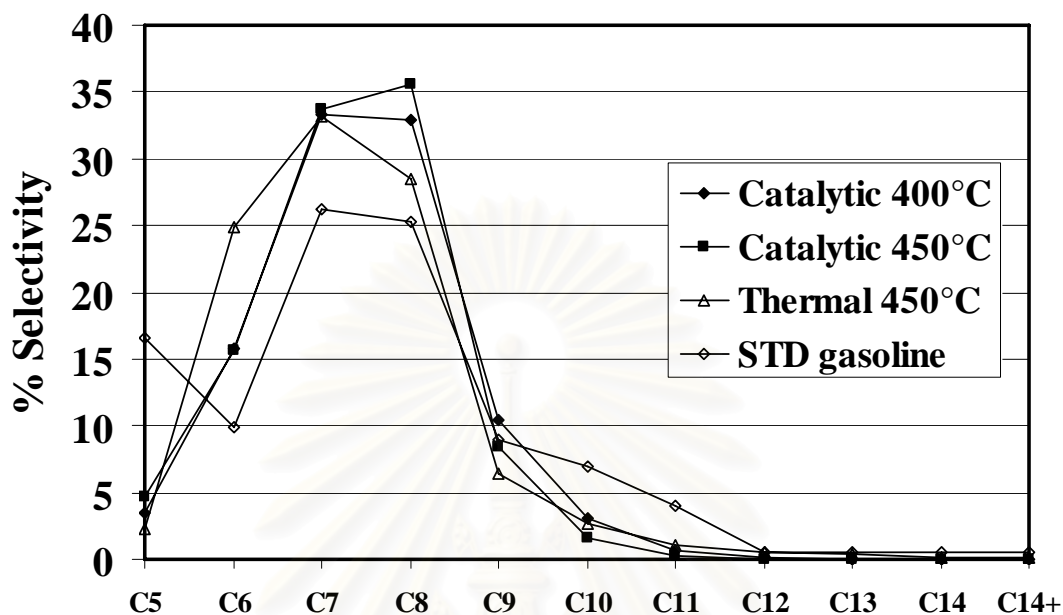


Figure 4.18 Carbon distribution numbers of distillate oils from thermal and catalytic cracking of HDPE over ZSM-5/Al-HMS-60 (1:1) composite catalysts at 400°C and 450°C.

4.3.2 Effect of catalytic to plastic ratio

The 1:1 composite ZSM-5/Al-HMS-60 composite catalyst (ZSM-5/Al-HMS-60 (1:1)) was used to study the effect of catalytic to plastic ratio on its activity. Conversion and product yields for the thermal cracking and catalytic cracking of HDPE over ZSM-5/Al-HMS-60 (1:1) composite catalysts with various catalytic to plastic ratios at 400°C are shown in Table 4.8. When the catalytic cracking was performed, high conversions of HDPE were observed with tremendous decrease of residue. It is suggested that the composite catalyst accelerated the cracking of HDPE into light hydrocarbons. When the catalytic to plastic ratios increased, the amount of residue decreased from 8.30 wt% to 1.60 wt%. It is suggested that the reactions were more accelerated in degradation because the acidity increased. A change in product yields was observed by an increasing trend of liquid products from 2 to 10 wt% of catalyst and a reduction of liquid products at 20 wt%. The result may be explained that the waxy residue decomposed into light hydrocarbons resulting in high product

yields especially in liquid fraction. On the other hand, with 20 wt% of catalyst to plastic ratio, high gas fraction was noticed and high value of coke (0.90 wt%) was produced. This can be explained that the highest acidity was obtained at 20 wt% catalytic to plastic resulting in gas yield. For 5-10 wt% of catalyst, high value of conversion, lower gas fraction and less coke deposited were obtained at 400°C compared to the 20 wt% of catalyst. In addition, the 10 wt% of catalyst gave slightly higher values of liquid fraction in heavy oils and least coke deposited on catalyst. Therefore, the 10 wt% of composite catalyst was the suitable catalyst in this study.

Table 4.8 Thermal cracking and catalytic cracking of HDPE over ZSM-5/Al-HMS-60 (1:1) composite catalysts with various catalytic to plastic ratios

% weight of catalyst	2% catalyst	5% catalyst	10% catalyst	20% catalyst	Thermal
Conversion (%)	91.7±0.1	96.2±0.0	96.4±0.0	98.4±0.0	4.6±0.2
Product yield (%)					
1. gas fraction	62.8±0.0	60.7±0.1	59.0±0.2	66.1±0.1	4.6±0.2
2. liquid fraction	28.9±0.1	35.5±0.1	37.4±0.2	32.3±0.1	0.0±0.0
- % heavy oil	15.1	19.9	21.7	17.0	-
- % distillate oil	13.8	15.6	15.7	15.3	-
3. residue	8.3±0.1	3.8±0.0	3.6±0.0	1.6±0.0	95.4±0.2
- wax	6.6	3.3	3.2	0.7	-
- solid coke	1.7	0.5	0.4	0.9	-
Total volume of liquid fraction (cm ³)	2.2	2.5	2.6	2.1	-
Liquid fraction density (g/cm ³)	0.66	0.71	0.71	0.75	-

Reaction condition: 400°C, 30 min, 20 cm³/min.N₂ flow.

Figure 4.19 shows the accumulative volume of liquid fractions in the graduated cylinder and the temperature of the reactor increased as a function of lapsed time. Although the initial rates of liquid fraction formation for 20 wt% and 10 wt% of catalyst to plastic ratio were similar, but the overall content of liquid fraction was slightly different.

Figure 4.20 shows product distribution of gas fraction obtained by thermal cracking and catalytic cracking of HDPE over ZSM-5/Al-HMS-60 (1:1) composite

catalysts with various catalytic to plastic ratios at 400°C. In the presence of any catalytic to plastic ratios catalysts, the product distribution in gas fraction was different from that in the absence of catalyst or thermal pyrolysis. For catalytic cracking, the major components of gas fraction were C₃ (propene), C₅+, and C₄ (iso-butene). While thermal cracking, the major components of gas fraction were C₂ (ethene), C₃ (propene), and C₅+

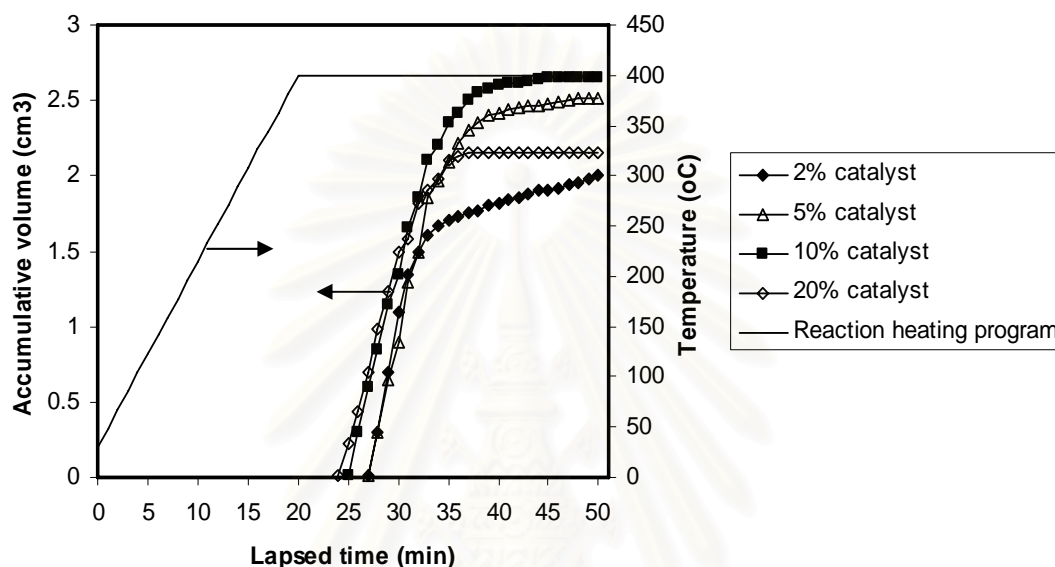


Figure 4.19 Accumulative volume of liquid fractions obtained by catalytic cracking of HDPE over ZSM-5/Al-HMS-60 (1:1) composite catalysts with various catalytic to plastic ratios.

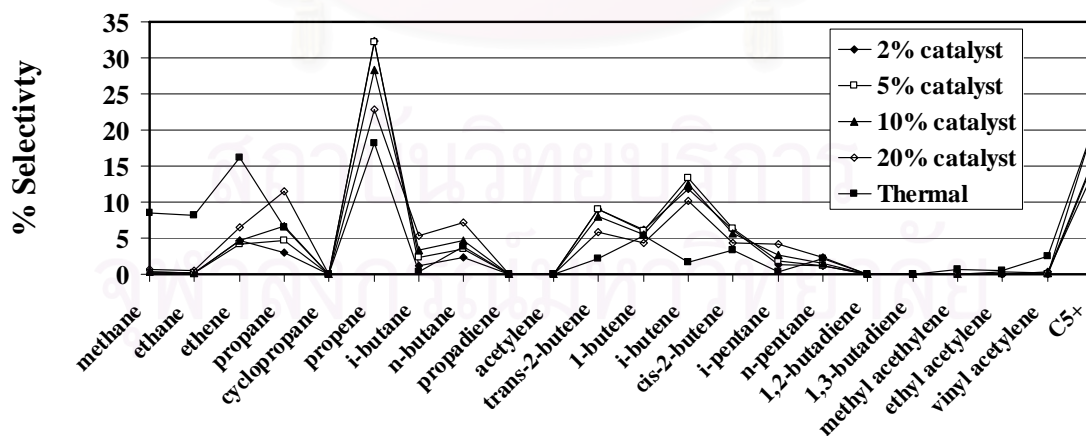


Figure 4.20 Distribution of gas fraction obtained by thermal cracking and catalytic cracking of HDPE over ZSM-5/Al-HMS-60 (1:1) composite catalysts with various catalytic to plastic ratios.

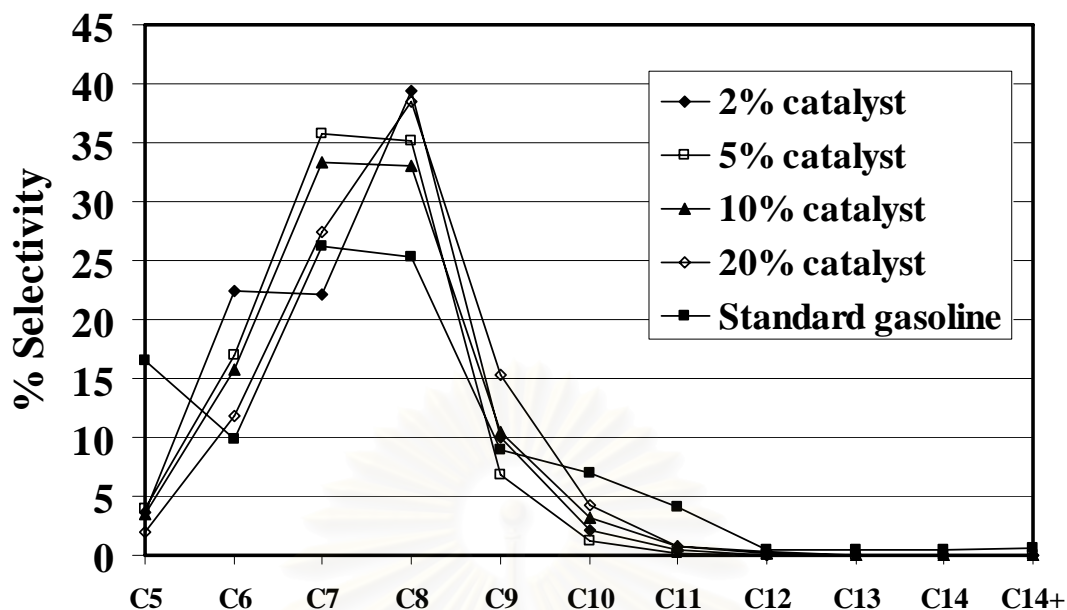


Figure 4.21 Carbon number distribution of distillate oils from catalytic cracking of HDPE over ZSM-5/Al-HMS-60 (1:1) composite catalysts with various catalytic to plastic ratios.

Figure 4.21 shows product distributions of distillate oil obtained by catalytic cracking of HDPE over ZSM-5/Al-HMS-60 (1:1) composite catalysts at 400°C with various catalytic to plastic ratios. The distillate oil components were mainly composed of hydrocarbons in the range of C₇ to C₈ for 5-20 wt% of catalyst, which were similar to the gasoline standard. When the catalytic to plastic ratio increased, the liquid fractions of heavier hydrocarbon (C₉-C₁₀) slightly increased. For 2 wt% catalytic to plastic ratio, liquid products obtained were in a wide range of hydrocarbon (C₆-C₈).

Therefore, it has been concluded that acidity and active site increased with increasing catalytic to plastic ratio. That results in faster rate of reaction, high conversion and product yields. However, there was no significant effect on product distribution in both gas and liquid phase. Thus, the 10 wt% catalytic to plastic ratio was chosen for further study due to the high conversion, high liquid fraction, and low coke.

4.3.3 Effect of ZSM-5:Al-HMS ratio in composite catalyst

Conversions and product yields for catalytic cracking of HDPE over ZSM-5/Al-HMS-60 composite catalysts with various ZSM-5:Al-HMS ratios in composite

catalyst were performed at 400°C and 10 wt% catalyst, compared to those over pure ZSM-5 and Al-HMS-60. The data are shown in Table 4.9. Conversions of pure ZSM-5 and the 2:1, 1:1, and 1:2 composites were not different and high values of gas fraction were obtained. In contrast, conversion of HDPE over pure Al-HMS-60 was lower and high liquid fraction was obtained. These results indicated that ZSM-5 had high performance in cracking of HDPE over Al-HMS-60 due to high acidity of ZSM-5 (0.429 mmole/g) over Al-HMS-60 (0.342 mmole/g). In addition, high fraction of gas product was obtained because small pore size of ZSM-5 can allow straight carbon chain structure of HDPE to access the active sites and restrict the product exit. In contrast to ZSM-5, Al-HMS-60 had low acidity and large pore size thus large molecules of HDPE were cracked into small hydrocarbon oligomers and produced more liquids which enriched in heavy oil content. For the 2:1, 1:1, and 1:2 composite catalysts, the conversions were not different but the product selectivity was significantly changed. With increasing the Al-HMS-60 content, the values of gas fraction decreased while the liquid fraction was increased. The high content of heavy oil was also observed compared to pure ZSM-5. The data suggested with increasing Al-HMS-60 content, decreasing of acidity and increasing the content of large pore size of Al-HMS, the reaction produced more liquids. Thus, the composite catalysts can act as pure ZSM-5 and Al-HMS-60 depending on the desired product. For example, if high distillate liquid fraction was desired, high content of Al-HMS-60 in composite catalyst such as the 1:2 composition was suggested however high solid coke was its drawback. For the 1:1 composite catalyst, conversion and product yields were not different from the 1:2 composite catalyst except the high content of heavy oil and low values of distillate oil and solid coke. In this work, the 1:1 composite catalyst was chosen for further studied in this work due to the lowest yield of solid coke as 0.41 wt% and high yield of liquid fraction.

Figure 4.22 shows the accumulative volume of liquid fractions in the graduated cylinder and the temperature of the reactor increased as a function of lapsed time. Although the initial rates of liquid fraction formation for all ratios were similar, but that of the 1:1 composite catalyst (50 wt% of ZSM-5) was faster than other ratios.

Table 4.9 Catalytic cracking of HDPE over ZSM-5/Al-HMS-60 composite catalysts with various ZSM-5:Al-HMS ratios in composite catalyst

ZSM-5:Al-HMS ratio in composite catalyst	ZSM-5 (100 wt% of ZSM-5)	2:1 (67 wt% of ZSM-5)	1:1 (50 wt% of ZSM-5)	1:2 (33 wt% of ZSM-5)	Al-HMS60 (0 wt% of ZSM-5)
Conversion (%)	97.5±0.1	96.6±0.0	96.4±0.0	96.4±0.0	93.9±0.1
Product yield (%)					
1. gas fraction	67.1±0.1	64.5±0.1	59.0±0.2	58.8±0.2	39.4±0.2
2. liquid fraction	30.4±0.0	32.1±0.1	37.4±0.2	37.6±0.2	54.5±0.1
- % heavy oil	13.9	19.7	21.7	18.5	36.1
- % distillate oil	16.5	12.4	15.7	19.1	18.4
3. residue	2.5±0.1	3.4±0.0	3.6±0.0	3.6±0.0	6.1±0.1
- wax	1.6	2.9	3.2	2.7	4.8
- solid coke	0.9	0.5	0.4	0.9	1.3
Total volume of liquid fraction (cm ³)	2.2	2.3	2.6	2.6	3.7
Liquid fraction density (g/cm ³)	0.69	0.70	0.71	0.71	0.74

Reaction condition: 10 wt% of catalyst, 400°C, 30 min, 20 cm³/min.N₂ flow.

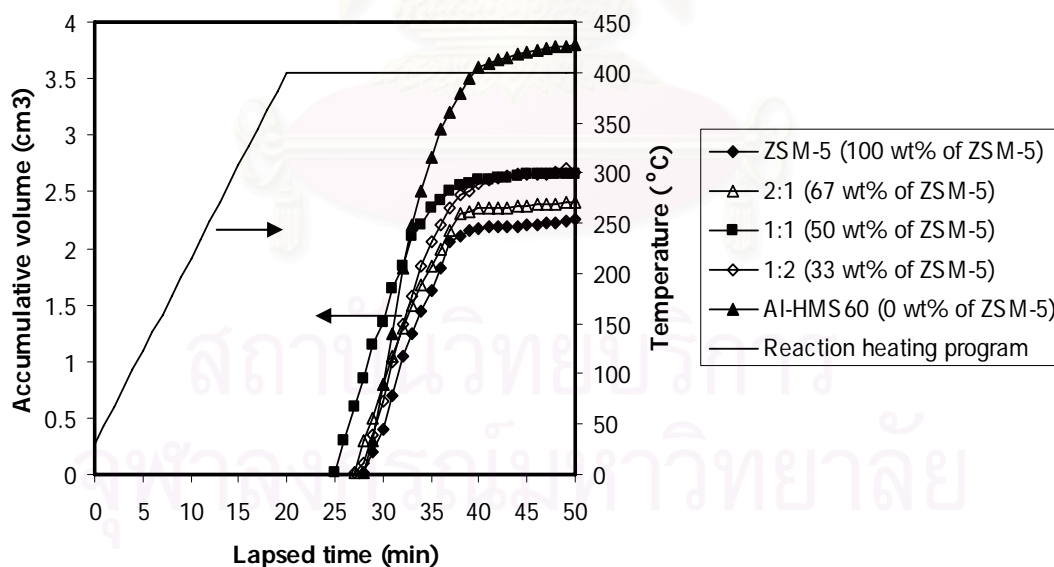


Figure 4.22 Accumulative volume of liquid fractions obtained by catalytic cracking of HDPE over ZSM-5/Al-HMS-60 composite catalysts with various ZSM-5:Al-HMS ratios in composite catalyst.

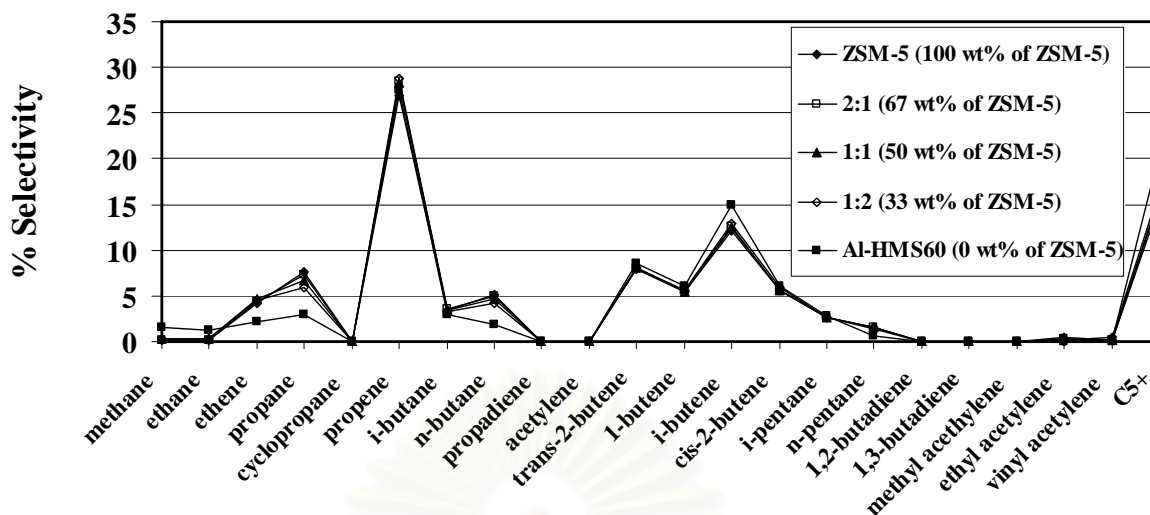


Figure 4.23 Distribution of gas fraction obtained by catalytic cracking of HDPE over ZSM-5/Al-HMS-60 composite catalysts with various ZSM-5:Al-HMS ratios in composite catalyst.

Figure 4.23 shows distribution of gas fraction obtained by catalytic cracking of HDPE over ZSM-5/Al-HMS-60 composite catalysts with various ZSM-5:Al-HMS ratios in composite catalyst. For all composite ratios, the major components in gas fraction were mainly C_3 (propene) and C_4 (iso-butene). While pure Al-HMS-60 yielded C_4 (iso-butene) and C_{5+} more than other composite ratios due to the high content of large pore size of Al-HMS-60.

Figure 4.24 shows product distribution of distillate oil obtained by catalytic cracking of HDPE over ZSM-5/Al-HMS-60 composite catalysts with various ZSM-5:Al-HMS ratios in composite catalyst. The distillate oil components of composites were mainly in hydrocarbons range from C_7 to C_8 that were similar to the standard gasoline oil except 0 wt% of ZSM-5 (pure Al-HMS) that obtained wide range of hydrocarbons from C_6 - C_8 due to the high content of large pore size of Al-HMS-60.

Therefore, it has been concluded that with increasing ZSM-5:Al-HMS ratios, acidity increased and large pore size of Al-HMS decreased. That results in high gas fraction, high solid coke and low liquid yield. However, there was no significant effect on product distribution in both gas and liquid phase. Thus, the 1:1 ZSM-5:Al-HMS ratio was chosen for further study due to the high conversion, high liquid fraction, and low coke.

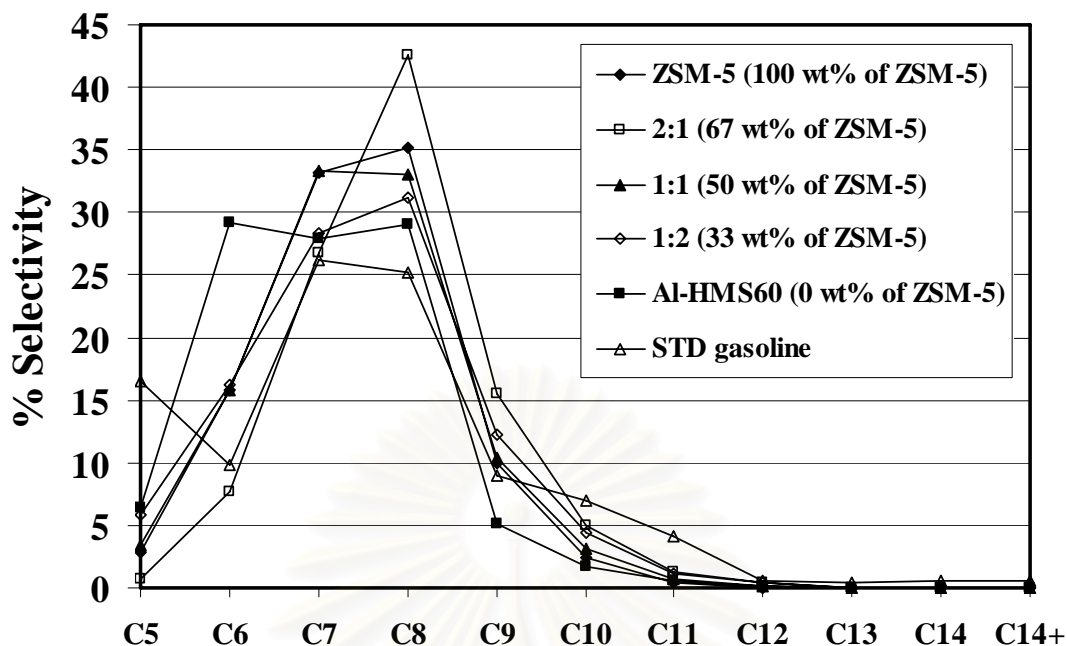


Figure 4.24 Carbon number distribution of distillate oils from catalytic cracking of HDPE over ZSM-5/Al-HMS-60 composite catalysts with various ZSM-5:Al-HMS ratios in composite catalyst.

4.3.4 Effect of aluminium content in catalyst

To study effect of aluminium contents in Al-HMS catalyst, the cracking of HDPE over ZSM-5/Al-HMS (1:1) composite catalyst with various Si/Al ratios in Al-HMS were performed at 400°C and 10 wt% of catalyst to plastic ratio. Their catalytic activities are shown in Table 4.10. When aluminium contents increased, conversions of HDPE were not different but product selectivities were significantly different. For this study, the 1:1 composite of ZSM-5/Al-HMS-60 ratio gave high yield of liquid fraction and distillate oil and less solid coke than others. This may be due to the acidity of Al-HMS and the value of the ratio of peak area between tetrahedral and octahedral aluminium. Figure 4.25 shows the accumulative volume of liquid fractions in the graduated cylinder and the temperature of the reactor increased as a function of lapsed time. Although the initial rates of liquid fraction formation for all catalysts were similar, but the 1:1 composite of ZSM-5:Al-HMS-60 catalyst gave faster kinetic rate than other catalysts.

Table 4.10 Catalytic cracking of HDPE over ZSM-5/Al-HMS composite catalysts with various Si/Al ratios in Al-HMS

Si/Al ratio in gel in Al-HMS (ZSM-5:Al-HMS ratio)	20 (1:1)	60 (1:1)	200 (1:1)
Conversion (%)	96.1±0.1	96.4±0.0	96.6±0.0
Product yield (%)			
1. gas fraction	66.3±0.1	59.0±0.2	70.7±0.1
2. liquid fraction	29.8±0.0	37.4±0.2	25.9±0.1
- % heavy oil	23.0	21.7	20.0
- % distillate oil	6.8	15.7	5.9
3. residue	3.9±0.1	3.6±0.0	3.4±0.0
- wax	2.8	3.2	2.5
- solid coke	1.1	0.4	0.9
Total volume of liquid fraction (cm ³)	2.0	2.6	1.8
Liquid fraction density (g/ cm ³)	0.74	0.71	0.73

Reaction condition: ZSM-5:Al-HMS ratio of 1:1, 10 wt% of catalyst, 400°C,

30 min, 20 cm³/min.N₂ flow.

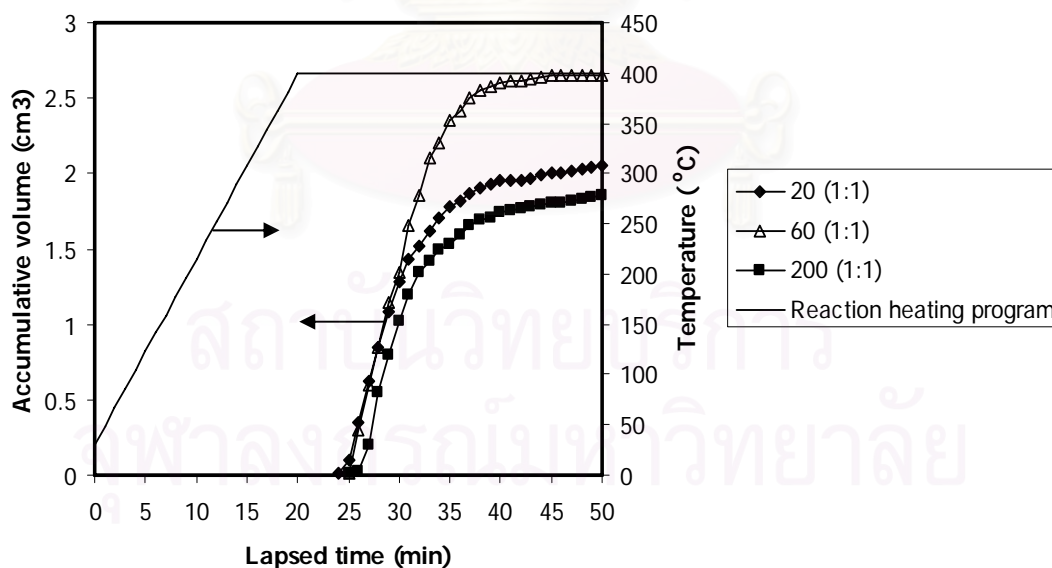


Figure 4.25 Accumulative volume of liquid fractions obtained by catalytic cracking of HDPE over ZSM-5/Al-HMS composite catalysts with various aluminium contents in Al-HMS.

Figure 4.26 shows product distribution of gas fraction obtained by catalytic cracking of HDPE over ZSM-5/Al-HMS composite catalysts with various aluminium contents in Al-HMS. For all aluminium contents, the distributions of gas fraction were in the same trend. The major components of gas fraction were C₃ (propene), C₅₊ and C₄ (iso-butene).

Figure 4.27 shows product distribution of distillate oil obtained by catalytic cracking of HDPE over ZSM-5/Al-HMS composite catalysts with various aluminium contents in Al-HMS comparing with the commercial SUPELCO standard gasoline fraction. The distillate oil components from catalytic crackings were composed of hydrocarbons in the range of C₅-C₁₂ but mainly in C₇ to C₈ as the standard gasoline.

Therefore, it has been concluded that with increasing aluminium contents, acidity increased and the ratio of peak area between tetrahedral and octahedral aluminium decreased. That results in high conversion and the value of product yields. However, there was no significant effect on product distribution in both gas and liquid phase. Thus, the ZSM-5:Al-HMS-60 was chosen for further study due to the high liquid fraction, and low coke.

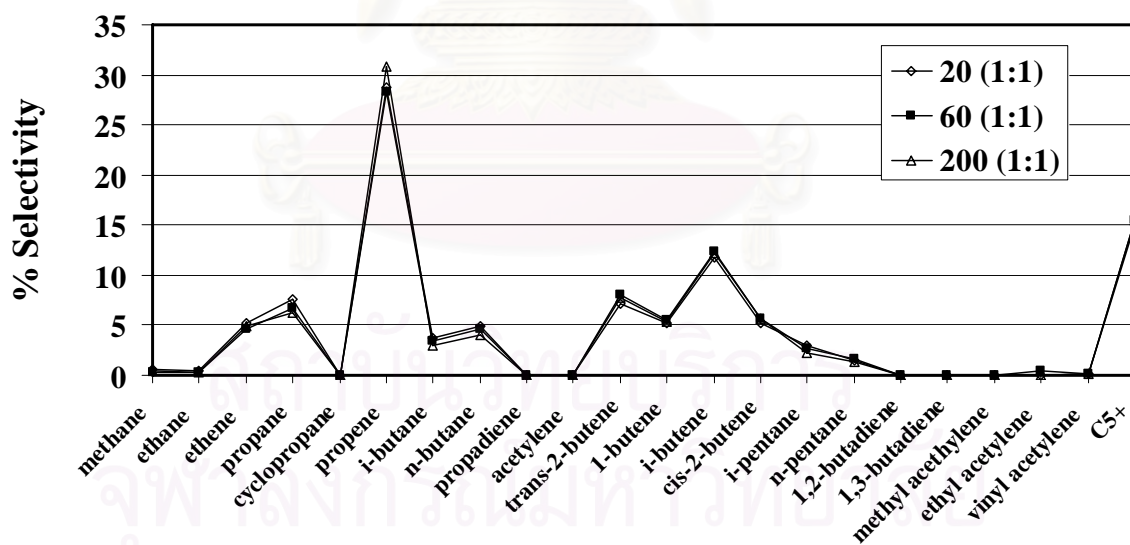


Figure 4.26 Distribution of gas fraction obtained by catalytic cracking of HDPE over ZSM-5/Al-HMS composite catalysts with various aluminium contents in Al-HMS.

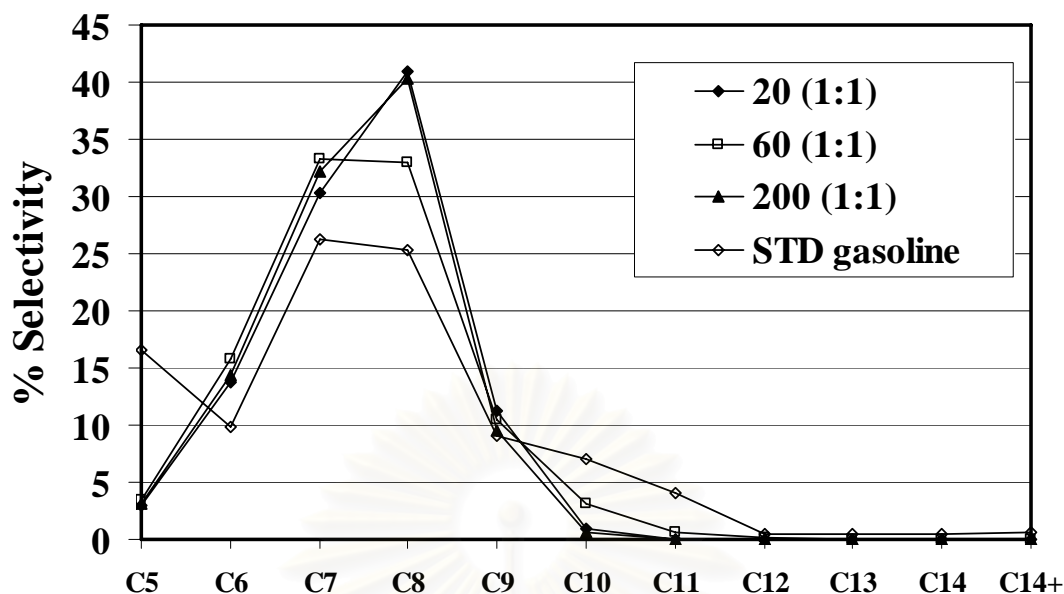


Figure 4.27 Carbon number distribution of distillate oils from the commercial SUPELCO standard gasoline fraction and catalytic cracking of HDPE over ZSM-5/Al-HMS composite catalysts with various aluminium contents in Al-HMS.

4.4 Activity of ZSM-5/Al-HMS composite catalysts in PP Cracking

4.4.1 Effect of Temperature

ZSM-5/Al-HMS-60 composite catalyst with the ZSM-5:Al-HMS-60 ratio of 1:1 was used for studying the effect of temperature on its activity. Conversion and product yields for thermal and catalytic cracking of PP over ZSM-5/Al-HMS-60 (1:1) at 350°C, 400°C and 450°C are shown in Table 4.11. For thermal cracking, conversion increased when temperature increased. When the reaction temperature for catalytic cracking increased from 350°C to 450°C, PP conversions increased and product selectivity for gas fraction increased from 37.70 wt% to 43.80 wt%. For 350°C, even though catalytic conversion was high as 67.60 wt% which corresponded to yield of residue as 32.40 wt%, the white candle wax remained in the reactor and it was difficult to remove and find for solid coke. While at 400°C and 450°C, high values of PP conversion were obtained about 96 wt%, but yield of solid coke at 450°C was higher than that at 400°C. In addition, liquid fraction obtained was also lower while the gas fraction was higher. This can be explained that increasing reaction temperature, PP diffuses into the catalyst pore easier and generates more carbocation intermediates which resulting light hydrocarbon products. When the different

conversions between catalytic and thermal cracking were compared, the highest conversion was obtained from the temperature of 350°C, which suggested the performance of composite catalyst. However, the reaction temperature at 400°C for 30 min was chosen for further studies of PP cracking in order to compare with HDPE cracking. And, it will be noted that the conversion of PP at 400°C resulted from both thermal and catalyst performance.

Figure 4.28 shows the accumulative volume of liquid fractions in the graduated cylinder and the temperature of the reactor increased as a function of lapsed time. Although the initial rate of liquid fraction formation at 450°C was faster than that those at 400°C, but liquid volume of both were not different. If the reaction temperature was performed at 350°C, the reaction time should be longer than 30 min in order to allow the reaction to reach equilibrium and gave highest performance of the composite catalyst alone. Thus, the reaction temperature at 400°C was chosen for the reaction time at 30 min.

Table 4.11 Thermal and catalytic cracking of PP over ZSM-5/Al-HMS-60 (1:1) composite catalysts at various reaction temperatures

Reaction temperature	350°C		400°C		450°C	
	Thermal	Catalytic	Thermal	Catalytic	Thermal	Catalytic
Cracking						
Conversion (%)	2.7±0.1	67.6±0.0	67.0±0.0	96.1±0.1	94.1±0.1	96.3±0.1
Product yield (%)						
1. gas fraction	2.7±0.1	37.7±0.0	24.7±0.2	42.9±0.1	25.8±0.0	43.8±0.0
2. liquid fraction	0.0±0.0	29.9±0.0	42.3±0.2	53.2±0.2	68.3±0.1	52.5±0.1
- % heavy oil	-	20.7	31.4	42.6	42.9	41.1
- % distillate oil	-	9.3	10.9	10.6	25.4	11.4
3. residue	97.3±0.1	32.4±0.0	33.0±0.0	3.9±0.1	5.9±0.1	3.7±0.1
- wax	97.3	32.4	33.0	3.1	5.9	2.7
- solid coke	-	0.0	-	0.8	-	1.0
Total volume of liquid fraction (cm ³)	-	2.0	2.9	3.6	4.6	3.5
Liquid fraction density (g/cm ³)	-	0.75	0.74	0.75	0.74	0.75
Δ conversion (%)	64.9		29.1		2.2	

Reaction condition: 10 wt% of catalyst, 30 min, 20 cm³/min.N₂ flow.

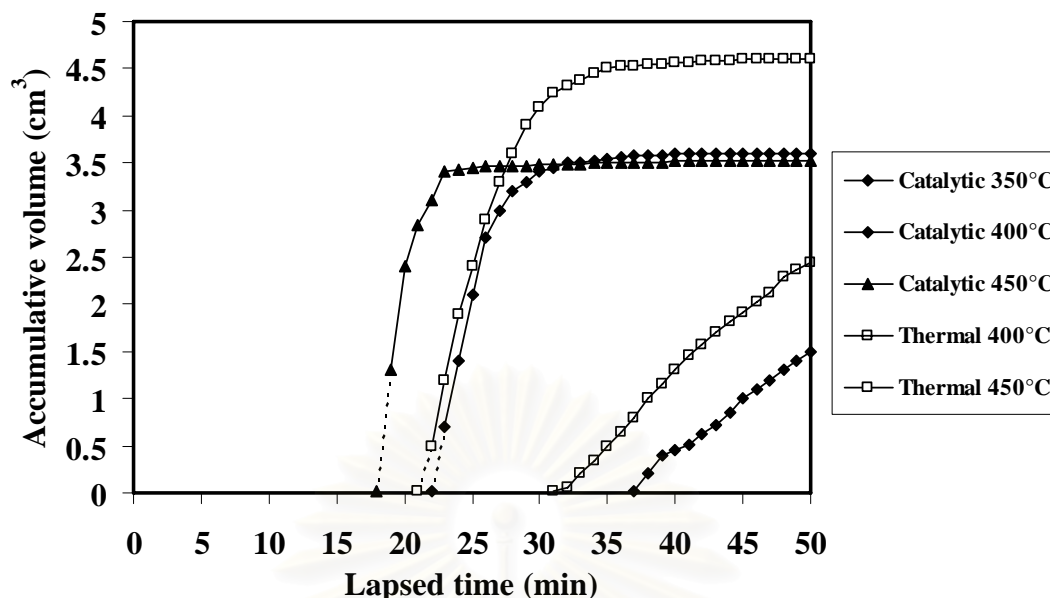


Figure 4.28 Accumulative volume of liquid fractions obtained by thermal and catalytic cracking of PP over ZSM-5/Al-HMS-60 (1:1) composite catalysts at 350°C, 400°C and 450°C.

Figure 4.29 shows product distribution of gas fraction obtained by catalytic cracking of PP over ZSM-5/Al-HMS-60 (1:1) composite catalysts at 350°C, 400°C and 450°C. All reactions showed similar trend in product distribution of gas fraction as follows; C_3 (propene) > C_5 + > C_4 (iso-butene), whereas thermal cracking major product was C_3 (propene) for 400 and 450°C, and was C_5 (n-pentane) for 350°C. During thermal cracking, a radical is formed through H-transfer reaction. The radical can also be formed through chain isomerization reaction being n-alkane such as n-pentane at mild condition (350°C). When temperature increased to 400-450°C, radicals can decompose through the so-called “ β scission” to form a smaller radical and an olefin (ethane and propene).

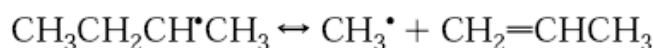
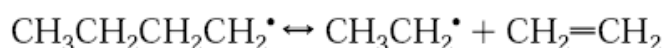
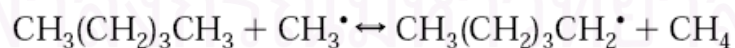


Figure 4.30 shows product distribution of distillate oil obtained by thermal and catalytic cracking of PP over ZSM-5/Al-HMS-60 (1:1) composite catalysts at 350°C, 400°C and 450°C. In case of catalytic cracking, distillate oils were mainly composed

of hydrocarbons in the range of C₇ to C₈ as the standard gasoline oil. When the reaction temperature increased from 400°C to 450°C, the liquid fractions of heavier hydrocarbon (C₉-C₁₀) increased. However, this change was not significant. In case of 350°C, the heavier hydrocarbons (C₉-C₁₀) were higher than the others significantly. The thermal crackings contained mainly C₆ and C₉ product and the compositions of distillate oils were also in similar trend.

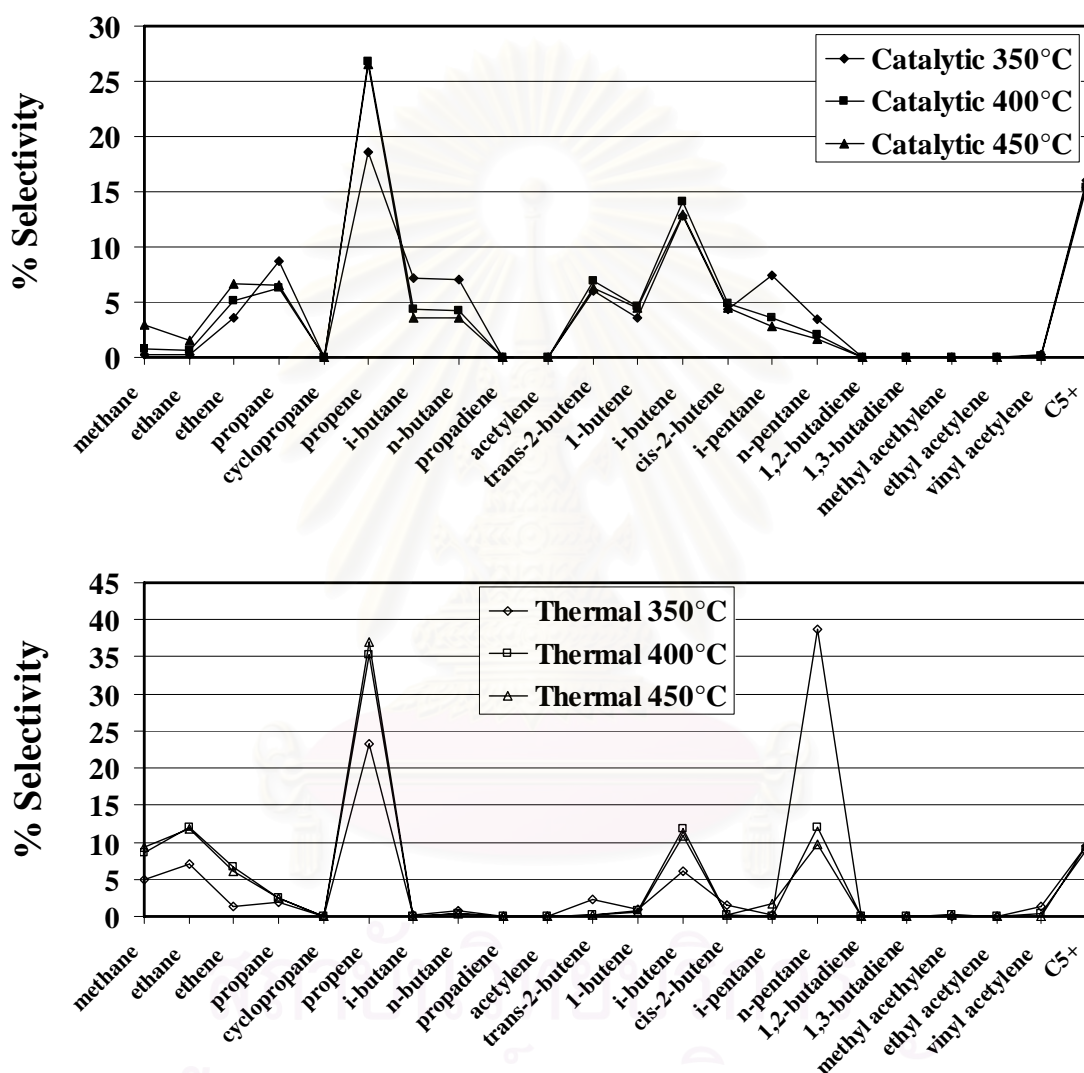


Figure 4.29 Distribution of gas fraction obtained by thermal and catalytic cracking of PP over ZSM-5/Al-HMS-60 (1:1) composite catalysts at 350°C, 400°C and 450°C.

Therefore, it has been concluded that with increasing the reaction temperature, PP diffuses into the catalyst pore easier and generates more carbocation intermediates. That results in faster rate of reaction, high conversion and product yields. However,

there was no effect on product distribution in both gas and liquid phase. Thus, the reaction temperature at 400°C was chosen for further study due to the high conversion, high liquid fraction, and low coke and in order to compare with HDPE cracking.

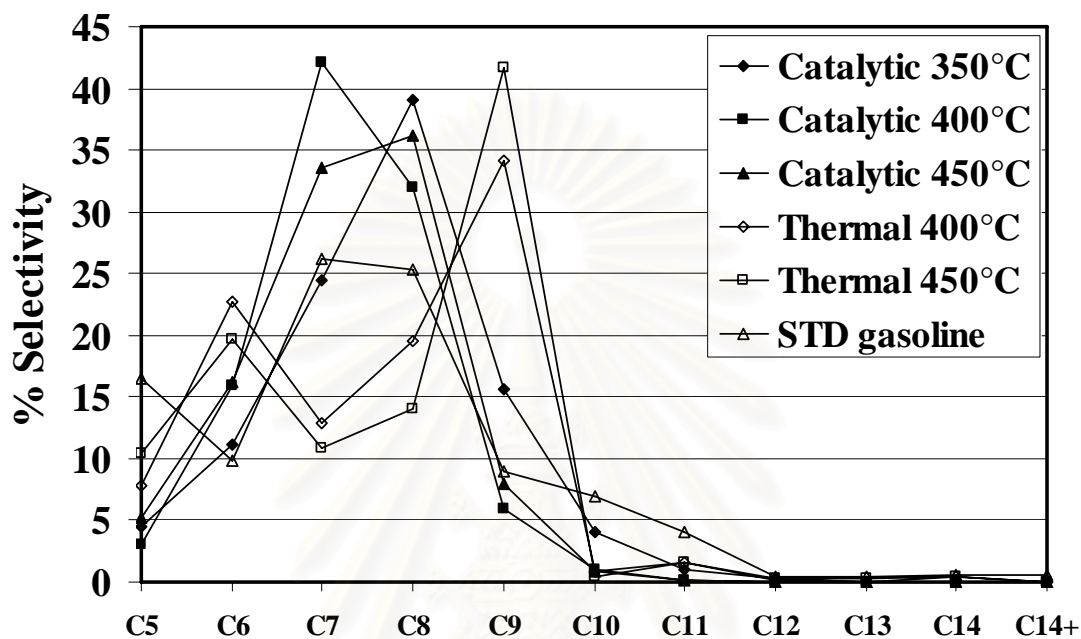


Figure 4.30 Carbon number distribution of distillate oils from thermal and catalytic cracking of PP over ZSM-5/Al-HMS-60 (1:1) composite catalysts at 350°C, 400°C and 450°C.

4.4.2 Effect of catalytic to plastic ratio

ZSM-5/Al-HMS-60 (1:1) composite catalyst was used for studying the effect of catalytic to plastic ratio on its activity. The values of conversion and the product yields for the thermal cracking and catalytic cracking of PP over ZSM-5/Al-HMS-60 (1:1) composite catalysts with various catalytic to plastic ratios and the thermal cracking at 400°C are shown in Table 4.12. For thermal cracking at 400°C, the white candle wax remained in the reactor after the reaction. With increasing the weight percent of catalyst in the reaction from 2 to 20 wt%, high conversions were obtained over 95%. Selectivities to liquid fraction were mainly obtained and be in the same range for 2 to 10 wt% of catalyst whereas the high value of gas fraction was noticed for 20 wt% of catalyst. This can be explained that with increasing the catalytic to plastic ratio, acidity and active site increased. For 5 wt% of catalyst, slightly higher in

liquid fraction and lower in gas fraction and solid coke deposited were obtained. It suggested that 5 wt% of catalyst enhanced high molecular weight hydrocarbons to break into light hydrocarbons in the heavy oil fraction. Thus, the 5 wt% of catalyst was chosen for further study.

Table 4.12 Thermal cracking and catalytic cracking of PP over ZSM-5/Al-HMS-60 (1:1) composite catalysts with various catalytic to plastic

% weight of catalyst	2% catalyst	5% catalyst	10% catalyst	20% catalyst	Thermal
Conversion (%)	95.9±0.1	96.8±0.0	96.1±0.1	94.9±0.1	67.0±0.0
Product yield (%)					
1. gas fraction	42.5±0.1	37.5±0.1	42.9±0.1	56.7±0.1	24.7±0.2
2. liquid fraction	53.4±0.0	59.3±0.1	53.2±0.2	38.2±0.0	42.3±0.2
- % heavy oil	43.8	49.1	42.6	18.8	31.4
- % distillate oil	9.6	10.2	10.6	19.4	10.9
3. residue	4.1±0.1	3.2±0.0	3.9±0.1	5.1±0.1	33.0±0.0
- wax	2.0	2.4	3.1	4.2	-
- solid coke	2.1	0.8	0.8	0.9	-
Total volume of liquid fraction (cm ³)	3.5	3.9	3.6	2.6	2.9
Liquid fraction density (g/cm ³)	0.75	0.76	0.75	0.74	0.74

Reaction condition: 400°C, 30 min, 20 cm³/min.N₂ flow.

Figure 4.31 shows the accumulative volume of liquid fractions in the graduated cylinder and the temperature of the reactor increased as a function of lapsed time. Although the initial rates of liquid fraction formation for 5 wt% and 10 wt% of catalytic to plastic ratio were not different but the overall rates of liquid fraction formation over 5 wt% of catalytic to plastic ratio was faster than that over 10 wt%.

Figure 4.32 shows distribution of gas fraction obtained by thermal cracking and catalytic cracking of PP over ZSM-5/Al-HMS-60 (1:1) composite catalysts with various catalytic to plastic ratios at 400°C. In the presence of catalysts, the product distributions in gas fraction were different from that in the absence of catalyst or thermal pyrolysis. For catalytic cracking, the major components of gas fraction were mainly C₃ (propene) and C₄ (iso-butene). Thermal cracking produced mainly C₃ (propene) and high contents in methane, ethane, iso-butene, and n-pentane.

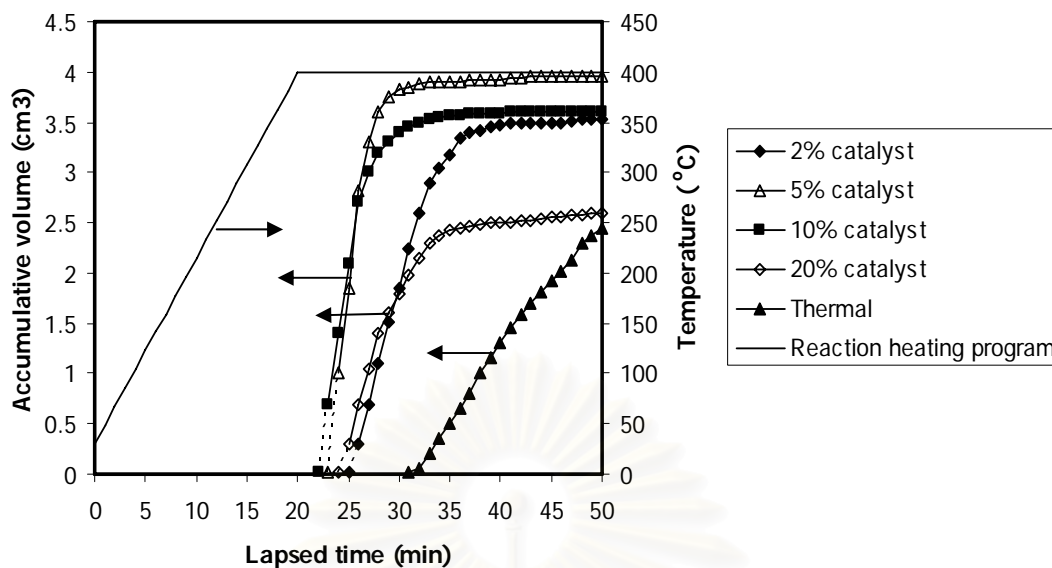


Figure 4.31 Accumulative volume of liquid fractions obtained by thermal cracking and catalytic cracking of PP over ZSM-5/Al-HMS-60 composite catalysts with various catalytic to plastic ratios.

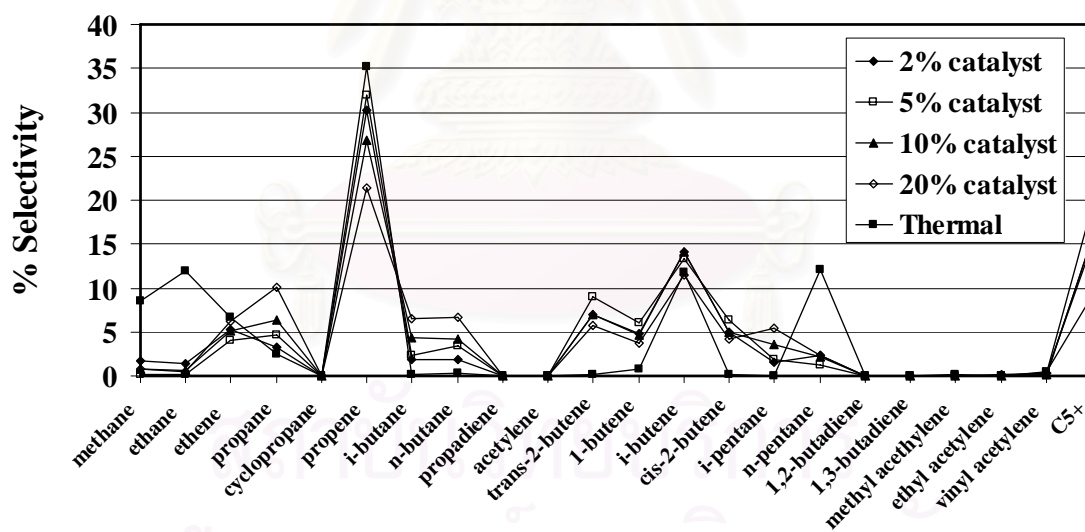


Figure 4.32 Distribution of gas fraction obtained by thermal cracking and catalytic cracking of PP over ZSM-5/Al-HMS-60 (1:1) composite catalysts with various catalytic to plastic ratios.

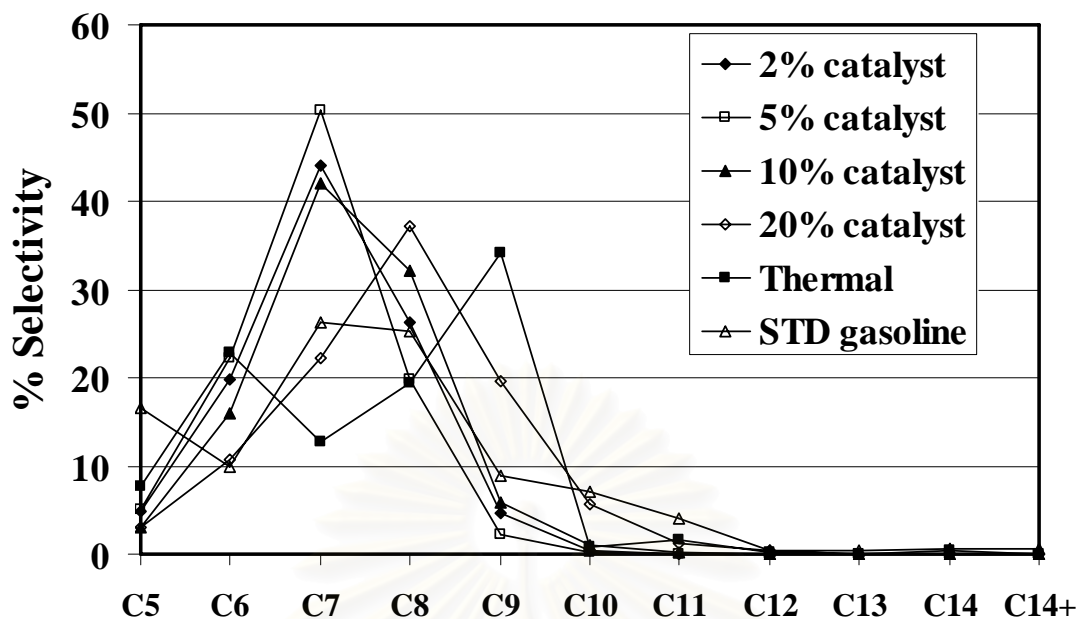


Figure 4.33 Carbon number distribution of distillate oils from the thermal cracking and catalytic cracking of PP over ZSM-5/Al-HMS-60 composite catalysts with various catalytic to plastic ratios.

Figure 4.33 shows product distribution of distillate oil obtained by catalytic cracking of PP over ZSM-5/Al-HMS-60 (1:1) composite catalysts at 400°C with various catalytic to plastic ratios and the thermal cracking. For the thermal cracking, the liquid fraction was mainly C₉ components and high value of C₆. The distillate oil components were mainly in the range of C₇ to C₈ as the standard gasoline oil but for 20 wt% of catalyst to plastic ratios, the oil component was enriched in C₈ more than C₇.

Therefore, it has been concluded that with increasing catalytic to plastic ratio, increasing acidity and active site increased. That results in faster rate of reaction, high conversion and product yields. However, there was no significant effect on product distribution in both gas and liquid phase. Thus, the 5 wt% catalytic to plastic ratio was chosen for further study due to the high conversion, high liquid fraction, and low coke.

4.4.3 Effect of ZSM-5:Al-HMS ratio in composite catalyst

The values of conversion and product yield for catalytic cracking of PP over ZSM-5/Al-HMS-60 composite catalysts with various ZSM-5:Al-HMS ratios in composite catalyst at 400°C and 5 wt% of catalyst to plastic are shown in Table 4.13. Conversion of the 2:1, 1:1, and 1:2 composites were slightly closed about 96-97 wt% but the selectivities in products were slightly different. With decreasing the ZSM-5 content, the yields of gas fraction decreased and the yields of liquid fraction increased. As the result of increasing Al-HMS-60, acidity of catalyst reduced. Large molecules of PP were cracked into small hydrocarbon oligomers and produced more liquids which enriched in heavy oil content. However, there was no difference in conversion and product yields between the 1:1 and 1:2 composite catalysts. Thus, the 1:1 composite catalyst was chosen for further studied in this work due to low yield of solid coke as 0.8 wt% and high yield of liquid fraction.

Table 4.13 Catalytic cracking of PP over ZSM-5/Al-HMS-60 composite catalysts with various ZSM-5:Al-HMS ratios in composite catalyst

ZSM-5:Al-HMS ratio in composite catalyst	ZSM-5 (100 wt% of ZSM-5)	2:1 (67 wt% of ZSM-5)	1:1 (50 wt% of ZSM-5)	1:2 (33 wt% of ZSM-5)	Al-HMS60 (0 wt% of ZSM-5)
Conversion (%)	93.5±0.1	96.3±0.1	96.8±0.0	96.5±0.1	96.5±0.1
Product yield (%)					
1. gas fraction	55.5±0.1	40.5±0.1	37.5±0.1	36.2±0.2	24.6±0.0
2. liquid fraction	38.0±0.0	55.8±0.2	59.3±0.1	60.3±0.1	71.9±0.1
- % heavy oil	32.5	45.0	49.1	48.1	56.6
- % distillate oil	5.5	10.8	10.2	12.2	15.3
3. residue	6.5±0.1	3.7±0.1	3.2±0.0	3.5±0.1	3.5±0.1
- wax	5.5	2.9	2.4	2.5	2.6
- solid coke	1.0	0.8	0.8	1.0	0.9
Total volume of liquid fraction (cm ³)	2.5	3.7	3.9	4.0	4.9
Liquid fraction density (g/cm ³)	0.76	0.76	0.76	0.75	0.74

Reaction condition: 5 wt% of catalyst, 400°C, 30 min, 20 cm³/min.N₂ flow.

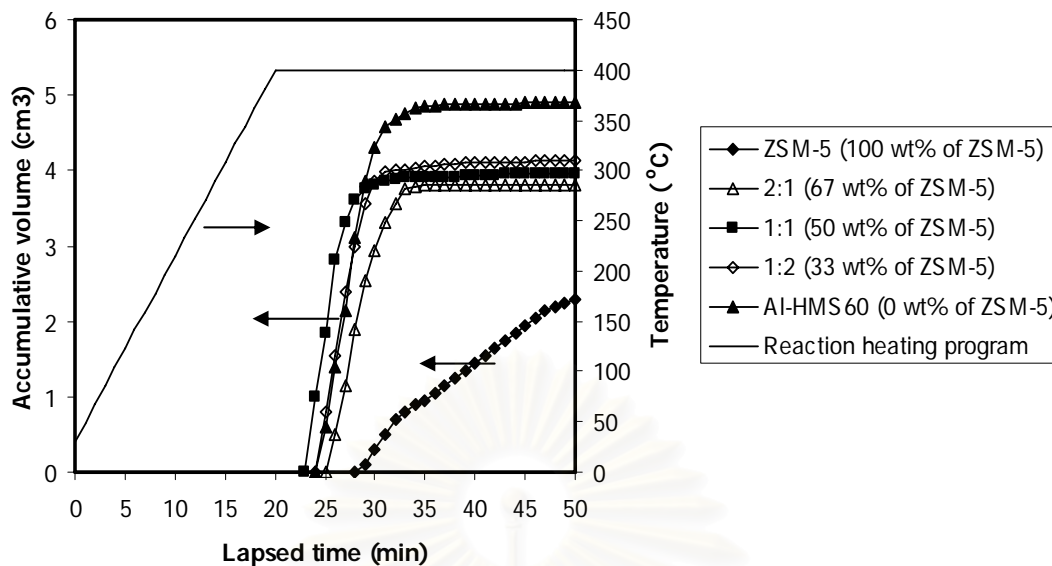


Figure 4.34 Accumulative volume of liquid fractions obtained by catalytic cracking of PP over ZSM-5/Al-HMS-60 composite catalysts with various ZSM-5:Al-HMS ratios in composite catalyst.

Figure 4.34 shows the accumulative volume of liquid fractions in the graduated cylinder and the temperature of the reactor increased as a function of lapsed time. The initial rates of liquid formation for the composite catalyst with different ZSM-5:Al-HMS ratios were in the following order: 1:1 (50 wt% of ZSM-5) > 1:2 (33 wt%) = Al-HMS 60 (0 wt%) > 2:1 (67 wt%) > ZSM-5 (100 wt%).

Figure 4.35 shows product distribution of gas fraction obtained by catalytic cracking of PP over ZSM-5/Al-HMS-60 composite catalysts with various ZSM-5:Al-HMS ratios. For all ZSM-5:Al-HMS ratios, the major components in gas fraction were C₃ (propene), C₄ (iso-butene) and C₅₊, except ZSM-5 (100 wt%) obtained more light molecule C₃ (propene and propane) and C₂ (ethene) because of small pore size of ZSM-5. For pure Al-HMS-60 (0 wt% of ZSM-5), the yield of C₄ (iso-butene) and C₅₊ obtained more than other ratios, that means this ratio was more selectivity in liquid fraction due to large pore size of Al-HMS.

Figure 4.36 shows product distribution of distillate oil obtained by catalytic cracking of PP over ZSM-5/Al-HMS-60 composite catalysts with various ZSM-5:Al-HMS ratios in composite catalyst. The components of distillate oil were mainly in the hydrocarbon range of C₇-C₈ as the standard gasoline oil, except at 0 and 50 wt% of ZSM-5 in the ZSM-5/Al-HMS-60 composite catalyst. The pure Al-HMS-60 (0 wt%

of ZSM-5 in catalyst) obtained wide range of hydrocarbons mainly in C₆-C₈ while the 50 wt% of ZSM-5 in catalyst gave narrow range of hydrocarbon mainly in C₇.

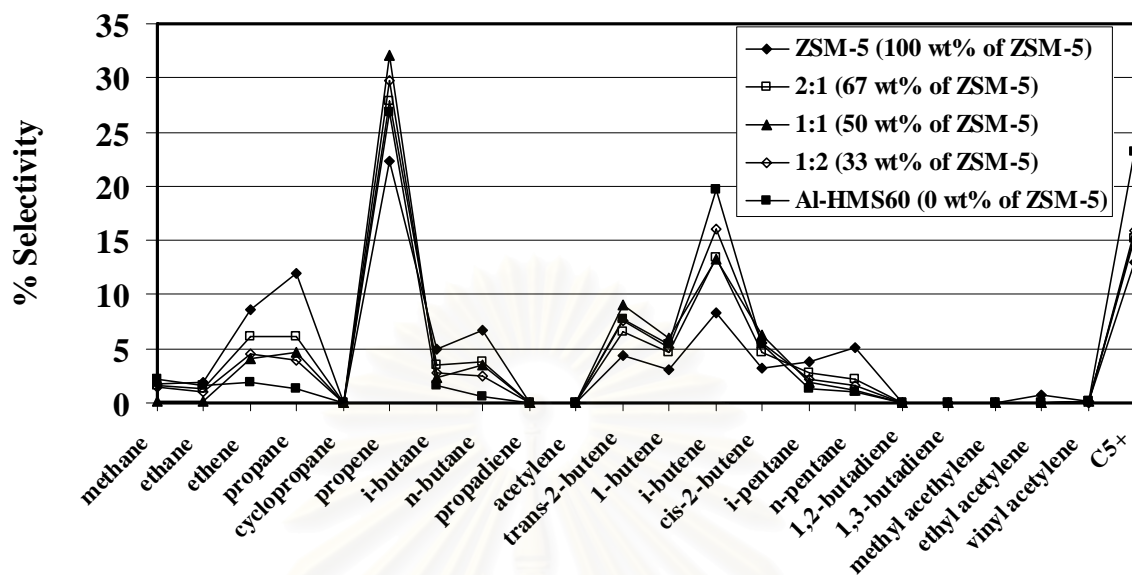


Figure 4.35 Distribution of gas fraction obtained by catalytic cracking of PP over ZSM-5/Al-HMS-60 composite catalysts with various ZSM-5:Al-HMS ratios in composite catalyst.

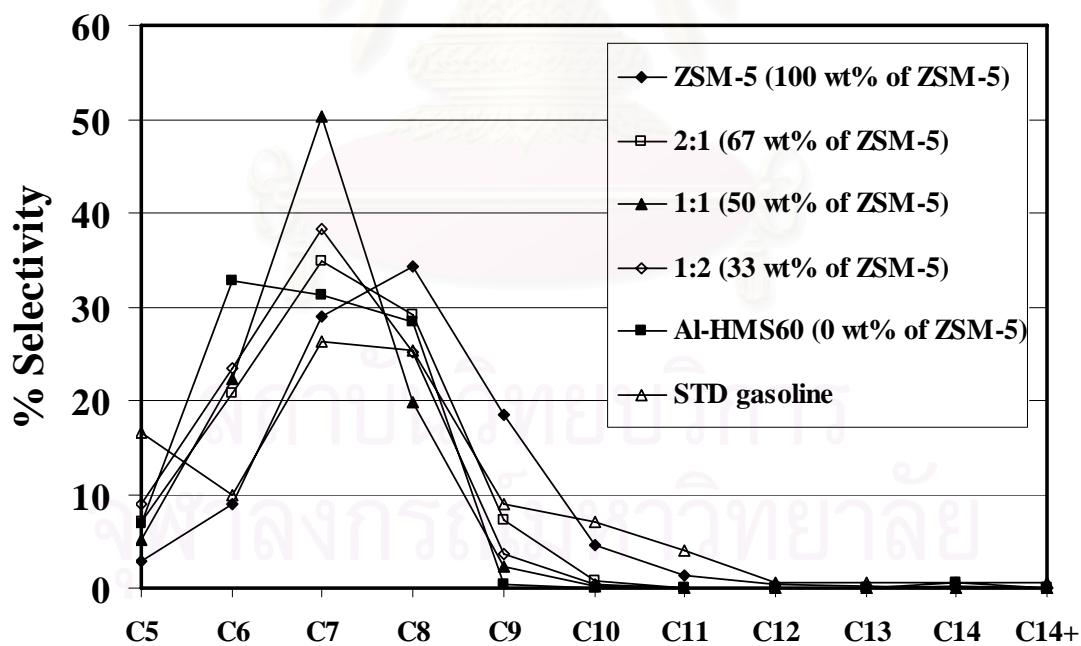


Figure 4.36 Carbon number distribution of distillate oils from catalytic cracking of PP over ZSM-5/Al-HMS-60 composite catalysts with various ZSM-5:Al-HMS ratios in composite catalyst.

Therefore, it has been concluded that with increasing ZSM-5:Al-HMS ratios, acidity increased and the content of large pore size of Al-HMS decreased. That results in high conversion and the value of product yields. However, there was no significant effect on product distribution in both gas and liquid phase. Thus, the 1:1 ZSM-5:Al-HMS ratio was chosen for further study due to the high conversion, high liquid fraction, and low coke.

4.4.4 Effect of aluminium content in catalyst

To study the effect of aluminium contents (Si/Al ratio) in Al-HMS in the composite catalyst, the ZSM-5/Al-HMS composites with the weight ratio of ZSM-5:Al-HMS as 1:1 were performed with different Si/Al ratios in Al-HMS. The data are shown in Table 4.14. With increasing the aluminium contents, high values of conversion were obtained about 96-97 wt%. There was no difference in conversion and product selectivity for composite catalysts with various Si/Al ratios in gel of Al-HMS. This may be because the reaction temperature for cracking of PP is too high, therefore we can not observe the different from conversion and the yield of products.

Table 4.14 Catalytic cracking of PP over ZSM-5/Al-HMS composite catalysts with various aluminium contents in Al-HMS

Si/Al ratio in gel in Al-HMS (ZSM-5:Al-HMS ratio)	20 (1:1)	60 (1:1)	200 (1:1)
Conversion (%)	96.3±0.1	96.8±0.0	96.3±0.1
Product yield (%)			
1. gas fraction	37.7±0.1	37.5±0.1	40.9±0.3
2. liquid fraction	58.6±0.0	59.3±0.1	55.4±0.4
- % heavy oil	47.7	49.1	48.7
- % distillate oil	10.9	10.2	6.7
3. residue	3.7±0.1	3.2±0.0	3.7±0.1
- wax	2.8	2.4	2.9
- solid coke	0.9	0.8	0.8
Total volume of liquid fraction (cm ³)	3.9	3.9	3.7
Liquid fraction density (g/ cm ³)	0.75	0.76	0.76

Reaction condition: 1:1 ZSM-5:Al-HMS ratio, 5 wt% of catalyst, 400°C, 30 min, 20 cm³/min.N₂ flow.

Figure 4.37 shows the accumulative volume of liquid fractions in the graduated cylinder and the temperature of the reactor increased as a function of lapsed time. Although the initial rates of liquid fraction formation of aluminium contents (Si/Al ratio) were in the order of $20 > 60 > 200$, the ZSM-5/Al-HMS composite catalyst with Si/Al ratio in Al-HMS of 20 and 60 were not significant in the overall kinetic rate.

Figure 4.38 shows product distribution of gas fraction obtained by catalytic cracking of PP over ZSM-5/Al-HMS composite catalysts with various aluminium contents in Al-HMS. For all aluminium contents, the distributions of gas fraction were similar. The major components of gas fraction were mainly C₃ (propene), C₅₊ and C₄ (iso-butene).

Figure 4.39 shows product distribution of distillate oil obtained by catalytic cracking of PP over ZSM-5/Al-HMS composite catalysts with various aluminium contents in Al-HMS comparing with the commercial SUPELCO standard gasoline fraction. The component of standard gasoline was mainly in the range of C₇ to C₈. For catalytic cracking in this study, the distillate oils were mainly consisted of hydrocarbons in the range of C₇ to C₈ for the composite with Al-HMS 200 and in the wide range of C₆-C₈ for one with Al-HMS 20. For the composite with Al-HMS 60 distillate oil components mainly obtained hydrocarbon in the narrow range of C₇.

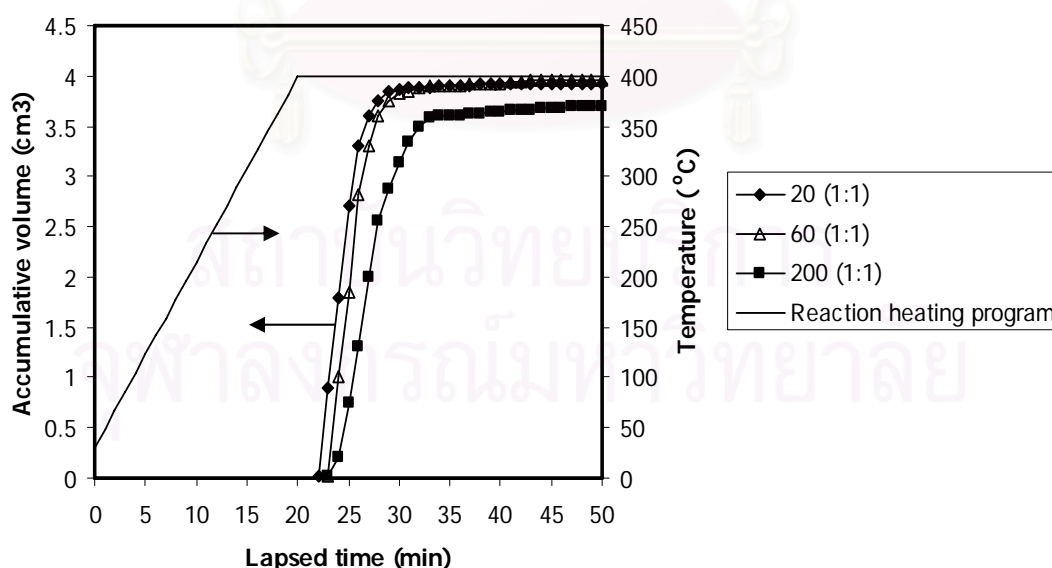


Figure 4.37 Accumulative volume of liquid fractions obtained by catalytic cracking of PP over ZSM-5/Al-HMS composite catalysts with various aluminium contents in Al-HMS.

Therefore, it has been concluded that with increasing aluminium contents, acidity increased. That results in high conversion. However, there was no significant effect on product distribution in both gas and liquid phase. Thus, the ZSM-5:Al-HMS-60 was chosen for further study due to the high liquid fraction, and low coke.

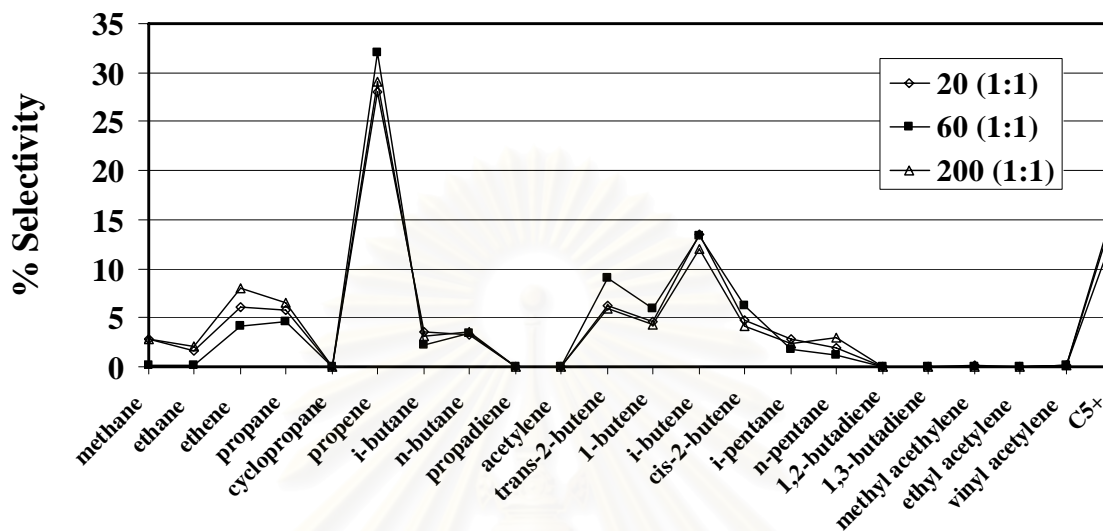


Figure 4.38 Distribution of gas fraction obtained by catalytic cracking of PP over ZSM-5/Al-HMS composite catalysts with various aluminium contents in Al-HMS.

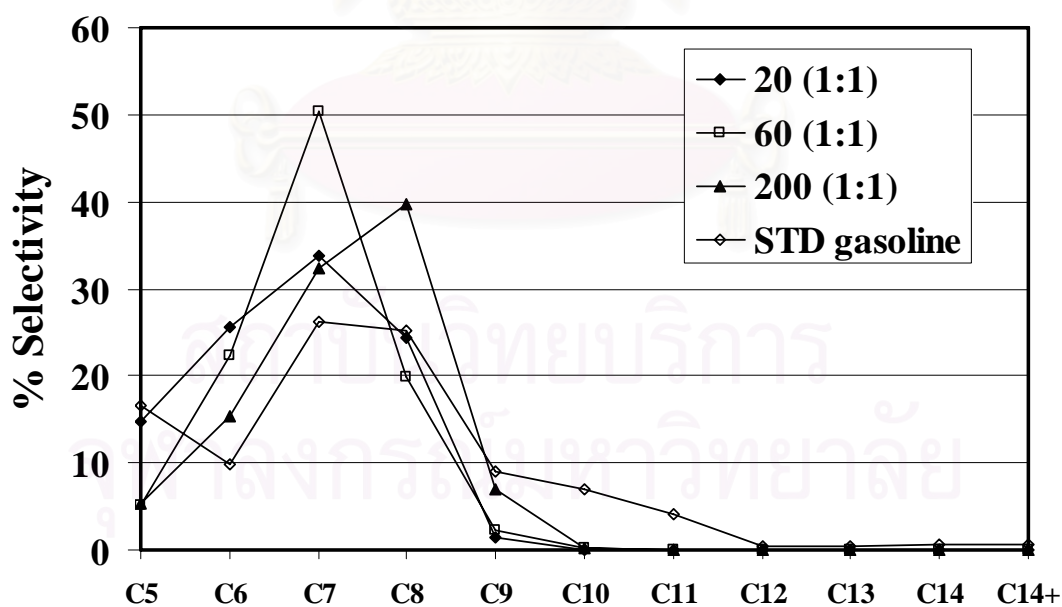


Figure 4.39 Carbon number distribution of distillate oils from the commercial SUPELCO standard gasoline fraction and catalytic cracking of PP over ZSM-5/Al-HMS composite catalysts with various aluminium contents in Al-HMS.

4.5 Catalyst Regeneration

4.5.1 The characterization of regenerated catalyst

4.5.1.1 XRD Results

ZSM-5/Al-HMS 60 composite catalyst with the weight ratio of 1:1 became black after the first round of cracking reaction due to the deposition of coke on the surface and in the pores. After regeneration by calcination the used catalyst in a muffle furnace at 550°C for 10 h, the catalyst turned white. The XRD patterns of both fresh and the regenerated composite catalysts are shown in Figure 4.40. The hexagonal structure of Al-HMS and the MFI structure of ZSM-5 were still remained for the regenerated composite catalyst as in the fresh catalyst. The small shift of the low 2θ peaks of the regenerated composite catalyst to higher values of 2θ indicates the decrease of d-spacings and the contraction of the unit cell in the hexagonal structure of Al-HMS.

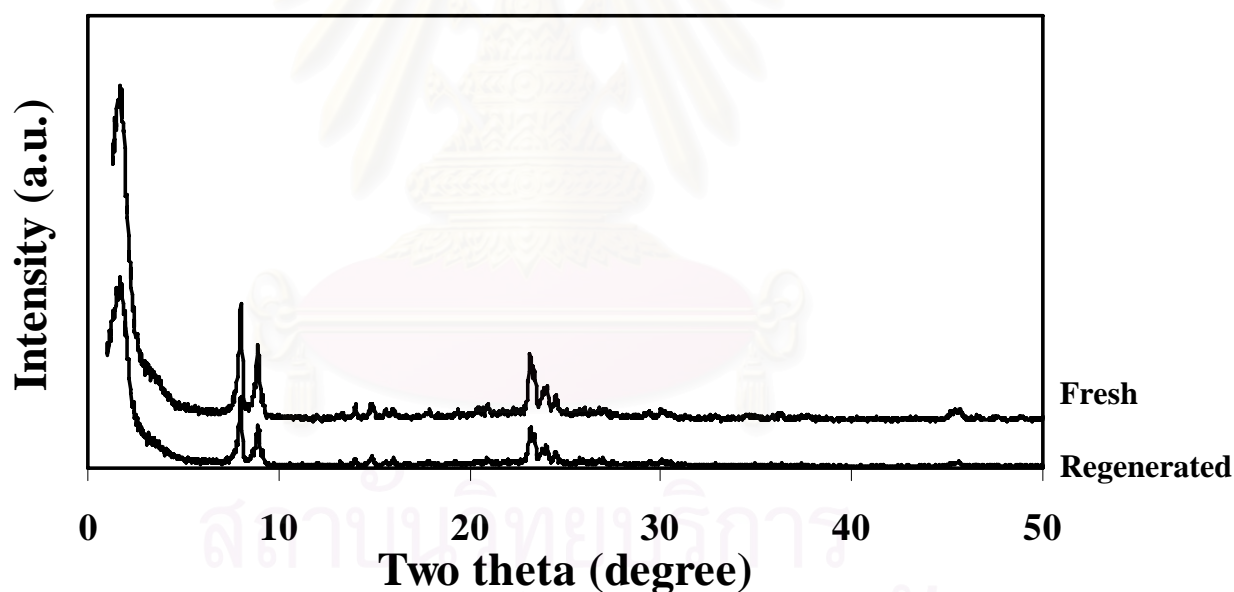


Figure 4.40 XRD patterns of fresh and regenerated ZSM-5/Al-HMS-60 (1:1) composite catalyst.

4.5.1.2 Nitrogen Adsorption-Desorption

The adsorption isotherms of fresh and regenerated catalyst are exhibited in Figure 4.41. As compare to the adsorption isotherm of fresh ZSM-5/Al-HMS-60 (1:1) composite catalyst, the regenerated ZSM-5/Al-HMS-60 (1:1) composite catalyst was also shown the adsorption isotherm of mesoporous materials

with the reduction of surface area from 539 m²/g in the fresh catalyst to 484 m²/g in the regenerated catalyst. The reduction of surface area approximately 10% may be due to many reasons, such as the unstability of hexagonal structure of Al-HMS as seen in the XRD result.

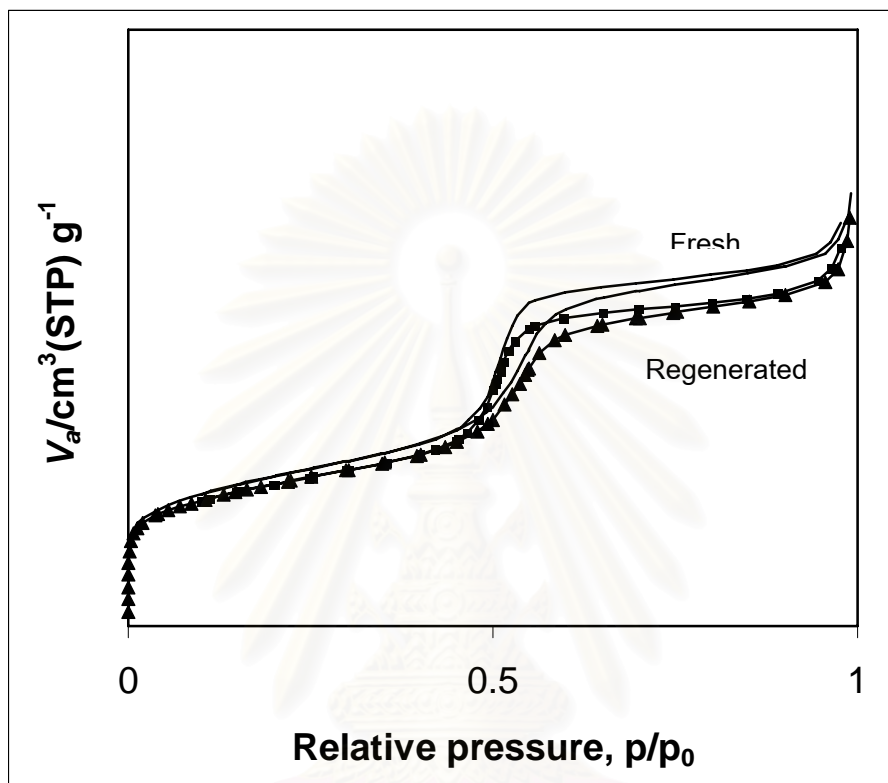


Figure 4.41 Adsorption isotherms of fresh and regenerated ZSM-5/Al-HMS-60 (1:1) composite catalyst from N₂ adsorption measurement.

4.5.2 Activity of regenerated catalyst

4.5.2.1 Activity of regenerated catalyst in HDPE Cracking

The catalytic cracking of HDPE was carried out at the optimal condition: reaction temperature of 400°C for 30 min, 10 wt% of ZSM-5/Al-HMS 60 (1:1) catalyst to plastic. The conversion and product yields obtained are shown in Table 4.10.

Table 4.15 Catalytic cracking of HDPE using the fresh and the regenerated ZSM-5/Al-HMS-60 (1:1) composite catalysts

ZSM-5:Al-HMS-60 catalyst 1:1	Fresh	Regenerated
Conversion (%)	96.4±0.0	94.6±0.2
Product yield (%)		
1. gas fraction	59.0±0.2	63.6±0.0
2. liquid fraction	37.4±0.2	31.0±0.2
- % heavy oil	21.7	16.0
- % distillate oil	15.7	15.0
3. residue	3.6±0.0	5.4±0.2
- wax	3.2	4.7
- solid coke	0.4	0.7
Total volume of liquid fraction (cm ³)	2.6	2.2
Liquid fraction density (g/cm ³)	0.71	0.70

Reaction condition: 10 wt% of catalyst, 400°C, 30 min, 20 cm³/min.N₂ flow.

From Table 4.15, very high conversion values about 94.6 wt% was still obtained over the regenerated catalyst. As compared to the fresh catalyst, the conversion of the regenerated catalyst was slightly lower. The yield of gas fraction obtains for the regenerated catalyst was higher while the yield of liquid fraction was lower. Besides, the fraction of heavy oil was lower. It may be explained by the reduction of specific surface area caused by the instability of Al-HMS structure. The contraction of hexagonal structure may result in collapse of pores and prohibit the large hydrocarbon molecules to access the mesopores.

Figure 4.42 shows the accumulative volume of liquid fractions in the graduated cylinder and the temperature of the reactor increased as a function of lapsed time. The initial rates of liquid fraction formation for both catalysts were similar, but the overall content of liquid fraction was slightly different.

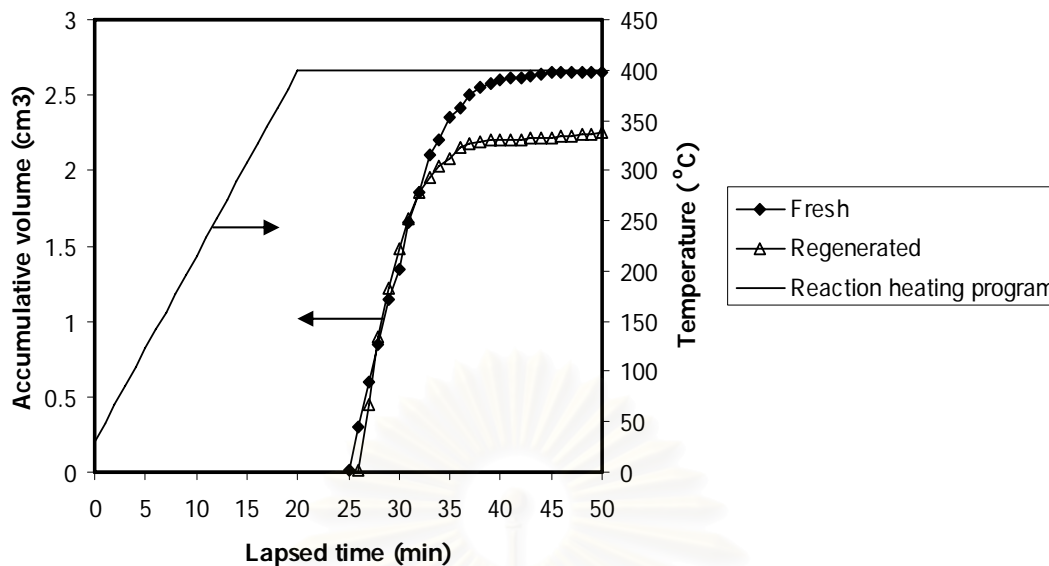


Figure 4.42 Accumulative volume of liquid fraction obtained by catalytic cracking of HDPE using the fresh and the regenerated ZSM-5/Al-HMS-60 (1:1) composite catalysts.

Figure 4.43 shows distribution of gas fraction obtained by catalytic cracking of HDPE over the fresh and the regenerated ZSM-5/Al-HMS-60 (1:1) composite catalysts. For both catalysts, the distributions of gas fraction were in the same trend. The major components of gas fraction were C₃ (propene), C₅₊ and C₄ (iso-butene).

Figure 4.44 shows product distribution of distillate oil obtained by catalytic cracking of HDPE over the fresh and the regenerated ZSM-5/Al-HMS-60 (1:1) composite catalysts and the commercial SUPELCO standard gasoline fraction. The distillate oil components from catalytic cracking of both catalysts were mainly composed of hydrocarbons in the range of C₇ to C₈, are similar to the standard gasoline. However, parafinic and olefinic hydrocarbons could not be identified.

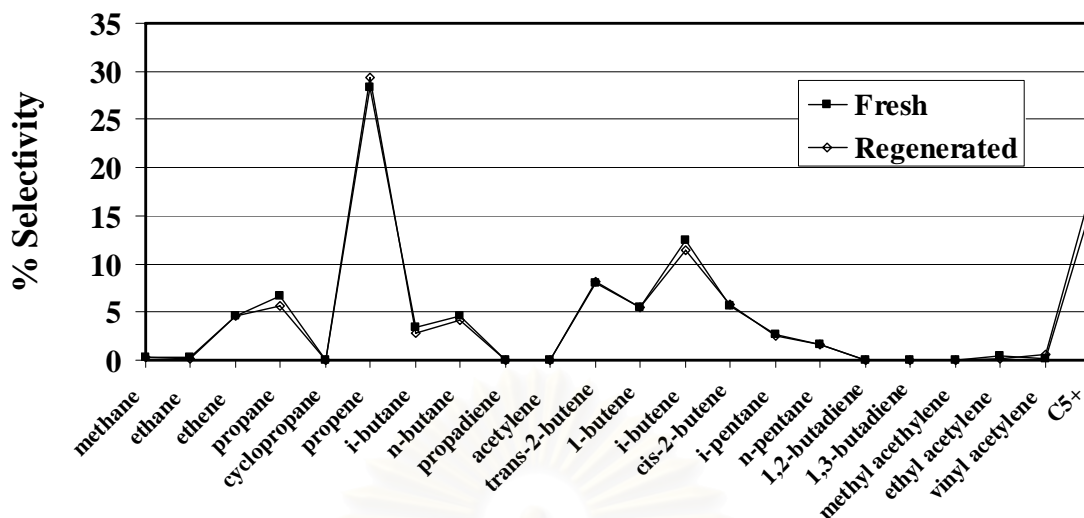


Figure 4.43 Distribution of gas fraction obtained by catalytic cracking of HDPE using the fresh and the regenerated ZSM-5/Al-HMS-60 (1:1) composite catalysts.

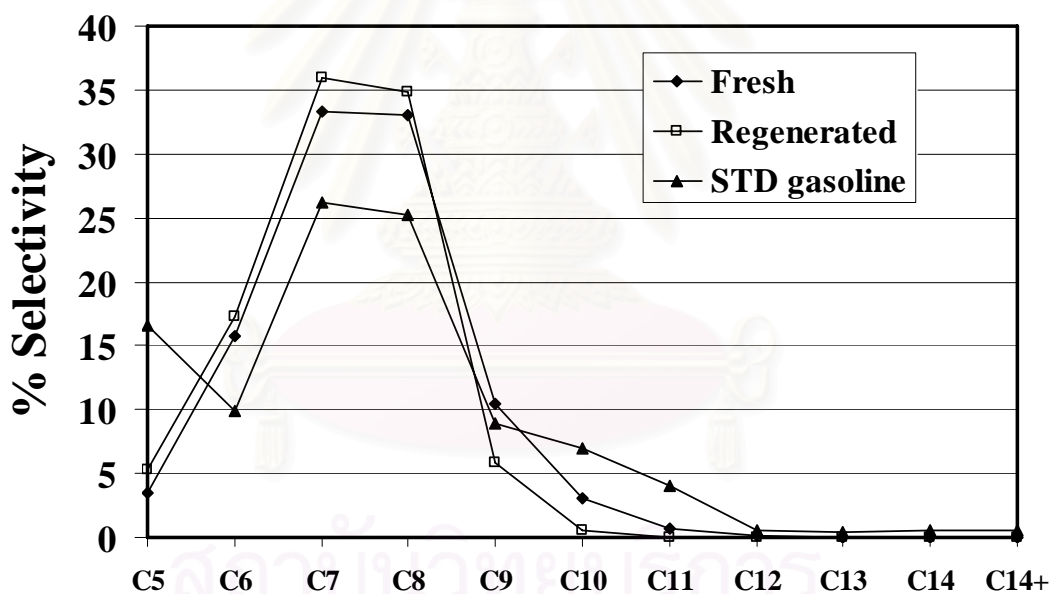


Figure 4.44 Carbon number distributions of distillate oils obtained by the commercial SUPELCO standard gasoline fraction and catalytic cracking of HDPE using the fresh and the regenerated ZSM-5/Al-HMS-60 (1:1) composite catalysts.

4.5.2.2 Activity of regenerated catalyst in PP Cracking

The catalytic cracking of PP was carried out at the optimal condition: reaction temperature of 400°C for 30 min, using 5 wt% of ZSM-5/Al-HMS 60 (1:1) catalyst to plastic. The conversion and product distribution obtained are shown in Table 4.14.

Table 4.16 Catalytic cracking of PP using the fresh and the regenerated ZSM-5/Al-HMS-60 (1:1) composite catalysts

ZSM-5:Al-HMS-60 catalyst 1:1	Fresh	Regenerated
Conversion (%)	96.8±0.0	95.2±0.2
Product yield (%)		
1. gas fraction	37.5±0.1	38.4±0.2
2. liquid fraction	59.3±0.1	56.8±0.0
- % heavy oil	49.1	45.4
- % distillate oil	10.2	11.4
3. residue	3.2±0.0	4.8±0.2
- wax	2.4	4.0
- solid coke	0.8	0.8
Total volume of liquid fraction (cm ³)	3.9	3.8
Liquid fraction density (g/cm ³)	0.76	0.75

Reaction condition: 5 wt% of catalyst, 400°C, 30 min, 20 cm³/min N₂ flow

From Table 4.16, very high conversion values about 95.2 wt% was obtained with the regenerated catalyst. As compared to the fresh catalyst, the conversion of the regenerated catalyst was not different. The yield of gas fraction was not much different while the yield of liquid fraction was slightly lower. The content of heavy oil fraction was decreased. This may also due to the relatively less specific surface area.

Figure 4.45 shows the accumulative volume of liquid fractions in the graduated cylinder and the temperature of the reactor increased as a function of lapsed time. This figure shows the initial kinetic rates of liquid fraction formation for fresh ZSM-5:Al-HMS 60 ratio 1:1 composite catalyst were not significantly faster than the regenerated catalyst.

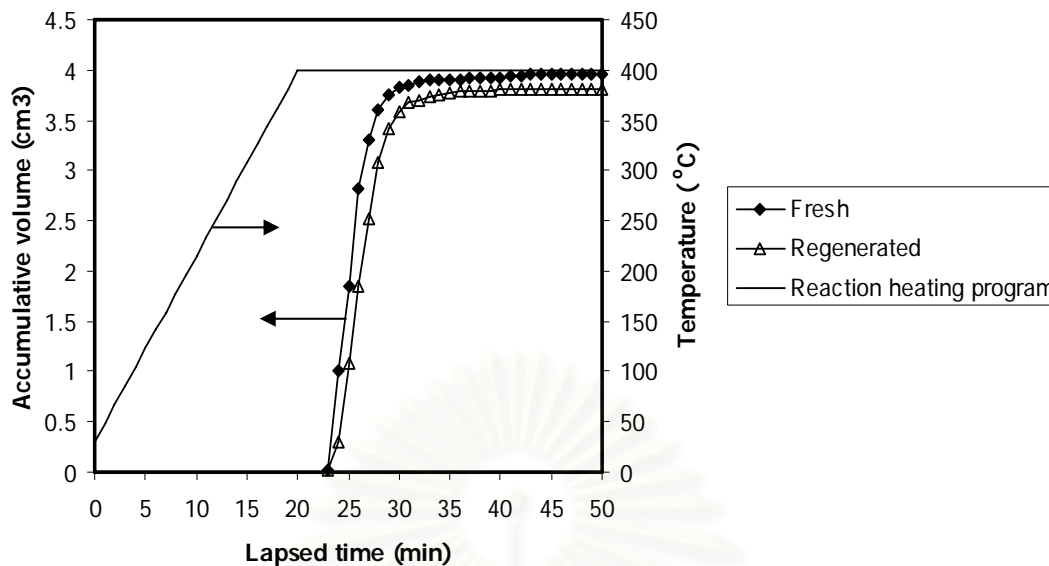


Figure 4.45 Accumulative volume of liquid fraction obtained by catalytic cracking of PP using the fresh and the regenerated ZSM-5/Al-HMS-60 (1:1) composite catalysts.

Figure 4.46 shows the distribution of gas fraction obtained from catalytic cracking of PP over the fresh and the regenerated ZSM-5/Al-HMS-60 (1:1) composite catalysts. For both catalysts, the distributions of gas fraction were similar. The majority in component of gas fraction was C₃ (propene), C₅₊ and C₄ (iso-butene).

Figure 4.47 shows the product distribution of distillate oil obtained from catalytic cracking of PP over the fresh and the regenerated ZSM-5/Al-HMS-60 (1:1) composite catalysts, comparing with the commercial SUPELCO standard gasoline fraction. The distillate oil components of catalytic cracking composed of hydrocarbons in the range of C₅ to C₉, but mainly in C₇ with different from standard gasoline composed of hydrocarbons in the range of C₅ to C₁₂ and mainly in C₇-C₈. However, the relative lighter hydrocarbon component was noticed for the fresh catalysts.

It can be concluded that the reuse of catalyst in this research is plausible for one cycle. The conversion and product yield is not significantly different. However, more cycles of regenerated catalyst should be studied for life time of catalyst.

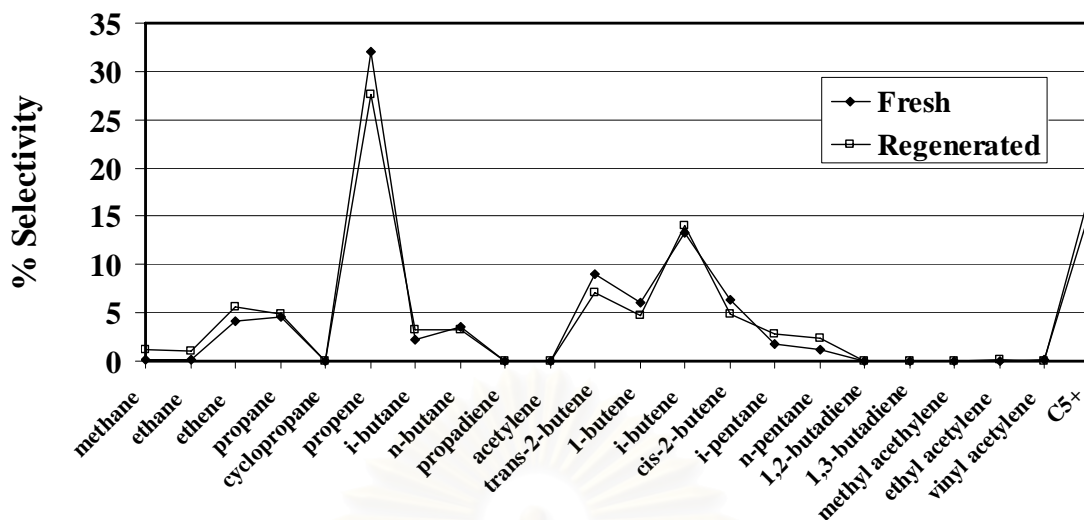


Figure 4.46 Distribution of gas fraction obtained by catalytic cracking of PP using the fresh and the regenerated ZSM-5/Al-HMS-60 (1:1) composite catalysts.

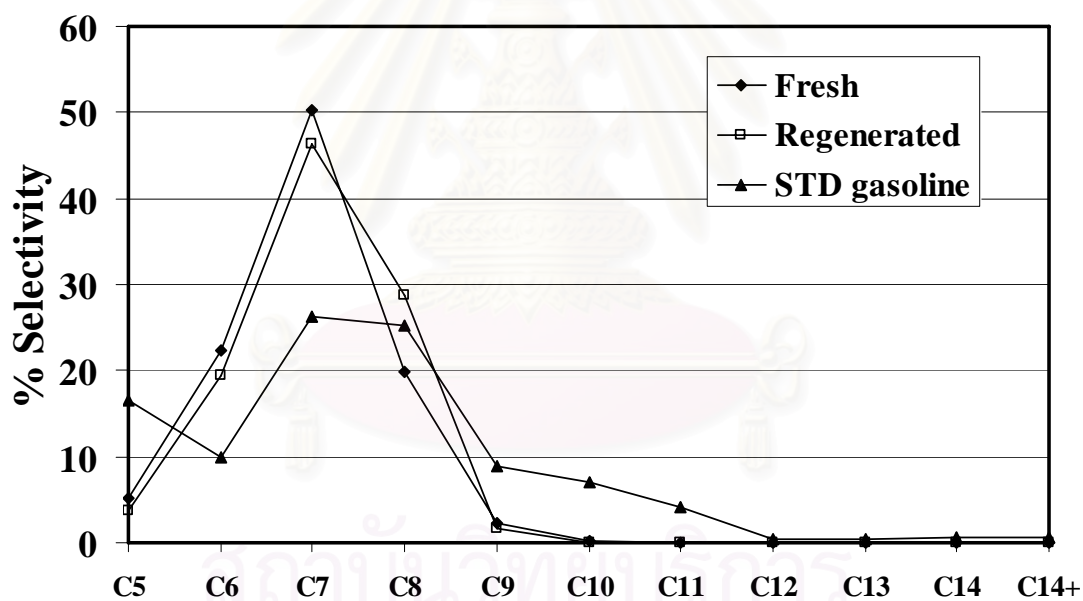


Figure 4.47 Carbon number distributions of distillate oils obtained by the commercial SUPELCO standard gasoline fraction and catalytic cracking of PP using the fresh and the regenerated ZSM-5/Al-HMS-60 (1:1) composite catalysts.

CHAPTER V

CONCLUSION

ZSM-5 microporous and Al-HMS mesoporous molecular sieve have been synthesized by the procedure reported by Vorranch J.[84] for ZSM-5, Metha S.[85]. for Al-HMS. The calcined catalysts were treated with a solution of ammonium chloride to remove the non-framework aluminium. All synthesized catalysts were characterized using XRD, ICP-AES, ^{27}Al -MAS-NMR, N_2 adsorption-desorption, NH_3 -TPD and SEM techniques. XRD patterns of both catalysts showed the characteristic peaks similar to that of ZSM-5 and HMS. Morphology of ZSM-5 was rectangle-formed and cross-formed particle while Al-HMS was spherical particle. ^{27}Al -MAS-NMR spectra of ZSM-5 showed all aluminium were in tetrahedral framework while those in Al-HMS were in framework and non-framework. When Si/Al ratios increased, the relative intensities of tetrahedral Al to octahedral Al increased in Al-HMS. Adsorption-desorption isotherm of N_2 on ZSM-5 and Al-HMS exhibited pattern of type I and IV which are typical shape for micropores and mesopores, respectively. The specific surface area in the mesopores increased with the decrease of aluminum content. The number of acid sites also decreased when aluminum content in catalyst decreased. The composite catalysts were synthesized by physically mixing method. XRD patterns showed both characteristic peaks of pure catalysts. N_2 adsorption-desorption isotherm of the composite exhibited pattern of type IV and having value of surface area between both pure catalysts.

The catalytic cracking of HDPE and PP were chosen to test catalytic activity of ZSM-5/Al-HMS-60 ratio 1:1 catalyst. The results showed the catalytic cracking of polymer process depended on physical characteristics of the catalysts and structural nature of the polymers. % Conversion of polymer and % yield of products by catalytic cracking are higher than thermal cracking. The value of % conversion increases when reaction temperature increased. The maximum conversion was obtained at temperature higher than 400°C . When increases ratio of catalytic to plastic at 400°C of temperature reaction, the conversion increases in HDPE but for the PP cracking % conversion is maximal at 5 wt% ratio. In case of ratio of ZSM-5 per Al-HMS-60, the value % conversion of the composites are not significant but the ratio 1:1 of

composite gives high value of liquid fraction and lowest value of coke over cracking of HDPE and PP. For the effect of aluminium content, the conversion is very close but the ZSM-5/Al-HMS-60 composite obtains the highest yield of liquid and the lowest yield of coke in HDPE and PP cracking. The optimum condition for catalytic cracking of composite ZSM-5/Al-HMS catalyst is temperature of reaction at 400°C, ratio of ZSM-5 per Al-HMS as 1:1 (50 wt% of ZSM-5) and Si/Al ratio 60 of Al-HMS wherewith HDPE and PP using catalytic to plastic ratios are 10 and 5 wt%, respectively.

The major component of gas fractions are C₃ (propene), C₄ (iso-butene) and C₅₊ from HDPE and PP cracking. The distillate oil components are mainly in the range of C₇ to C₈. The carbon number distribution over ZSM-5/Al-HMS composite catalyst was similar to that for commercial gasoline fraction hydrocarbon based on the boiling point range using n-paraffins as reference.

The regenerated ZSM-5/Al-HMS-60 ratio 1:1 composite catalyst was tested for catalytic cracking of HDPE and PP at the optimum condition. It was found that the structure of ZSM-5/Al-HMS composite catalyst is stable. XRD patterns of the MFI of ZSM-5 and the hexagonal structure HMS were still remained for the regenerated ZSM-5/Al-HMS-60 ratio 1:1 composite catalyst with almost the same crystallinity as the unused catalyst while surface area was reduced about 10% from the fresh. The regenerated catalyst provided relatively higher yield of gas fraction and lower yield of liquid fraction comparing to the fresh catalyst. Distribution of gas fraction and liquid fraction are not significantly different using the fresh or the regenerated catalyst.

The suggestions for future work

1. To compare ZSM-5/Al-HMS-60 ratio 1:1 composite catalyst with zeolite and other mesoporous materials for catalytic cracking of HDPE and PP under the same condition.
2. To investigate the efficiency of ZSM-5/Al-HMS-60 ratio 1:1 composite for catalytic cracking of mixed plastic containing HDPE, LDPE, PP, PS, PET.

REFERENCES

- [1] Klaus, T. municipal waste [Online]. Available from :
www.vitalgraphics.net/waste.html [2007, June 24]
- [2] Blackburn, M.; CMAI Europe Ltd. Global PVC Market. Seminar, 2006.
- [3] Aguado, J; Serrano, D.P. Feedstock recycling of plastic waste, RCC, Cambridge, 1999.
- [4] Kaminsky, W.; Schlesselmann, B.; and Simon, C. Olefins from polyolefins and mixed plastic by pyrolysis. J. Anal. Appl. Pyrolysis 32 (1995):19.
- [5] Conesa, J.A.; Fant, R.; Marcilla, A.; and Garcia, A.N. Pyrolysis of polyethylene in a fluidized bed reactor. Energy Fuel 8 (1994): 1238.
- [6] Wanpler, T.P. Thermometric behavior of polyolefins. J. Anal. Appl. Pyrolysis. 15 (1989): 187.
- [7] Ohkita, H.; Nishiyama, R.; Tochiyama, Y.; Mizushima, T.; Kakuta, N.; Morioka, Y.; Ueno, A.; Namiki, Y.; Tanifuji, S.; Katoh, H.; Sunazuka, H.; Nakayama, R.; and Kuroyanagi, T. Acid properties of silica-alumina catalysts and catalytic degradation of polyethylene. Ind. Eng. Chem. Res. 32 (1993): 3112.
- [8] Kim, J.R.; Yoon, J.H.; and Park, D.W. Catalytic recycling of the mixture of polypropylene and polystyrene. Polym. Degrad. Stab. 76 (2002): 61.
- [9] Cordona, S.C.; and Corma, A. Kinetic study of the catalytic cracking of polypropylene in a semibatch stirred reactor. Catal. Today 75 (2002): 239.
- [10] Manos, G.; Gaeforth, A.; and Dwyer, J. Catalytic degradation of high-density polyethylene over different zeolitic structures. Ind. Eng. Chem. Res. 39 (2000): 1198.
- [11] Manos, G.; Garforth, A.; and Dwyer, J. Catalytic degradation of high-density polyethylene on an ultrastable-Y zeolite. Nature of initial polymer reactions, pattern of formation of gas and liquid products, and temperature effects. Ind. Eng. Chem. Res. 39 (2000): 1203.
- [12] Westerhout, R.W.J.; Kuipers, J.A.M.; and Swaaij, W.P.M. Experimental determination of the yield of pyrolysis products of polyethene and

- polypropene: Influence of reaction conditions. Ind. Eng. Chem. Res. 37 (1998): 841.
- [13] Uddin, M.A.; Sakata, Y.; Muto, A.; Shiraga, Y.; Koizumi, K.; Kanada, Y.; and Murata, K. Catalytic degradation of polyethylene and polypropylene into liquid hydrocarbons with mesoporous silica. Micropor. Mesopor. Mater. 21 (1998): 557.
- [14] Kim, J.R.; Kim, Y.A.; Yoon, J.H.; Park, D.W.; and Woo, H.C. Catalytic degradation of polypropylene: effect of dealumination of clinoptilolite catalyst. Polym. Degrad. Stab. 75 (2002): 287.
- [15] Grieken, R.; Serrano, D.P.; Aguado, J.; Garcia, R.; and Rojo, C. Thermal and catalytic cracking of polyethylene under mild conditions. J. Anal. Appl. Pyrolysis 58-59 (2001): 127.
- [16] Hesse, N.D.; Lin, R.; Bonnet, E.; Cooper, J.; and White, R.L. In situ analysis of volatiles obtained from the catalytic cracking of polyethylene. J. Appl. Polym. Sci. 82 (2001): 3118.
- [17] Fernandes, Jr. V.J.; Araujo, A.S.; and Fernandes, G.J.T. Catalytic degradation of high density polyethylene by HZSM-5 zeolite. Stud. Surf. Sci. Catal. 105 (1997): 941.
- [18] Serrano, D.P.; Aguado, J.; Sotelo, J.L.; Grieken, R.V.; Escola, J.M.; and Menendez, J.M. Catalytic properties of MCM-41 for the feedstock recycling of plastic and lubricating oil wastes. Stud. Surf. Sci. Catal. 117 (1998): 437.
- [19] Manos, G.; Gaeforth, A.; and Dwyer, J. Catalytic degradation of HDPE over different zeolitic structures. Ind. Eng. Chem. Res. 39 (2000): 1198.
- [20] Makkee, M.; den Hollander, M.A.; Wissink, M. and Moulijn, J.A. Gasoline conversion: reactivity towards cracking with equilibrated FCC and ZSM-5 catalysts. Apply. Catal. A. 223 (2002): 85
- [21] Uddin, M.A.; Sakata, Y.; Muto, A.; and Shiraga, Y. Catalytic degradation of PE and PP into liquid hydrocarbons with mesoporous silica. Micropor. Mesopor. Mater. 21 (1998): 557.
- [22] Serrano, D.P.; Aguado, J.; and Escola, J.M. Catalytic conversion of polystyrene over HMCM-41, HZSM-5 and amorphous SiO₂-Al₂O₃: comparison with thermal cracking. Apply. Catal. B. 25 (2000): 181.

- [23] Serrano, D.P.; Aguado, J.; and Escola, J.M. Catalytic conversion of polyolefins into liquid fuels over MCM-41: comparison with ZSM-5 and amorphous SiO₂-Al₂O₃. Energy & Fuels 11 (1997): 1225.
- [24] Serrano, D.P.; Aguado, J.; and Escola, J.M. Catalytic cracking of a polyolefin mixture over different acid solid catalysts. Ind. Eng. Chem. Res. 39 (2000): 1177.
- [25] Aguado, J.; Serrano, D.P.; Sotelo, J.L.; Van Grieken, R.; and Escola, J.M. Influence of the Operating Variables on the Catalytic Conversion of a Polyolefin Mixture over HMCM-41 and Nanosized HZSM-5. Ind. Eng. Chem. Res. 40 (2001): 5696.
- [26] Kloetstra, K.R.; Zandbergen, H.W.; Jansen, J.C.; and Van Bekkum, H. Overgrowth of mesoporous MCM-41 on faujasite. Micropor. Mater. 6 (1996): 287.
- [27] Kloetstra, K. R.; Jansen, J. C.; van Bekkum, H. Solid mesoporous base catalysts comprising of MCM-41 supported intraporous cesium oxide. Studies Surface Science Catal. 105 (1997): 431.
- [28] Kloetstra, K. R.; van Bekkum, H.; Jansen, J. C. New organic chemical conversions over MCM-41-type materials. J. Chem. Soc., Chem. Commun. 117 (1997): 2281.
- [29] Karlsson, A.; Stocker, M.; and Schmidt, R. In *Proceedings of the 12th International Zeolite Conference*; MRS: Warrendale, PA, 1999; Vol. 1, p 713.
- [30] Karlsson, A.; Stocker, M.; and Schmidt, R. Composites of micro- and mesoporous materials: simultaneous syntheses of MFI/MCM-41 like phases by a mixed template approach. Micropor. Mesopor. Mater. 27 (1999): 181.
- [31] Huang, L.; and Li, Q. In *Proceedings of the 12th International Zeolite Conference*; MRS: Warrendale, PA, 1999; Vol. 1, p 707.
- [32] Guo, W.; Huang, L.; Deng, P.; Xue, Z.; and Li, Q. Characterization of Beta/MCM-41 composite molecular sieve compared with the mechanical mixture. Micropor. Mesopor. Mater. 44-45 (2001): 427.
- [33] Garcia, R.A.; Serrano, D.P.; and Otero, D. Catalytic cracking of HDPE over hybrid zeolitic-mesoporous materials. J. Anal. Appl. Pyrolysis. 74 (2005): 379.

- [34] Mokaya, M.; and Jones, W. Physicochemical Characterisation and Catalytic Activity of Primary Amine Templated Aluminosilicate Mesoporous Catalysts. J. Catalysis. 172 (1997): 211
- [35] Bhatia, S.; Ooi, Y.S.; Zakaria, R.; and Mohamed A.R. Synthesis of composite material MCM-41/Beta and its catalytic performance in waste used palm oil cracking. Apply. Catal. A. 274 (2004); 15
- [36] Farrauto, R.J.; and Bartholomew, C.H. Fundamentals of Industrial catalytic processes, Blackie Academic and Professional, London UK: Chapman & Hill Boundry Row, 1997, 7.
- [37] McBain, J.W. The Sorption of Gases and Vapors by Solids, London: Rutledge & Sons, 1932, 17.
- [38] Colella, C; Gualtieri, A. F. Cronstedt's zeolite. Micropor. Mesopor. Mater. 105 (2007): 213.
- [39] Smart, L. Zeolites and related structures. In Solid State Chemistry: An Introduction, Moore, E. Ed.; Champman and Hall: London, (1995); 238.
- [40] Loewenstein, W. Am. The distribution of aluminum in the tetrahedra of silicates and aluminates. Mineral. 39 (1954): 92.
- [41] Derouane, E.G. New aspects of molecular shape-selectivity: Catalytic by zeolite ZSM-5. Studies Surface Science Catal. 5 (1980): 5.
- [42] Szostak, R. Molecular Sieve Principles of Synthesis and Identification, New York: Van Nostrand Reinhold, 1988, 1-45.
- [43] Szostak, R. Molecular Sieves: Principles of Synthesis and Identification. New York: Van Nostrand Reinhold, 1989.
- [44] Breck, D. Zeolite Molecular Sieves: Structure, Chemistry, and Use. New York: John Wiley & Sons, 1974.
- [45] Meisel, S.L.; McCullough, J.P.; Lechthaler C.H.; and Weisz P.B. Gasoline from methanol in one step. Chemtech 6 (1976): 86.
- [46] Kokotailo, G.T.; Lawton, S.L.; Olson D.H.; and Meier W.M. Structure of synthetic zeolite ZSM-5. Nature 272 (1978): 437.
- [47] Olson, D.H.; Kokotailo, G.T.; Lawton S.L.; and Meier, W.M. Crystal Structure and Structure-Related Properties of ZSM-5. J. Phys. Chem 85 (1981): 2238.

- [48] Beck, J.S.; Vartuli, J.C.; Roth, W.J.; Leonowicz, M.E.; Kresge, C.T.; Schmitt, K.D.; Chu, C.T.-W.; Olson, D.H.; Sheppard, E.W.; Mccullen, S.B.; Higgins, J.B.; and Schlenker, J.L. A New Family of Mesoporous Molecular Sieves Prepared with Liquid Crystal Templates. J. Am. Chem. Soc. 114 (1992): 10834.
- [49] Inagaki, S.; Fukushima, Y.; and Kuroda, K. Synthesis of Highly Ordered Mesoporous Materials from a Layered Polysilicate. J. Chem. Soc., Chem. Commun. (1993): 680.
- [50] Tanev, P.T.; Chibwe, M.; and Pinnavaia, T.J. Titanium-Containing Mesoporous Molecular Sieves for Catalytic Oxidation of Aromatic Compounds. Nature 368 (1994): 321.
- [51] Zhao, D.; Feng, J.; Huo, Q.; Melosh, N.; Fredrickson, G.H.; Chmelka, B.F.; and Stucky, G.D. Triblock Copolymer Syntheses of Mesoporous Silica with Periodic 50-300 Angstrom Pores. Science. 279 (1998): 548.
- [52] Tuel, A. Modification of Mesoporous Silica by Incorporation of Heteroelements in the Framework. Micropor. Mesopor. Mater. 27 (1999): 151.
- [53] Tanev, P.T.; and Pinnavaia, T.J. A Neutral Templating Route to Mesoporous Molecular Sieves. Science. 267 (1995): 865.
- [54] Ying, J.Y.; Mehnert, C.P.; Wong, M.S. Synthesis and Application of Supramolecular-Templated Mesoporous Materials. Angew. Chem. Int. Ed. 38 (1999): 56.
- [55] Inagaki, S.; Koiwai, A.; Suzuki, N.; Fukushima, Y.; and Kuroda, K. Synthesis of Highly Ordered Mesoporous Material, FSM-16, Derived from Kanemite. Bull. Chem. Soc. Jpn. 69 (1996): 1449-1457.
- [56] Ciesla, U.; and Schüth, F. Order Mesoporous Materials. Micropor. Mesopor. Mater. 27 (1999): 131.
- [57] Pauly, T.R.; and Pinnavaia, T.J. Pore Size Modification of Mesoporous HMS Molecular Sieve Silicas with Wormhole Framework Structures. Chem. Mater. 13 (2001): 987.
- [58] Zhao, D.; Huo, Q.; Feng, J.; Chmelka, B.F.; and Stucky, G.D. Nonionic Triblock and Star Diblock Copolymer and Oligomeric Surfactant Syntheses of Highly Ordered, Hydrothermally Stable, Mesoporous Silica Structure. J. Am. Chem. Soc. 120 (1998): 6024.

- [59] Zhang, W.; Pauly, T.R.; and Pinnavaia, T.J. Tailoring the Framework and Textural Mesoporous of HMS Molecular Sieve Through and Electrically Neutral (S^{0+}) Assembly Pathway. Chem. Mater. 9 (1997): 2491.
- [60] Chiranjeevi, T.; Kumar, P.; Maity, S.K.; Rana, M.S.; Murali Dhar, G.; and Prasada Rao, T.S.R. Characterization and Hydrodesulfurization Catalysis on WS_2 Supported on Mesoporous Al-HMS Materials. Micropor. Mesopor. Mater. 44-45 (2001): 547.
- [61] Yang, R.T.; Pinnavaia, T.J.; Li, W.; and Zhang, W. Fe^{3+} Exchanged Mesoporous Al-HMS and Al-MCM-41 Molecular Sieves for Selective Catalytic Reduction of NO with NH_3 . J. Catal. 172 (1997): 488.
- [62] Yin, D.; Li, W.; Yang, W.; Xiang, H.; Sun, Y.; Zhong, B.; and Peng, S. Mesoporous HMS Molecular Sieves Supported Cobalt Catalysts for Fischer-Tropsch Synthesis. Micropor. Mesopor. Mater. 47 (2001): 15.
- [63] Pinnavaia, T.J. and Liu, Y. Mesocellular aluminosilicate foams (MSU-S/F) and large pore hexagonal mesostructures (MSU-S/H) assembled from zeolite seeds: hydrothermal stability and properties as cumene cracking catalysts. Studies Surface Science Catal. 142 (2002): 1075.
- [64] Callister, W.D.J. Materials science and engineering - An introduction, 4th ed., John Wiley & Sons, USA, 1997.
- [65] Elliott, S. The physics and chemistry of solids, John Wiley & Sons, Chichester, 1998.
- [66] Rouquerol, F.; Rouquerol, J.; and Sing, K. Adsorption by powders and porous solids, Academic Press, San Diego, USA, 1999.
- [67] Zworykin, V.K.; Hiller, J.; and Snyder, R.L.; ASTM Bulletin 117 (1942): 15.
- [68] Lewis, D.W.; Catlow, C.R.A.; and Sankar, G. Structure of Iron-Substituted ZSM-5. J. Phys. Chem. 99 (1995): 2377.
- [69] Hunger, M.; Schenk, U.; Breuninger, R.; Glaser, R.; and Weikamp, J. Characterization of the acid sites in MCM-41 type materials by spectroscopic and catalytic technique. Micropor. Mesopor. Mater. 27 (1999): 261.
- [70] Vela, N.P., Olson, L.K., and Caruso, J.A. Elemental speciation with plasma mass spectrometry. Analytical Chemistry. 65 ,13 (1993); 585A
- [71] Scherzer, J. Octane-enhancing, zeolitic FCC catalyst: scientific and technical aspect. Catal. Rev.-Sci. Eng. 31 (1989): 83.

- [72] Kevan, L.; Hartmann, M. Transition-Metal Ions in Aluminophosphate and Silicoaluminophosphate Molecular Sieves: Location, Interaction with Adsorbates and Catalytic Properties. Chem. Rev. 99 (1999): 635.
- [73] Yury, V.K. Chemical mechanisms of catalytic cracking over solid acidic catalyst: alkanes and alkenes. Taylor & Francis. 48 (2001): 85.
- [74] Greensfelder, B.S.; Voge, H.H.; and Good, G.M. Catalytic and thermal cracking of pure hydrocarbons. Ind. Eng. Chem. Res. 41 (1949): 2573.
- [75] Thomas, C.L. Chemistry of cracking catalysts. Ind. Eng. Chem. Res. 41 (1949): 2564.
- [76] Sie, S.T. Acid-catalyzed cracking of paraffinics Part2. Evidence for the protonated cyclopropane mechanism from catalytic cracking experiments. Indian Eng. Chem. 32 (1993): 397.
- [77] Williams, B.A.; Babitz, S.M.; Miller, J.T.; Snurr, R.Q.; and Kung, H.H. The role of acid strength and pore diffusion in the enhanced cracking activity of steamed zeolites Y. Apply. Catal. A. 32 (1999): 161.
- [78] Cumming, K.A.; and Wojciechowski, B.W. Hydrogen transfer, coke formation and catalyst decay and their role in the chain mechanism of catalytic cracking. Catal. Rev. Sci. Eng. 38 (1996): 101.
- [79] Wojciechowski, B.W.; and Abbot, J. The mechanism of catalytic cracking of n-alkanes on ZSM-5 zeolite. J. Chem. Eng. 63 (1985): 462.
- [80] Makkee, M.; Wissink, M.; and Moulijn, J.A. Gasoline conversion: reactivity towards cracking with equilibrated FCC and ZSM-5 catalysts. Apply. Catal. A. 223 (2002): 85.
- [81] Ishihara, Y.; Nanbu, H.; Saido, K.; Ikemura, T.; and Takesue, T. Mechanism for gas formation in polyethylene catalytic decomposition. Polymer 33 (1992): 3482.
- [82] Ishihara, Y.; Nanbu, H.; Saido, K.; Ikemura, T.; Takesue, T.; and Kuroki, T. Mechanism for gas formation in catalytic decomposition of polypropylene. Fuel 72 (1993): 1115.
- [83] Huang, L.; Guo, W.; Deng, P.; Xue, Z.; and Li, Q. Investigation of synthesizing MCM-41/ZSM-5 composites. J. Phys. Chem. B. 104 (2000): 2817.

- [84] Vorranutch J. Effect of silica sources on properties of ZSM-5 and product selectivity of catalytic plastic cracking. Senior project, Department of Chemistry, Faculty of Science, Chulalongkorn University, 2005.
- [85] Metha S. Tungsten oxide catalyst on various supports for metathesis reaction of 1-hexene. Master degree thesis, Department of Chemistry, Faculty of Science, Chulalongkorn University, 2003.
- [86] Soamwadee, C.; Rangson, K.; Aticha, C.; Thallada, B.; Akio, N.; Akinori, M.; Yusaku, S. Catalytic degradation of polyolefins over hexagonal mesoporous silica : Effect of aluminium addition. J. Anal. Appl. Pyrolysis. 80 (2007): 360.



สถาบันวิทยบริการ
จุฬาลงกรณ์มหาวิทยาลัย



APPENDICES

สถาบันวิทยบริการ
จุฬาลงกรณ์มหาวิทยาลัย

Appendix

A-1 Calculation of Selectivity to Other Hydrocarbons

% Selectivity of gas fraction and liquid fraction

$$\% \text{ Selectivity of X} = \frac{\text{concentration of X} \times 100}{\text{total concentration of fractions}}$$

$$\text{Concentration of X} = \frac{b \times c}{a}$$

a = Peak area of X in standard gas or liquid fraction

b = % molar of X in standard gas or liquid fraction

c = Peak area of X in sample products

สถาบันวิทยบริการ
จุฬาลงกรณ์มหาวิทยาลัย

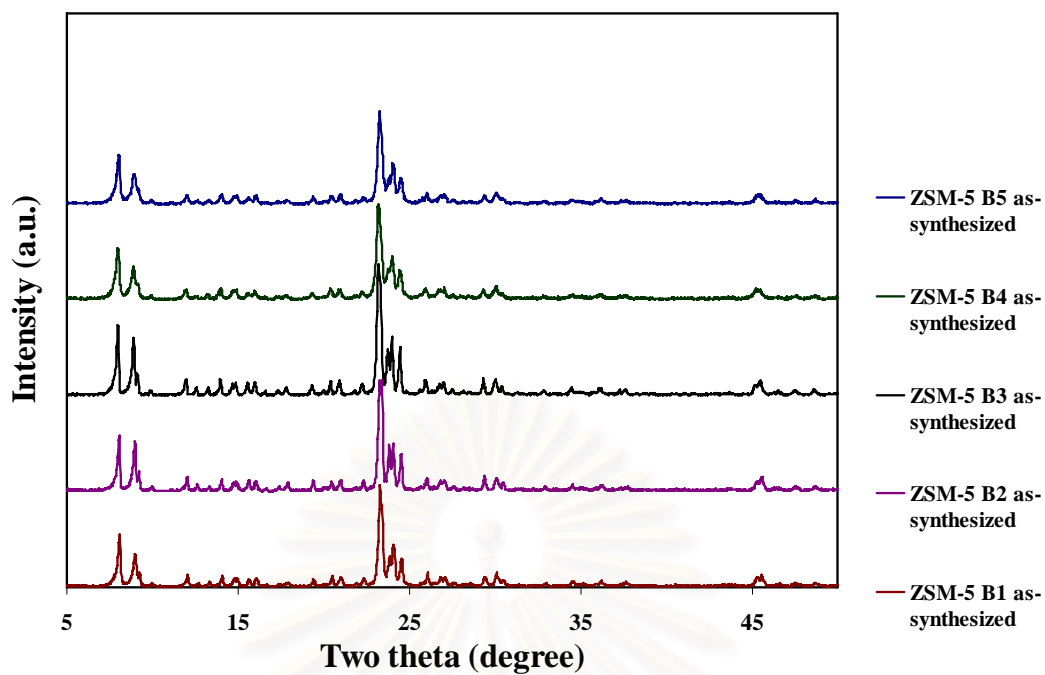


Figure A-1 XRD patterns of as-synthesized of ZSM-5.

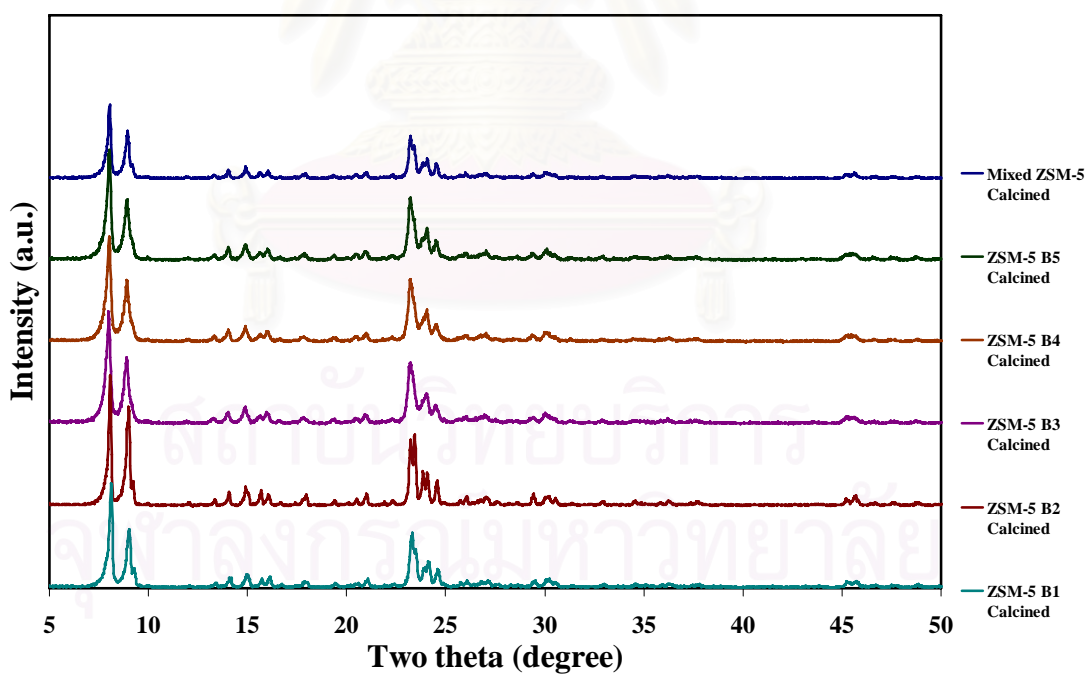


Figure A-2 XRD patterns of the calcined of ZSM-5.

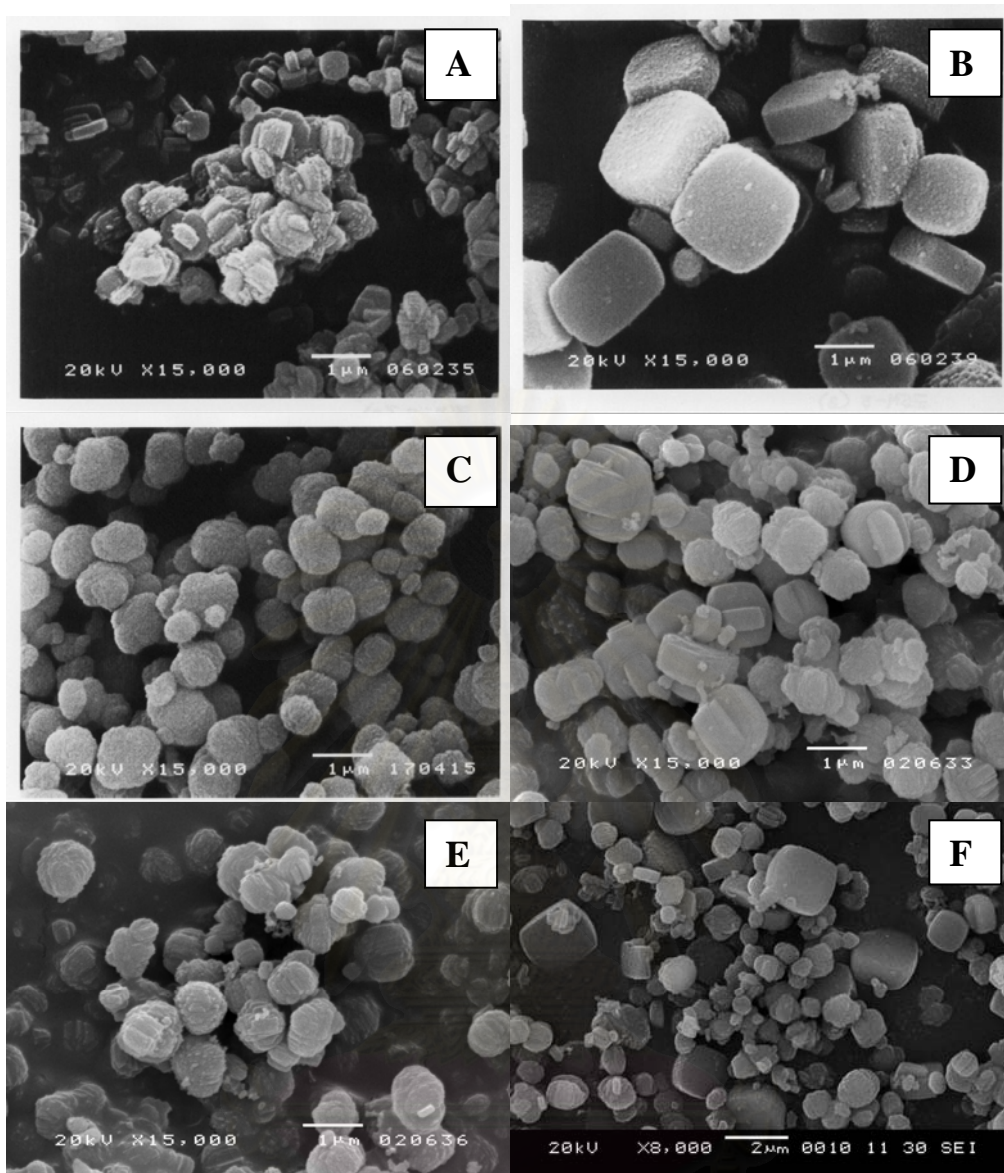


Figure A-3 SEM images of calcined sample ZSM-5: (A) ZSM-5 B1, (B) ZSM-5 B2, (C) ZSM-5 B3, (D) ZSM-5 B4, (E) ZSM-5 B5, and (F) mixed ZSM-5.

จุฬาลงกรณ์มหาวิทยาลัย

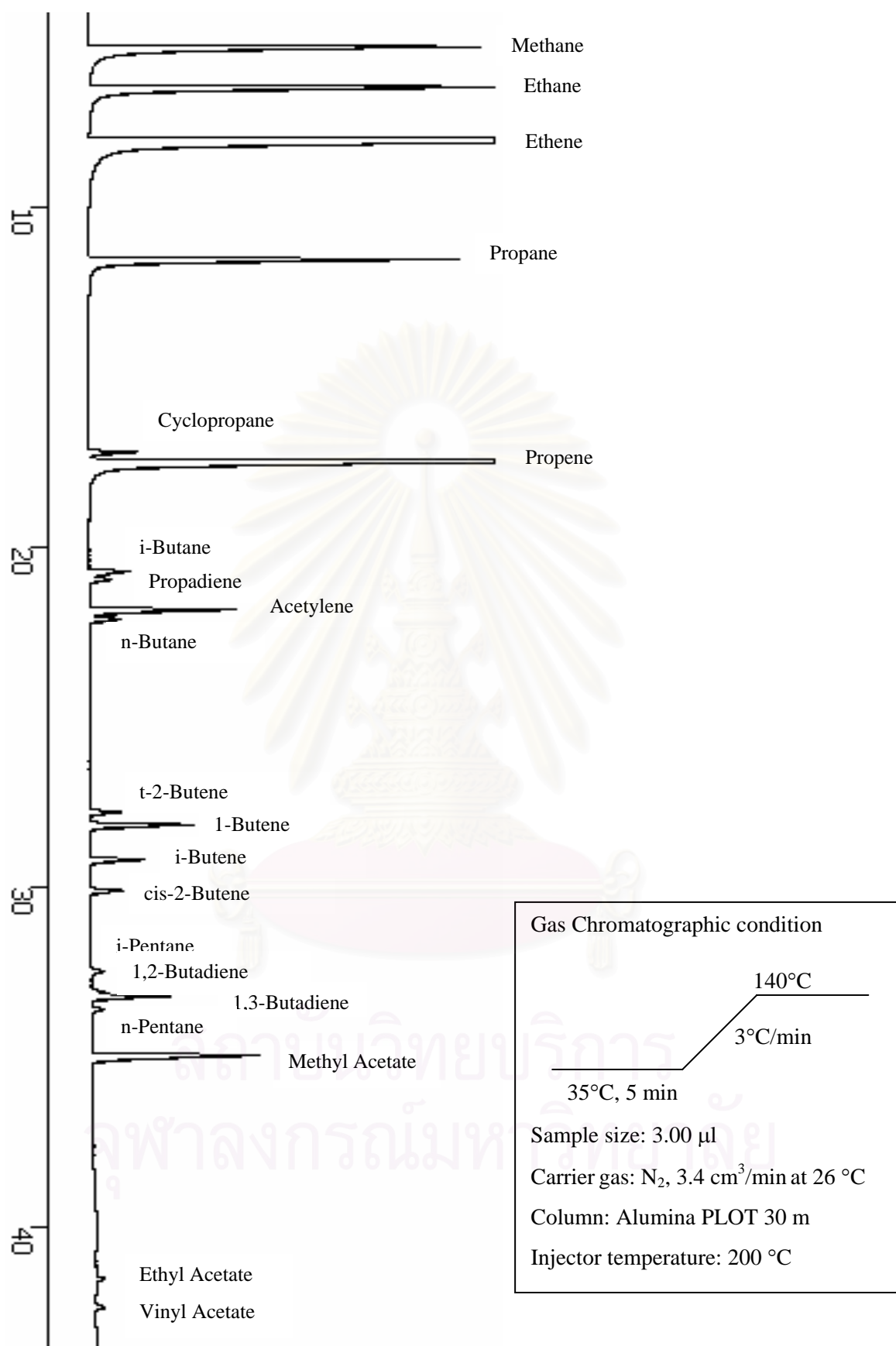


Figure A-4 Gas chromatogram of standard mixture gas.

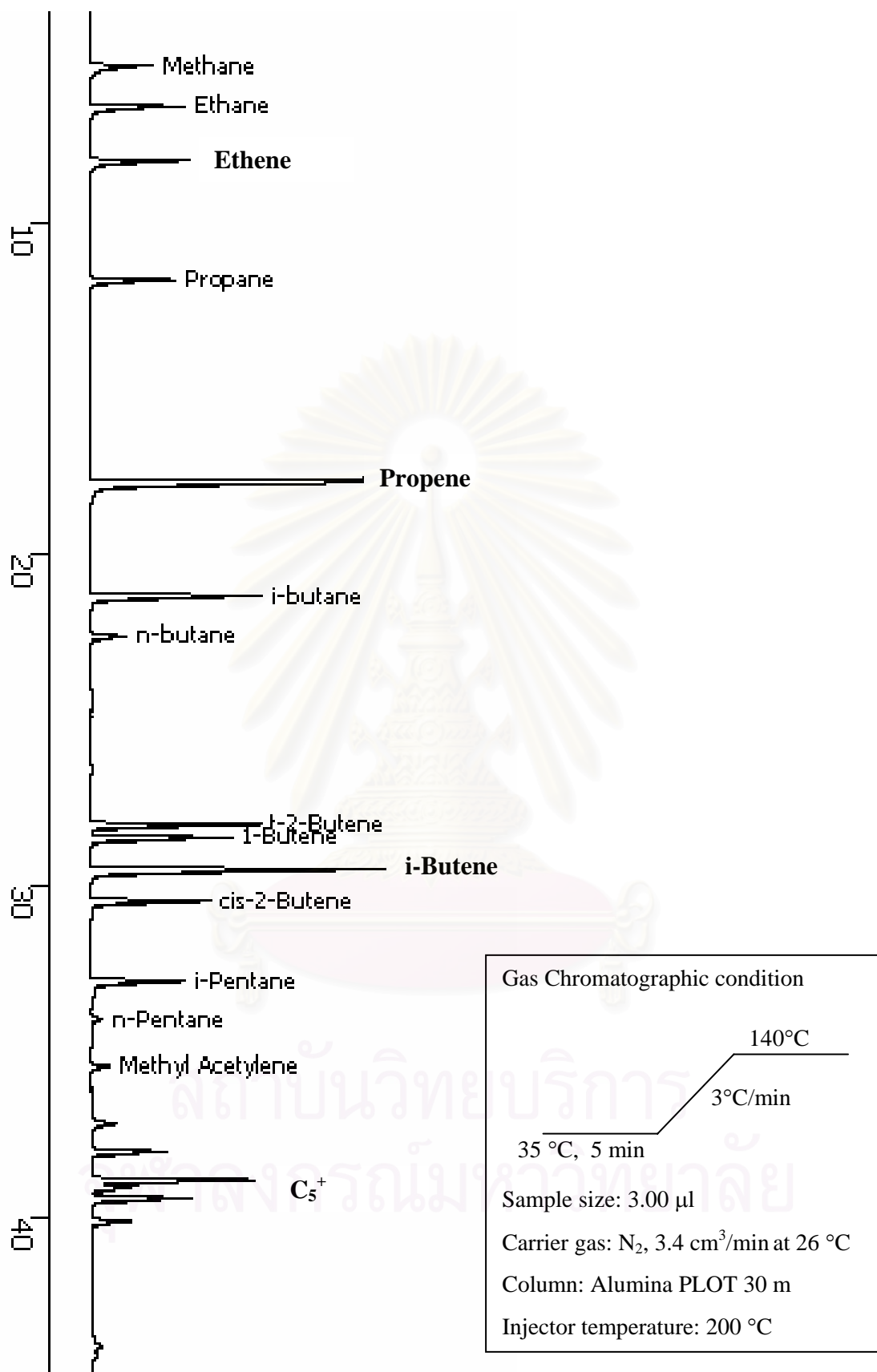


Figure A-5 Gas chromatogram of gas product obtained from catalytic cracking of PP over ZSM-5/Al-HMS-60 (1:1) at 400°C, 5 wt% of catalyst.

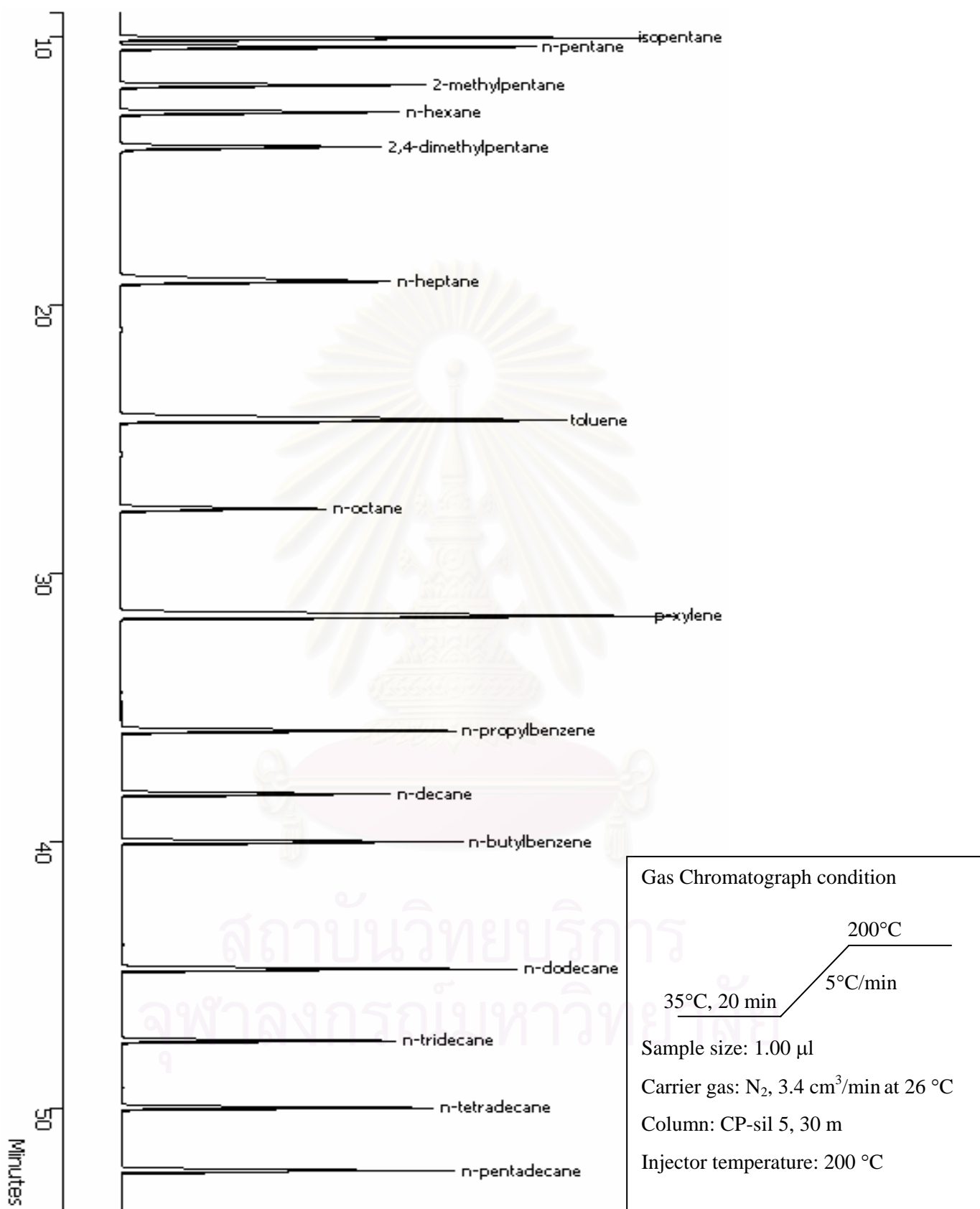


Figure A-6 Liquid chromatogram of standard gasoline (SUPELCO).

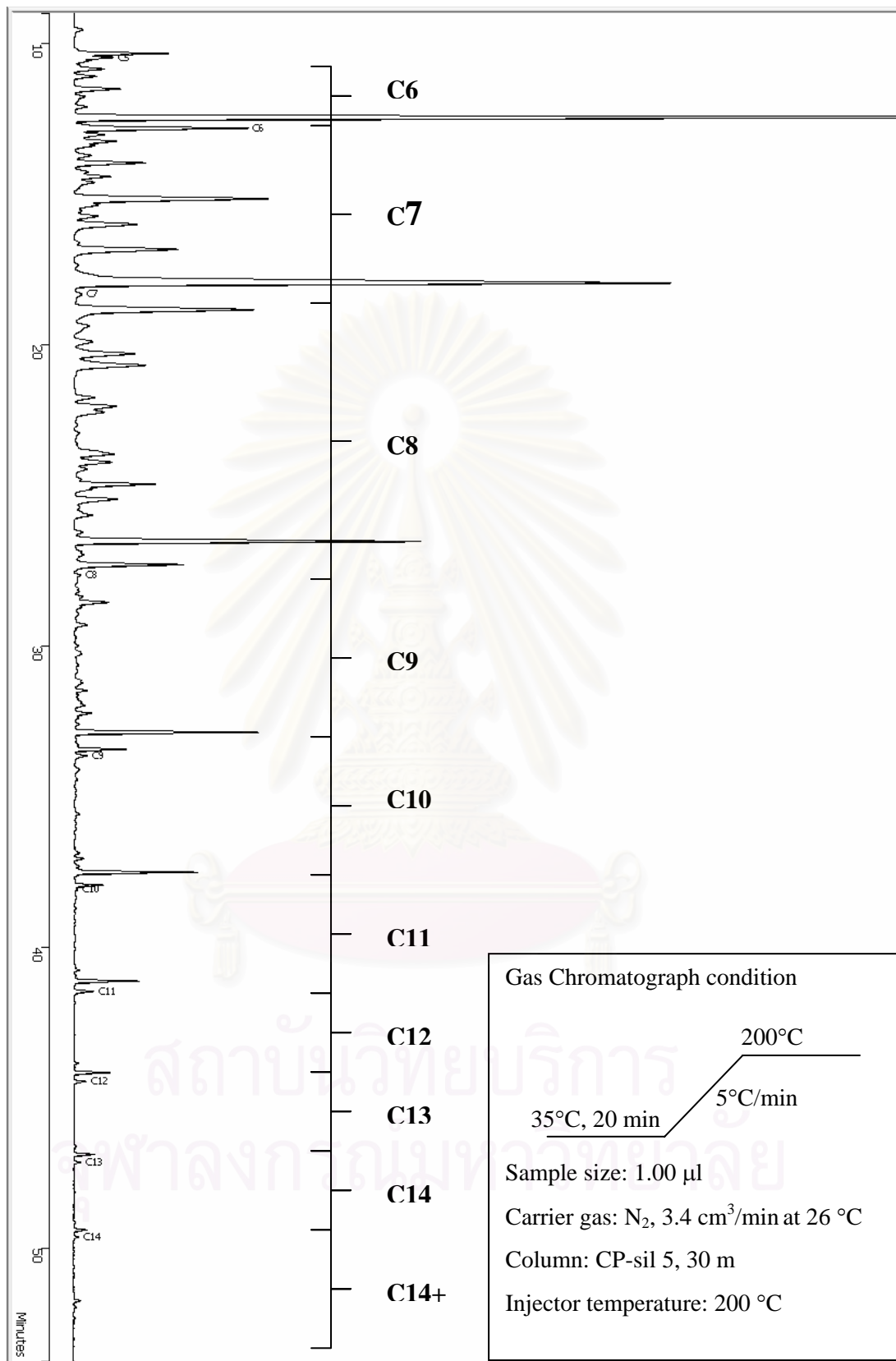
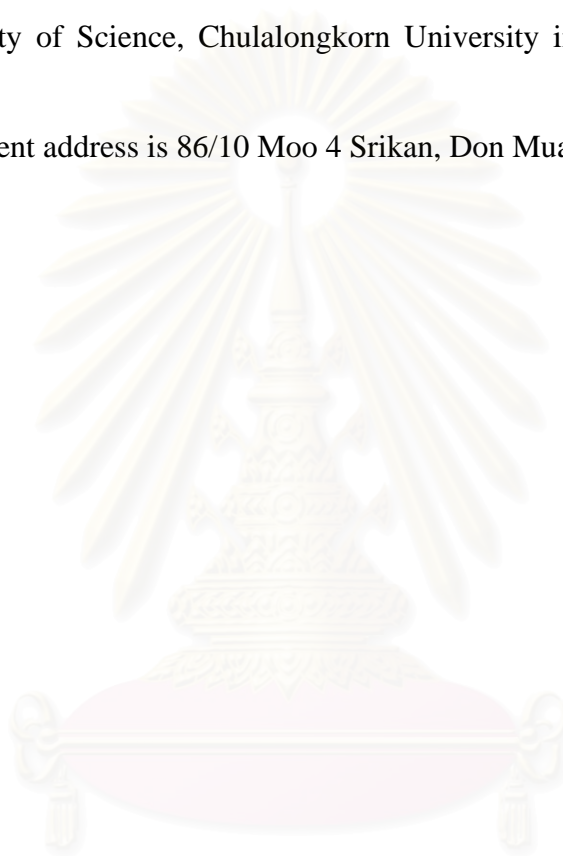


Figure A-7 Liquid chromatogram of liquid product obtained from thermal cracking of HDPE at 450°C.

VITAE

Mr. Rangson Katsutath was born on April 24, 1982 in Bangkok, Thailand. He received a Bachelor's Degree of Science in Chemistry from Mahidol University in 2004. He continued his Master's Degree study in Petrochemistry and Polymer Science Program, Faculty of Science, Chulalongkorn University in 2004 and completed in 2008.

His present address is 86/10 Moo 4 Srikan, Don Muang, Bangkok, Thailand



สถาบันวิทยบริการ
จุฬาลงกรณ์มหาวิทยาลัย